

University of Nebraska - Lincoln

DigitalCommons@University of Nebraska - Lincoln

Kenneth Bloom Publications

Research Papers in Physics and Astronomy

8-1-2001

Measurement of the $t\bar{t}$ production cross section in $p\bar{p}$ collisions at $\sqrt{s} = 1.8$ TeV

T. Affolder

Ernest Orlando Lawrence Berkeley National Laboratory, Berkeley, California

Kenneth A. Bloom

University of Nebraska-Lincoln, kenbloom@unl.edu

Collider Detector at Fermilab Collaboration

Follow this and additional works at: <https://digitalcommons.unl.edu/physicsbloom>



Part of the [Physics Commons](#)

Affolder, T.; Bloom, Kenneth A.; and Fermilab Collaboration, Collider Detector at, "Measurement of the $t\bar{t}$ production cross section in $p\bar{p}$ collisions at $\sqrt{s} = 1.8$ TeV" (2001). *Kenneth Bloom Publications*. 86. <https://digitalcommons.unl.edu/physicsbloom/86>

This Article is brought to you for free and open access by the Research Papers in Physics and Astronomy at DigitalCommons@University of Nebraska - Lincoln. It has been accepted for inclusion in Kenneth Bloom Publications by an authorized administrator of DigitalCommons@University of Nebraska - Lincoln.

Measurement of the $t\bar{t}$ production cross section in $p\bar{p}$ collisions at $\sqrt{s} = 1.8$ TeV

T. Affolder,²³ H. Akimoto,⁴⁵ A. Akopian,³⁸ M. G. Albrow,¹¹ P. Amaral,⁸ S. R. Amendolia,³⁴ D. Amidei,²⁶ K. Anikeev,²⁴ J. Antos,¹ G. Apollinari,¹¹ T. Arisawa,⁴⁵ T. Asakawa,⁴³ W. Ashmanskas,⁸ F. Azfar,³¹ P. Azzi-Bacchetta,³² N. Bacchetta,³² M. W. Bailey,²⁸ S. Bailey,¹⁶ P. de Barbaro,³⁷ A. Barbaro-Galtieri,²³ V. E. Barnes,³⁶ B. A. Barnett,¹⁹ S. Baroiant,⁵ M. Barone,¹³ G. Bauer,²⁴ F. Bedeschi,³⁴ S. Belforte,⁴² W. H. Bell,¹⁵ G. Bellettini,³⁴ J. Bellinger,⁴⁶ D. Benjamin,¹⁰ J. Bensinger,⁴ A. Beretvas,¹¹ J. P. Berge,¹¹ J. Berryhill,⁸ B. Bevensee,³³ A. Bhatti,³⁸ M. Binkley,¹¹ D. Bisello,³² M. Bishai,¹¹ R. E. Blair,² C. Blocker,⁴ K. Bloom,²⁶ B. Blumenfeld,¹⁹ S. R. Blusk,³⁷ A. Bocci,³⁸ A. Bodek,³⁷ W. Bokhari,³³ G. Bolla,³⁶ Y. Bonushkin,⁶ D. Bortoletto,³⁶ J. Boudreau,³⁵ A. Brandl,²⁸ S. van den Brink,¹⁹ C. Bromberg,²⁷ M. Brozovic,¹⁰ N. Bruner,²⁸ E. Buckley-Geer,¹¹ J. Budagov,⁹ H. S. Budd,³⁷ K. Burkett,¹⁶ G. Busetto,³² A. Byon-Wagner,¹¹ K. L. Byrum,² P. Calafiura,²³ M. Campbell,²⁶ W. Carithers,²³ J. Carlson,²⁶ D. Carlsmith,⁴⁶ W. Caskey,⁵ J. Cassada,³⁷ A. Castro,³² D. Cauz,⁴² A. Cerri,³⁴ A. W. Chan,¹ P. S. Chang,¹ P. T. Chang,¹ J. Chapman,²⁶ C. Chen,³³ Y. C. Chen,¹ M.-T. Cheng,¹ M. Chertok,⁴⁰ G. Chiarelli,³⁴ I. Chirikov-Zorin,⁹ G. Chlachidze,⁹ F. Chlebana,¹¹ L. Christofek,¹⁸ M. L. Chu,¹ Y. S. Chung,³⁷ C. I. Ciobanu,²⁹ A. G. Clark,¹⁴ A. Connolly,²³ J. Conway,³⁹ M. Cordelli,¹³ J. Cranshaw,⁴¹ D. Cronin-Hennessy,¹⁰ R. Cropp,²⁵ R. Culbertson,¹¹ D. Dagenhart,⁴⁴ S. D'Auria,¹⁵ F. DeJongh,¹¹ S. Dell'Agnello,¹³ M. Dell'Orso,³⁴ L. Demortier,³⁸ M. Deninno,³ P. F. Derwent,¹¹ T. Devlin,³⁹ J. R. Dittmann,¹¹ S. Donati,³⁴ J. Done,⁴⁰ T. Dorigo,¹⁶ N. Eddy,¹⁸ K. Einsweiler,²³ J. E. Elias,¹¹ E. Engels, Jr.,³⁵ R. Erbacher,¹¹ D. Errede,¹⁸ S. Errede,¹⁸ Q. Fan,³⁷ R. G. Feild,⁴⁷ J. P. Fernandez,¹¹ C. Ferretti,³⁴ R. D. Field,¹² I. Fiori,³ B. Flaughner,¹¹ G. W. Foster,¹¹ M. Franklin,¹⁶ J. Freeman,¹¹ J. Friedman,²⁴ Y. Fukui,²² I. Furic,²⁴ S. Galeotti,³⁴ M. Gallinaro,³⁸ T. Gao,³³ M. Garcia-Sciveres,²³ A. F. Garfinkel,³⁶ P. Gatti,³² C. Gay,⁴⁷ D. W. Gerdes,²⁶ P. Giannetti,³⁴ P. Giromini,¹³ V. Glagolev,⁹ D. Glenzinski,¹¹ M. Gold,²⁸ J. Goldstein,¹¹ A. Gordon,¹⁶ I. Gorelov,²⁸ A. T. Goshaw,¹⁰ Y. Gotra,³⁵ K. Goulianos,³⁸ C. Green,³⁶ G. Grim,⁵ P. Gris,¹¹ L. Groer,³⁹ C. Grosso-Pilcher,⁸ M. Guenther,³⁶ G. Guillian,²⁶ J. Guimaraes da Costa,¹⁶ R. M. Haas,¹² C. Haber,²³ E. Hafen,²⁴ S. R. Hahn,¹¹ C. Hall,¹⁶ T. Handa,¹⁷ R. Handler,⁴⁶ W. Hao,⁴¹ F. Happacher,¹³ K. Hara,⁴³ A. D. Hardman,³⁶ R. M. Harris,¹¹ F. Hartmann,²⁰ K. Hatakeyama,³⁸ J. Hauser,⁶ J. Heinrich,³³ A. Heiss,²⁰ M. Herndon,¹⁹ C. Hill,⁵ K. D. Hoffman,³⁶ C. Holck,³³ R. Hollebeek,³³ L. Holloway,¹⁸ R. Hughes,²⁹ J. Huston,²⁷ J. Huth,¹⁶ H. Ikeda,⁴³ J. Incandela,¹¹ G. Introzzi,³⁴ J. Iwai,⁴⁵ Y. Iwata,¹⁷ E. James,²⁶ M. Jones,³³ U. Joshi,¹¹ H. Kambara,¹⁴ T. Kamon,⁴⁰ T. Kaneko,⁴³ K. Karr,⁴⁴ H. Kasha,⁴⁷ Y. Kato,³⁰ T. A. Keaffaber,³⁶ K. Kelley,²⁴ M. Kelly,²⁶ R. D. Kennedy,¹¹ R. Kephart,¹¹ D. Khazins,¹⁰ T. Kikuchi,⁴³ B. Kilminster,³⁷ B. J. Kim,²¹ D. H. Kim,²¹ H. S. Kim,¹⁸ M. J. Kim,²¹ S. H. Kim,⁴³ Y. K. Kim,²³ M. Kirby,¹⁰ M. Kirk,⁴ L. Kirsch,⁴ S. Klimenko,¹² P. Koehn,²⁹ A. Königter,²⁰ K. Kondo,⁴⁵ J. Konigsberg,¹² K. Kordas,²⁵ A. Korn,²⁴ A. Korytov,¹² E. Kovacs,² J. Kroll,³³ M. Kruse,³⁷ S. E. Kuhlmann,² K. Kurino,¹⁷ T. Kuwabara,⁴³ A. T. Laasanen,³⁶ N. Lai,⁸ S. Lami,³⁸ S. Lammel,¹¹ J. I. Lamoureux,⁴ J. Lancaster,¹⁰ M. Lancaster,²³ R. Lander,⁵ G. Latino,³⁴ T. LeCompte,² A. M. Lee IV,¹⁰ K. Lee,⁴¹ S. Leone,³⁴ J. D. Lewis,¹¹ M. Lindgren,⁶ J. B. Liu,³⁷ Y. C. Liu,¹ D. O. Litvintsev,⁸ O. Lobbani,⁴¹ N. Lockyer,³³ J. Loken,³¹ M. Loreti,³² D. Lucchesi,³² P. Lukens,¹¹ S. Lusin,⁴⁶ L. Lyons,³¹ J. Lys,²³ R. Madrak,¹⁶ K. Maeshima,¹¹ P. Maksimovic,¹⁶ L. Malferrari,³ M. Mangano,³⁴ M. Mariotti,³² G. Martignon,³² A. Martin,⁴⁷ J. A. J. Matthews,²⁸ J. Mayer,²⁵ P. Mazzanti,³ K. S. McFarland,³⁷ P. McIntyre,⁴⁰ E. McKigney,³³ M. Menguzzato,³² A. Menzione,³⁴ C. Mesropian,³⁸ A. Meyer,¹¹ T. Miao,¹¹ R. Miller,²⁷ J. S. Miller,²⁶ H. Minato,⁴³ S. Miscetti,¹³ M. Mishina,²² G. Mitselmakher,¹² N. Moggi,³ E. Moore,²⁸ R. Moore,²⁶ Y. Morita,²² T. Moulk,²⁴ M. Mulhearn,²⁴ A. Mukherjee,¹¹ T. Muller,²⁰ A. Munar,³⁴ P. Murat,¹¹ S. Murgia,²⁷ J. Nachtman,⁶ V. Nagaslaev,⁴¹ S. Nahn,⁴⁷ H. Nakada,⁴³ T. Nakaya,⁸ I. Nakano,¹⁷ C. Nelson,¹¹ T. Nelson,¹¹ C. Neu,²⁹ D. Neuberger,²⁰ C. Newman-Holmes,¹¹ C.-Y. P. Ngan,²⁴ H. Niu,⁴ L. Nodulman,² A. Nomerotski,¹² S. H. Oh,¹⁰ T. Ohmoto,¹⁷ T. Ohsugi,¹⁷ R. Oishi,⁴³ T. Okusawa,³⁰ J. Olsen,⁴⁶ W. Orejudos,²³ C. Pagliarone,³⁴ F. Palmonari,³⁴ R. Paoletti,³⁴ V. Papadimitriou,⁴¹ S. P. Pappas,⁴⁷ D. Partos,⁴ J. Patrick,¹¹ G. Pauletta,⁴² M. Paulini,^{23,*} C. Paus,²⁴ L. Pescara,³² T. J. Phillips,¹⁰ G. Piacentino,³⁴ K. T. Pitts,¹⁸ A. Pompos,³⁶ L. Pondrom,⁴⁶ G. Pope,³⁵ M. Popovic,²⁵ F. Prokoshin,⁹ J. Proudfoot,² F. Ptohos,¹³ O. Pukhov,⁹ G. Punzi,³⁴ K. Ragan,²⁵ A. Rakitine,²⁴ D. Reher,²³ A. Reichold,³¹ A. Ribon,³² W. Riegler,¹⁶ F. Rimondi,³ L. Ristori,³⁴ M. Riveline,²⁵ W. J. Robertson,¹⁰ A. Robinson,²⁵ T. Rodrigo,⁷ S. Rolli,⁴⁴ L. Rosenson,²⁴ R. Roser,¹¹ R. Rossin,³² A. Roy,²⁴ A. Safonov,³⁸ R. St. Denis,¹⁵ W. K. Sakumoto,³⁷ D. Saltzberg,⁶ C. Sanchez,²⁹ A. Sansoni,¹³ L. Santi,⁴² H. Sato,⁴³ P. Savard,²⁵ P. Schlabach,¹¹ E. E. Schmidt,¹¹ M. P. Schmidt,⁴⁷ M. Schmitt,¹⁶ L. Scodellaro,³² A. Scott,⁶ A. Scribano,³⁴ S. Segler,¹¹ S. Seidel,²⁸ Y. Seiya,⁴³ A. Semenov,⁹ F. Semeria,³ T. Shah,²⁴ M. D. Shapiro,²³ P. F. Shepard,³⁵ T. Shibayama,⁴³ M. Shimojima,⁴³ M. Shochet,⁸ A. Sidoti,³² J. Siegrist,²³ A. Sill,⁴¹ P. Sinervo,²⁵ P. Singh,¹⁸ A. J. Slaughter,⁴⁷ K. Sliwa,⁴⁴ C. Smith,¹⁹ F. D. Snider,¹¹ A. Solodsky,³⁸ J. Spalding,¹¹ T. Speer,¹⁴ P. Sphicas,²⁴ F. Spinella,³⁴ M. Spiropulu,¹⁶ L. Spiegel,¹¹ J. Steele,⁴⁶ A. Stefanini,³⁴ J. Strologas,¹⁸ F. Strumia,¹⁴ D. Stuart,¹¹ K. Sumorok,²⁴ T. Suzuki,⁴³ T. Takano,³⁰ R. Takashima,¹⁷ K. Takikawa,⁴³ P. Tamburello,¹⁰ M. Tanaka,⁴³ B. Tannenbaum,⁶ W. Taylor,²⁵ M. Tecchio,²⁶ R. Tesarek,¹¹ P. K. Teng,¹ K. Terashi,³⁸ S. Tether,²⁴ A. S. Thompson,¹⁵ R. Thurman-Keup,² P. Tipton,³⁷ S. Tkaczyk,¹¹ D. Toback,⁴⁰ K. Tollefson,³⁷ A. Tollestrup,¹¹ H. Toyoda,³⁰ W. Trischuk,²⁵ J. F. de Troconiz,¹⁶ J. Tseng,²⁴ N. Turini,³⁴ F. Ukegawa,⁴³ T. Vaiculis,³⁷ J. Valls,³⁹ S. Vejck III,¹¹ G. Velev,¹¹ R. Vidal,¹¹ R. Vilar,⁷ I. Volobouev,²³ D. Vucinic,²⁴ R. G. Wagner,² R. L. Wagner,¹¹ J. Wahl,⁸ N. B. Wallace,³⁹ A. M. Walsh,³⁹ C. Wang,¹⁰ M. J. Wang,¹ T. Watanabe,⁴³ D. Waters,³¹ T. Watts,³⁹ R. Webb,⁴⁰ H. Wenzel,²⁰ W. C. Wester III,¹¹ A. B. Wicklund,² E. Wicklund,¹¹ T. Wilkes,⁵ H. H. Williams,³³ P. Wilson,¹¹ B. L. Winer,²⁹ D. Winn,²⁶ S. Wolbers,¹¹ D. Wolinski,²⁶ J. Wolinski,²⁷ S. Wolinski,²⁶ S. Worm,²⁸ X. Wu,¹⁴

J. Wyss,³⁴ A. Yagil,¹¹ W. Yao,²³ G. P. Yeh,¹¹ P. Yeh,¹ J. Yoh,¹¹ C. Yosef,²⁷ T. Yoshida,³⁰ I. Yu,²¹ S. Yu,³³ Z. Yu,⁴⁷
 A. Zanetti,⁴² F. Zetti,²³ and S. Zucchelli³

(CDF Collaboration)

¹*Institute of Physics, Academia Sinica, Taipei, Taiwan 11529, Republic of China*

²*Argonne National Laboratory, Argonne, Illinois 60439*

³*Istituto Nazionale di Fisica Nucleare, University of Bologna, I-40127 Bologna, Italy*

⁴*Brandeis University, Waltham, Massachusetts 02254*

⁵*University of California at Davis, Davis, California 95616*

⁶*University of California at Los Angeles, Los Angeles, California 90024*

⁷*Instituto de Fisica de Cantabria, CSIC–University of Cantabria, 39005 Santander, Spain*

⁸*Enrico Fermi Institute, University of Chicago, Chicago, Illinois 60637*

⁹*Joint Institute for Nuclear Research, RU-141980 Dubna, Russia*

¹⁰*Duke University, Durham, North Carolina 27708*

¹¹*Fermi National Accelerator Laboratory, Batavia, Illinois 60510*

¹²*University of Florida, Gainesville, Florida 32611*

¹³*Laboratori Nazionali di Frascati, Istituto Nazionale di Fisica Nucleare, I-00044 Frascati, Italy*

¹⁴*University of Geneva, CH-1211 Geneva 4, Switzerland*

¹⁵*Glasgow University, Glasgow G12 8QQ, United Kingdom*

¹⁶*Harvard University, Cambridge, Massachusetts 02138*

¹⁷*Hiroshima University, Higashi-Hiroshima 724, Japan*

¹⁸*University of Illinois, Urbana, Illinois 61801*

¹⁹*The Johns Hopkins University, Baltimore, Maryland 21218*

²⁰*Institut für Experimentelle Kernphysik, Universität Karlsruhe, 76128 Karlsruhe, Germany*

²¹*Center for High Energy Physics, Kyungpook National University, Taegu 702-701, Korea,*

Seoul National University, Seoul 151-742, Korea,

and SungKyunKwan University, Suwon 440-746, Korea

²²*High Energy Accelerator Research Organization (KEK), Tsukuba, Ibaraki 305, Japan*

²³*Ernest Orlando Lawrence Berkeley National Laboratory, Berkeley, California 94720*

²⁴*Massachusetts Institute of Technology, Cambridge, Massachusetts 02139*

²⁵*Institute of Particle Physics, McGill University, Montreal, Canada H3A 2T8*

and University of Toronto, Toronto, Canada M5S 1A7

²⁶*University of Michigan, Ann Arbor, Michigan 48109*

²⁷*Michigan State University, East Lansing, Michigan 48824*

²⁸*University of New Mexico, Albuquerque, New Mexico 87131*

²⁹*The Ohio State University, Columbus, Ohio 43210*

³⁰*Osaka City University, Osaka 588, Japan*

³¹*University of Oxford, Oxford OX1 3RH, United Kingdom*

³²*Universita di Padova, Istituto Nazionale di Fisica Nucleare, Sezione di Padova, I-35131 Padova, Italy*

³³*University of Pennsylvania, Philadelphia, Pennsylvania 19104*

³⁴*Istituto Nazionale di Fisica Nucleare, University and Scuola Normale Superiore of Pisa, I-56100 Pisa, Italy*

³⁵*University of Pittsburgh, Pittsburgh, Pennsylvania 15260*

³⁶*Purdue University, West Lafayette, Indiana 47907*

³⁷*University of Rochester, Rochester, New York 14627*

³⁸*Rockefeller University, New York, New York 10021*

³⁹*Rutgers University, Piscataway, New Jersey 08855*

⁴⁰*Texas A&M University, College Station, Texas 77843*

⁴¹*Texas Tech University, Lubbock, Texas 79409*

⁴²*Istituto Nazionale di Fisica Nucleare, University of Trieste/Udine, Italy*

⁴³*University of Tsukuba, Tsukuba, Ibaraki 305, Japan*

⁴⁴*Tufts University, Medford, Massachusetts 02155*

⁴⁵*Waseda University, Tokyo 169, Japan*

⁴⁶*University of Wisconsin, Madison, Wisconsin 53706*

⁴⁷*Yale University, New Haven, Connecticut 06520*

(Received 18 January 2001; published 3 July 2001)

We update the measurement of the $t\bar{t}$ production cross section using the CDF detector at the Fermilab Tevatron. This measurement uses $t\bar{t}$ decays to the final states $e + \nu + \text{jets}$ and $\mu + \nu + \text{jets}$. We search for b quarks from t decays via secondary-vertex identification or the identification of semileptonic decays of the b and cascade c quarks. The background to the $t\bar{t}$ production is determined primarily through a Monte Carlo

simulation. However, we calibrate the simulation and evaluate its uncertainty using several independent data samples. For a top quark mass of $175 \text{ GeV}/c^2$, we measure $\sigma_{t\bar{t}} = 5.1 \pm 1.5 \text{ pb}$ and $\sigma_{t\bar{t}} = 9.2 \pm 4.3 \text{ pb}$ using the secondary vertex and the lepton tagging algorithms, respectively. Finally, we combine these results with those from other $t\bar{t}$ decay channels and obtain $\sigma_{t\bar{t}} = 6.5_{-1.4}^{+1.7} \text{ pb}$.

DOI: 10.1103/PhysRevD.64.032002

PACS number(s): 14.65.Ha, 13.85.Ni, 13.85.Qk

I. INTRODUCTION

In the standard model (SM) the top quark completes the third fermion generation. The measurement of the top-quark pair production cross section $\sigma_{t\bar{t}}$ is of interest as a test of quantum chromodynamics (QCD) predictions. Aside from the obvious observation that a deviation from these predictions could be indicative of new physics, recent QCD calculations predict $\sigma_{t\bar{t}}$ with an uncertainty smaller than 15% [1] which motivates measurements of comparable precision.

In $p\bar{p}$ collisions at $\sqrt{s} = 1.8 \text{ TeV}$ top quarks are pair produced through $q\bar{q}$ annihilation ($\approx 90\%$) or gluon fusion ($\approx 10\%$). In the SM framework the top quark decays into a W boson and a b quark. When one of the W bosons decays to an electron or a muon, the final state includes a charged lepton with high transverse momentum (p_T), a large transverse energy imbalance from the undetected neutrino, referred to as \cancel{E}_T , and four jets from the hadronized quarks. However, because of gluon radiation or jet merging, the number of detected jets may vary. We measure $\sigma_{t\bar{t}}$ using this final state, referred to in this paper as W +jets and selected from the data (105.1 pb^{-1}) collected by the collider detector at Fermilab (CDF) in the 1992–1995 collider run.

The same data set has been used in the previous CDF measurement of $\sigma_{t\bar{t}}$ [2]. This paper revises that measurement and expands on many of the analysis details. The selection of the W +jet sample follows the guidelines used in all previous CDF measurements of the top quark mass and production cross section [3,4].

As done in previous analyses, we employ two techniques to enhance the relative fraction of events coming from top quark decays with respect to the background. The first method searches a jet for the presence of a secondary vertex reconstructed using the silicon vertex detector (SVX) and displaced from the primary event vertex due to the long b -quark lifetime (SECVTX tag). The second method searches a jet for the presence of a lepton, indicative of a semileptonic b -decay. Since these leptons typically have low momentum compared to the lepton from the W decay, they are referred to as soft lepton tags (SLT).

In this analysis we use the same SECVTX and SLT algorithms as in Ref. [2]. Differently from Refs. [2,3,5], we search jets and not events for soft lepton tags; this approach has been used for the top quark mass measurement [4].

As a cross-check, we take advantage of a third algorithm, jet-probability, which uses the impact parameter significance of all tracks in a jet to derive a probability that the jet originates from the primary event vertex [6]. Jets with small probability of having zero lifetime are considered jet-probability

tags (JPB). The value of the jet-probability threshold is tuned to have higher tagging efficiency than SECVTX in jets originating from c quarks and a higher rate of fake tags in jets without heavy flavor. Since this tuning results in an efficiency for tagging b -quark jets which is comparable to that of SECVTX, the jet-probability algorithm is used only to provide important cross-checks of the background determination and of the cross section measured using SECVTX tags.

The method used to measure $\sigma_{t\bar{t}}$ is outlined in Ref. [5] and has since been improved. As summarized in Ref. [2], the method relies on the calculation of all the background contributions to the tagged W +jet sample. The excess over background of the W +3, 4 jet events with at least one tag is attributed to $t\bar{t}$ production and used to derive $\sigma_{t\bar{t}}$.

The major sources of background are the processes $p\bar{p} \rightarrow Wg$ with $g \rightarrow b\bar{b}$, $c\bar{c}$ (referred to as gluon splitting) and $p\bar{p} \rightarrow Wc$. The second largest source of background is mistags (tags in jets which do not contain heavy flavor). Smaller contributions come from other processes like non- W production, single top quark production, WW , WZ , ZZ and $Z \rightarrow \tau\tau$.

The method used to measure $\sigma_{t\bar{t}}$ relies on the correct calibration of the Monte Carlo generators and the detector simulation. Simulated events are produced with the HERWIG [7] or PYTHIA [8] Monte Carlo generators. Hadrons with heavy flavor (b and c) are decayed using the CLEO Monte Carlo calculation (QQ) [9]. All other particles are decayed, when appropriate, by the CDF detector simulation (QFL) which uses its own lifetime table for b and c -hadrons. QFL simulates the interaction of all particles in the final state with the CDF detector; the detector response is based on parametrizations that are functions of the particle kinematics and have been derived using the data.

This paper describes the work done to understand and improve the calibrations used in the method to calculate the background to $t\bar{t}$ events using independent data samples and the corresponding simulations. This work was primarily focused on the components with the largest influence on the determination of $\sigma_{t\bar{t}}$ mistags, the efficiencies of the tagging algorithms, and the fraction of W +jet direct production which contains heavy flavor. We summarize here the relevant conclusions.

We find that, in the jet- E_T range of interest for this study, the SECVTX tagging efficiency for b -quark jets (b -jets) is $(25 \pm 13)\%$ higher in control samples of data than in the Monte Carlo simulation of the same processes. Therefore we conclude that the b -jet tagging rate in Refs. [2,3] is underestimated by this factor. This data-to-simulation discrepancy is largely due to errors in the simulation that were found *a posteriori*. Instead of remaking the large Monte Carlo

*Now at Carnegie Mellon University, Pittsburgh, Pennsylvania 15213.

samples used in this paper we chose to rescale the simulated b -quark tagging rate by the factor of 1.25 ± 0.13 .

We find that the rate of SECVTX mistags in jets without heavy flavor is $(50 \pm 5)\%$ smaller than what we estimated in Refs. [2,3].

We find that the fraction of $g \rightarrow b\bar{b}$ and $g \rightarrow c\bar{c}$ in the W + jet direct production evaluated with HERWIG needs to be increased by $(39 \pm 19)\%$ and $(35 \pm 36)\%$, respectively.

These last two effects tend to cancel, leaving the net background to top approximately unchanged from our previous results in Refs. [2,3]. In the W + 3,4 jets sample we observe 29 events with one or more SECVTX tags and 25 events with one or more SLT tags. The expected backgrounds are 8.0 ± 1.0 and 13.2 ± 1.2 events, respectively. The excess of SECVTX tags yields the cross section $\sigma_{t\bar{t}} = 5.08 \pm 1.54$ pb and the excess of SLT tags yields $\sigma_{t\bar{t}} = 9.18 \pm 4.26$ pb for a top quark mass of $175 \text{ GeV}/c^2$.

Following a brief description of the CDF detector in Sec. II, Sec. III describes the triggers and the reconstruction of leptons, jets, and the missing transverse energy. The selection of W + jet events is detailed in Sec. IV, along with the selection of the Z + jet sample, which will be used to check the background calculation. The selection of other data samples used to calibrate the event generators and the detector simulation is described in Sec. V. Sections VI and VII are dedicated to the Monte Carlo generators and the CDF detector simulation (QFL), respectively. Section VIII describes the algorithms used for the identification of jets with heavy flavor. The efficiency of those algorithms is calculated in Sec. IX, which also includes numerous checks of the result and the evaluation of its systematic uncertainty. The new method for evaluating mistags and the determination of its accuracy is described in Sec. X. Section XI details the calibration of the $g \rightarrow b\bar{b}$ and $g \rightarrow c\bar{c}$ cross sections predicted by the HERWIG generator. Section XII describes the calculation of the backgrounds to the $t\bar{t}$ production. In Sec. XIII, we check the background calculation using the Z + jet sample. Additional checks of the background calculation are described in Sec. XIV. Finally, $\sigma_{t\bar{t}}$ is derived in Sec. XV. In Sec. XVI, we combine the present results with previous CDF measurements of $\sigma_{t\bar{t}}$ that have been derived using different data sets. We conclude in Sec. XVII.

II. THE CDF DETECTOR

CDF is a general purpose detector with azimuthal and forward-backward symmetry designed to study $p\bar{p}$ interactions. The CDF coordinate system has the z -axis pointing along the proton momentum and the x -axis located in the horizontal plane of the Tevatron storage ring pointing radially outward so that the y -axis points up. The coordinates r - ϕ are the standard cylindrical coordinates. A complete description of CDF can be found in Refs. [5,10]. The detector components most relevant to this analysis are summarized below.

A superconducting solenoid of length 4.8 m and radius 1.5 m generates a 1.4-T magnetic field. The solenoid contains three types of tracking chambers for detecting charged

particles and measuring their momenta. A four layer silicon microstrip vertex detector (SVX) surrounds the beryllium beam pipe of radius 1.9 cm. The SVX has an active length of 51 cm; the four layers of the SVX are at distances of approximately 2.9, 4.2, 5.5, and 7.9 cm from the beamline. Axial micro-strips with $60\text{-}\mu\text{m}$ pitch provide accurate track reconstruction in the r - ϕ plane transverse to the beam [11]. Outside the SVX there is a vertex drift chamber (VTX) which provides track information up to a radius of 22 cm and for pseudorapidities $|\eta| \leq 3.5$. The VTX measures the z -position of the primary vertex. Both the SVX and the VTX are mounted inside the CTC, a 3.2 m long drift chamber with an outer radius of 132 cm containing 84 concentric, cylindrical layers of sense wires, which are grouped into 8 alternating axial and stereo superlayers. The solenoid is surrounded by sampling calorimeters used to measure the electromagnetic and hadronic energy of jets and electrons. The calorimeters cover the pseudorapidity range $|\eta| \leq 4.2$. The calorimeters are segmented in η - ϕ towers pointing to the nominal interaction point. There are three separate η -regions of calorimeters. Each region has an electromagnetic calorimeter [central (CEM), plug (PEM), and forward (FEM)] and behind it a hadron calorimeter [CHA, PHA, and FHA, respectively]. Located six radiation lengths inside the CEM calorimeter, proportional wire chambers (CES) provide shower-position measurements in the z and r - ϕ view. Proportional chambers (CPR) located between the solenoid and the CEM detect early development of electromagnetic showers in the solenoid coil. These chambers provide r - ϕ information only.

The calorimeter acts as a hadron absorber for the central muon detection system (CMU). The CMU consists of four layers of drift chambers located outside the CHA calorimeter. The CMU system covers the pseudorapidity $|\eta| \leq 0.6$ and can be reached by muons with $p_T \geq 1.4 \text{ GeV}/c$. The CMU system is followed by 0.6 m of steel and four additional layers of drift chambers (CMP). The system of drift chambers CMX extends the muon detection to $|\eta| \leq 1.0$.

III. DATA COLLECTION AND IDENTIFICATION OF HIGH p_T LEPTONS AND JETS

The last collider run, called run I, lasted from August of 1992 till July of 1993 (run 1A) and from January of 1994 till July of 1995 (run 1B). The data collected during this run correspond to an integrated luminosity of $105.1 \pm 4.0 \text{ pb}^{-1}$ when using the total $p\bar{p}$ cross section value $80.03 \pm 2.24 \text{ mb}$ [12]. We begin this section with a description of the triggers used in this analysis. This is followed by subsections on the reconstruction and identification of electrons, muons, jets and neutrinos.

A. Triggers

A three-level trigger system is used to select events originating from $p\bar{p}$ interactions and containing electrons, muons, jets, or missing transverse energy (E_T).

The first-level trigger (L1) accepts events based on the identification of energy clusters in the calorimeter or track segments in the muon chambers. The L1 calorimeter trigger

requires a single CEM or CHA trigger tower with transverse energy greater than 8 or 12 GeV, respectively (these thresholds were set at 6 and 8 GeV during run 1A). The L1 muon trigger infers the track momentum from the deflection of the track segment in the muon chambers due to the magnetic field; it requires a minimum transverse momentum of 6 and 10 GeV/ c in the CMU and CMX chambers, respectively. A minimum energy of 300 MeV is required in the hadron calorimeter tower associated with the track segment.

The second-level trigger (L2) uses the calorimetry information with greater sophistication. The L2 trigger is a fast-bus based processor [13] with a decision time of approximately 20 μ s. It combines calorimetry towers forming electromagnetic and jet-like clusters. An electromagnetic cluster is constructed as a set of contiguous CEM (PEM) towers each with $E_T \geq 7$ GeV (4 GeV), including at least one seed tower with $E_T \geq 8$ GeV (6 GeV).

The L2 jet clusters are formed starting with a seed tower with $E_T \geq 3$ GeV and summing all contiguous towers with $E_T \geq 1$ GeV. A crude estimate of \cancel{E}_T is also available at this trigger level. The L2 trigger utilizes the list of r - ϕ tracks provided by the central fast tracker (CFT), a hardware processor which uses fast timing information from the CTC as input. The events used in this analysis were collected using the L2 high- p_T electron trigger, which requires an electromagnetic cluster of transverse energy greater than 16 GeV matched by a CFT track with transverse momentum $p_T \geq 12$ GeV/ c . A second trigger requires an electromagnetic cluster of $E_T \geq 16$ GeV and $\cancel{E}_T \geq 20$ GeV and is used to recover losses due to the CFT inefficiency. The L2 high- p_T muon trigger requires a CFT track with $p_T \geq 12$ GeV/ c pointing within 5° to a L1 track segment in the muon detectors. To ensure good efficiency, additional L2 muon triggers require only a L1 track segment accompanied by at least one jet cluster with $E_T \geq 15$ GeV or $\cancel{E}_T \geq 35$ GeV.

The L3 trigger decision is made after the full event reconstruction. Events accepted by the L2 trigger are processed by a farm of SGI processors running the full off-line reconstruction package. The level 3 electron trigger requires a CEM cluster with $E_T \geq 18$ GeV and a reconstructed track with $p_T \geq 13$ GeV/ c pointing to it. The ratio of hadronic to electromagnetic energy in the cluster is required to be less than 0.125. The level 3 muon trigger requires a match within 10 cm in the r - ϕ plane between a reconstructed track with $p_T > 18$ GeV/ c extrapolated to the radius of the muon detectors and a track segment in the muon chambers.

Trigger efficiencies have been measured directly using events with overlapping triggers. The electron trigger efficiency is found to be larger than 99.6% for electrons inside the detector fiducial volume. Likewise, the muon trigger efficiency is $(70 \pm 2)\%$; this includes an inefficiency due to the fact that the muon trigger does not cover the entire detector fiducial volume. The measured trigger efficiencies have been included in the detector simulation described in Sec. VII. A check of the muon trigger simulation was performed by comparing the rate of $W \rightarrow \mu\nu$ events in the data to that of a simulation of this process using the HERWIG generator (see Sec. VI) normalized to the same number of $W \rightarrow e\nu$ events. We observe agreement between data and simulation within

TABLE I. Selection requirements for primary electrons.

Variable	Cut
E/P	≤ 1.5
$E_{\text{had}}/E_{\text{em}}$	≤ 0.05
L_{shr}	≤ 0.2
$ \Delta x $	≤ 1.5 cm
$ \Delta z $	≤ 3.0 cm
χ^2_{strip}	≤ 10.0
$ z_{\text{ver}} $	≤ 60.0 cm
z -vertex match	≤ 5.0 cm
I	≤ 0.1

10%, and this difference is taken as the systematic error on the muon trigger simulation.

B. Electron reconstruction

The W +jet sample is selected requiring electrons reconstructed in the central pseudorapidity region $|\eta| \leq 1$. Stricter cuts, described in detail in Ref. [5], are applied to central electron candidates which passed the trigger prerequisites. The following variables are used to discriminate against charged hadrons: (1) the ratio of hadronic to electromagnetic energy of the cluster, $E_{\text{had}}/E_{\text{em}}$; (2) the ratio of cluster energy to track momentum, E/P ; (3) a comparison of the lateral shower profile in the calorimeter cluster with that of test-beam electrons, L_{shr} ; (4) the distance between the extrapolated track-position and the CES measurement in the r - ϕ and z views, Δx and Δz ; (5) a χ^2 comparison of the CES shower profile with those of test-beam electrons, χ^2_{strip} ; (6) the interaction vertex position, z_{ver} and the distance between the interaction vertex and the reconstructed track in the z -direction, z -vertex match; and (7) the isolation, I , defined as the ratio of the additional transverse energy in a cone of radius $R=0.4$ around the cluster axis to the transverse energy of the electron cluster. The electron selection criteria are listed in Table I.

Fiducial cuts on the electromagnetic shower position, as measured in the CES, are applied to insure that the electron candidate is away from the calorimeter boundaries and the energy is well measured.

Electrons from photon conversions are removed using an algorithm based on tracking information. Electron tracks close to a companion track with opposite charge are considered conversion candidates. The following variables are used to identify and remove photon conversions: (1) the difference of the polar angles, $\delta \cot \theta$; (2) the distance between the two tracks in the r - ϕ plane at the radius R_{conv} where the tracks are parallel, Δ_{sep} ; and (3) the conversion radial position, R_{conv} . If a companion track is not found, we identify conversion candidates using f_{VTX} which is the ratio of the measured to expected number of VTX hits associated to the electron candidate. Table II summarizes the criteria used to identify and remove electrons from photon conversions. The efficiency of the conversion algorithm is measured with a sample of photon conversions selected using the CPR detector. The efficiency of the conversion removal algorithm is

TABLE II. Criteria used to identify electrons from photon conversions.

Variable	Cut
$ \Delta_{\text{sep}} $	≤ 0.3 cm
$ \delta \cot \theta $	≤ 0.06
R_{conv}	-20 cm \leq and ≤ 50 cm
f_{VTX}	$\leq 20\%$

(90.7 ± 3.8)%. The fraction of electrons erroneously removed is estimated using a sample of $Z \rightarrow e^+e^-$ events to be (2.2 ± 0.6)% and is properly accounted for by the simulation.

The total primary electron identification efficiency has been measured using a sample of $Z \rightarrow e^+e^-$ decays and is listed in Table III.

When an electron candidate is found, the calorimeter towers belonging to the electron cluster are not used by the jet clustering algorithm.

C. Muon reconstruction

Muons are identified in the $|\eta| \leq 1.0$ region by extrapolating CTC tracks to the muon detectors and matching them to track segments reconstructed in the muon chambers. The following variables, described in detail in Ref. [5], are used to separate muon candidates from cosmic rays and from hadrons not contained by the calorimeter: (1) an energy deposition in the electromagnetic and hadronic calorimeter characteristic of minimum ionizing particles, E_{em} and E_{had} ; (2) the distance of closest approach of the reconstructed track to the beam line, d ; (3) the z -vertex match; (4) the matching distance between the extrapolated track and the track segment in the muon chamber, $\Delta x = r\Delta\phi$; and (5) the isolation I , the ratio of additional transverse energy in a cone of radius $R = 0.4$ around the track direction to the muon transverse momentum.

The muon selection criteria are listed in Table IV. The muon identification efficiency has been measured using a sample of $Z \rightarrow \mu^+\mu^-$ decays and is listed in Table III.

Leptons passing the requirements listed in Tables I and IV are labeled primary leptons. As a consequence of the high luminosity of the collider, approximately 50% of the events with a primary lepton contain multiple interactions which result in more than one primary vertex in the event. The ambiguity is resolved by selecting the vertex associated with the primary lepton track to evaluate jet pseudorapidities and the missing transverse energy.

TABLE III. Lepton identification efficiencies, including the isolation requirement, measured using a sample of $Z \rightarrow ll$ events collected during run 1B. In run 1A the muon efficiency is (7.8 ± 2.8)% lower.

Lepton type	Efficiency
Electrons	0.81 ± 0.02
Muons	0.93 ± 0.03

TABLE IV. Selection requirements for primary muons.

Variable	Cut
E_{em}	≤ 2 GeV
E_{had}	≤ 6 GeV
$E_{\text{em}} + E_{\text{had}}$	≥ 0.1 GeV
$ d $	≤ 0.3 cm
$ \Delta x $	≤ 2.0 cm (CMU) ≤ 5.0 cm (CMP, CMX)
$ z_{\text{ver}} $	≤ 60.0 cm
z -vertex match	≤ 5.0 cm
I	≤ 0.1

D. Jet reconstruction

The CDF jet reconstruction algorithm uses a cone of fixed radius in the η - ϕ space. In this analysis we use a cone of radius 0.4 which has been shown to contain approximately 70% of the jet energy [14]. A detailed description of the jet reconstruction algorithm can be found in Ref. [14].

The jet energy resolution can be parametrized as $\sigma(E_T)/E_T \approx 1/\sqrt{E_T}$, where E_T is measured in GeV. Effects which contribute to the resolution are the lower calorimeter response at the boundaries of different towers and of different calorimeter detectors, the loss of low momentum particles inside the magnetic field, the energy deposition in towers outside the clustering cone, the contribution of the underlying-event and energy losses due to minimum ionizing particles or neutrinos present in the jet. Corrections meant to reproduce the average jet E_T correctly (without improving the energy resolution) are often used [14,15]. The average jet energy correction factor ranges from approximately 1.7 to 1.1 as the jet transverse energy increases from 15 to 100 GeV.

Checks of the jet energy corrections have been performed in Ref. [5] by studying the momentum balance in γ +jet and Z +jet events. The energy imbalance is measured to be within 3% of the Z or photon energy. However, the uncertainty in the modeling of the large-angle gluon emission results in a 10% systematic uncertainty of the jet energy scale.

E. \cancel{E}_T and neutrino reconstruction

The presence of neutrinos is inferred from transverse energy imbalance in the detector. The transverse missing energy is defined as

$$\cancel{E}_T = - \left| \sum_i E_T^i \vec{n}_i \right|$$

where E_T^i is the magnitude of the transverse energy contained in each calorimeter tower i in the pseudorapidity region $|\eta| < 3.5$ and \vec{n}_i is the direction of the tower in the plane transverse to the beam direction. When a muon is present in the event, \cancel{E}_T is calculated as

$$\vec{E}_T = - \left| \sum_i E_T^i \vec{n}_i + \vec{p}_T^\mu \left(1 - \frac{E_T^\mu}{p_T^\mu} \right) \right|$$

where E_T^μ is the transverse energy deposited by the muon in the calorimeter and p_T^μ is the muon transverse momentum.

IV. SELECTION OF THE WZ +JET SAMPLES

The W +jet sample, which contains the $t\bar{t}$ signal, is selected from the high- p_T inclusive lepton data set by requiring at least one primary electron with $E_T \geq 20$ GeV or one primary muon with $p_T \geq 20$ GeV/ c , $\vec{E}_T \geq 20$ GeV and at least one jet with uncorrected transverse energy $E_T \geq 15$ GeV and pseudorapidity $|\eta| \leq 2$. An appreciable fraction of these events is due to Z +jet production. Some Z events can be identified and removed when the second lepton from the Z decay falls into the detector acceptance. Because W +jet and Z +jet events have similar production mechanisms, we will use the Z +jet sample to check our evaluation of the backgrounds to $t\bar{t}$ production. It is also interesting to study this sample because events in which one of the two leptons is not identified (unidentified Z 's) are a background to $t\bar{t}$ production. The following subsection explains the removal of dilepton events. The events surviving dilepton removal constitute the W +jet sample which is described in the last subsection.

A. Selection of the Z +jet sample

Z candidates are selected from the high- p_T lepton data set by requiring a primary lepton with $E_T \geq 20$ GeV and by searching for a second lepton with the same flavor and opposite charge which satisfies the criteria listed in Table V.

Searching for additional electrons we relax the isolation and $E_{\text{had}}/E_{\text{em}}$ cuts. We also search in the PEM and FEM detectors. Additional muons are searched for by relaxing all selection cuts defining primary muons. As shown in Table V, CTC tracks without a match to a track segment in the muon chambers but pointing to a calorimeter tower with a small energy deposition are also considered muon candidates.

Events are flagged as Z candidates if the invariant mass of the lepton pair falls in the range $70 \leq M_{ll} \leq 110$ GeV/ c^2 (see Fig. 1). The number of Z candidate events as a function of the jet multiplicity is shown in Table VI.

B. Dilepton removal

All events containing a primary lepton and at least one additional lepton selected using the criteria listed in Table V are removed from the W +jet sample. These events arise from $Z \rightarrow \tau^- \tau^+$, di-boson, Drell-Yan, and $t\bar{t}$ production. The $t\bar{t}$ production cross section using dilepton events has been measured in Ref. [16] and we want to avoid obvious correlations.

We also remove events containing an isolated track with $p_T \geq 10$ GeV/ c with charge opposite to the primary lepton [17]. The majority of these events originates from genuine dilepton events in which one lepton is outside the region covered by the calorimeters or the muon detectors.

TABLE V. Selection requirements for loose leptons.

Variable	Cut
Electrons	
$ \eta $	≤ 4.2
E_T	≥ 10 GeV
$E_{\text{had}}/E_{\text{em}}$	≤ 0.12
I	≤ 0.15
Muons with a track segment in the muon chambers	
p_T	≥ 10 GeV/ c
$ d $	≤ 0.5 cm
z -vertex match	≤ 10 cm
$ \Delta x $	≤ 10 cm
E_{em}	≤ 5 GeV
E_{had}	≤ 10 GeV
I	≤ 0.15
Muons without a track segment in the muon chambers	
p_T	≥ 10 GeV/ c
$ d $	≤ 0.5 cm
z -vertex match	≤ 10 cm
$E_{\text{em}} + E_{\text{had}}$	≤ 10 GeV
	$(E_{\text{em}} \leq 2 \text{ or } E_{\text{had}} \leq 6 \text{ GeV})$
I	≤ 0.15

Finally, to remove dileptons missed due to inefficiencies of the tracking system, we remove events in which a jet with $E_T \geq 15$ GeV and $|\eta| \leq 2$ has a large electromagnetic fraction ($E_{\text{em}}/E_{\text{em}+\text{had}} \geq 0.95$) and less than three tracks. These types of events are mostly produced by $Z \rightarrow e^+ e^-$ decays.

The dilepton removal reduces the acceptance for $t\bar{t}$ events by 17.2%.

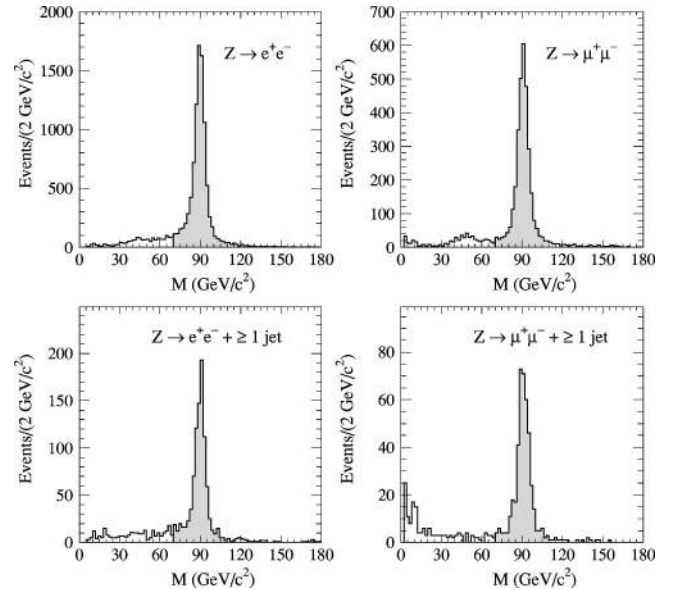


FIG. 1. Invariant mass distributions of electron and muon pairs before and after requiring the presence of at least one jet with $E_T \geq 15$ GeV and $|\eta| \leq 2$. The shaded area indicates the mass window used to select Z candidate events.

TABLE VI. Number of Z candidate events as a function of the observed jet multiplicity.

Jet multiplicity	$Z \rightarrow e^+ e^-$	$Z \rightarrow \mu^+ \mu^-$	Total
1 jet	791	357	1148
2 jets	107	52	159
3 jets	9	7	16
≥ 4 jets	3	1	4

C. The W +jet sample

The number of W events surviving the Z and dilepton removal is listed in Table VII as a function of the jet multiplicity. The transverse mass distribution of the W candidates is shown in Fig. 2.

V. ADDITIONAL DATA SAMPLES

In addition to the Z +jet sample, we use a number of independent data sets for the purpose of calibrating the Monte Carlo generators and the detector simulation. The generic-jet samples are described in subsection A. We will use these samples to derive the new parametrization of the mistag rate, to check our evaluation of the efficiency of the tagging algorithms, and to calibrate the calculation of the fraction of W +jet events with heavy flavor. Subsection B describes the low- p_T inclusive lepton sample which will be used to determine the efficiency of the tagging algorithms. Finally, subsection C details the selection of the isolated photon sample. We will use this sample to check the parametrization of the mistag rate of the tagging algorithms.

A. Generic-jet samples

The samples JET 20, JET 50, JET 70, and JET 100 are data collected requiring the presence of a L2 calorimeter cluster with transverse energy $E_T \geq 20, 50, 70,$ and 100 GeV, respectively.

The samples $\Sigma E_T 175$ and $\Sigma E_T 300$ are data collected requiring the scalar sum of the transverse energy of all calorimeter towers, as evaluated by the L2 trigger, to be larger than 175 and 300 GeV, respectively.

The last generic-jet sample, $\Sigma E_T 125$ 4 CL was collected requiring the presence of four L2 calorimeter clusters with $E_T \geq 15$ GeV and the scalar sum of the transverse energy of all calorimeter towers to be larger than 125 GeV.

The L2 triggers calculate the above quantities with respect to the nominal interaction point. Offline we take as event

TABLE VII. Number of W candidate events as a function of the observed jet multiplicity.

Jet multiplicity	$W \rightarrow e \nu$	$W \rightarrow \mu \nu$	Total
1 jet	5472	3982	9454
2 jets	744	626	1370
3 jets	111	84	198
≥ 4 jets	26	28	54

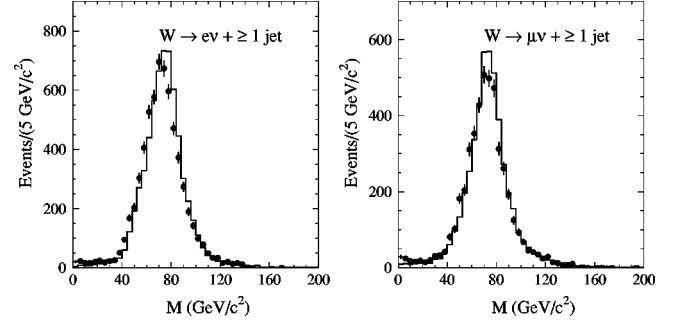


FIG. 2. Distribution of the transverse mass M of W candidates in the data (\bullet) and in a simulation using the HERWIG generator (solid histogram). We utilize measured quantities without the full set of corrections used to determine the W mass.

vertex the one with the largest $\sum_i p_T^i$ using all tracks i associated with the vertex. We retain the events in which the L2 requirements are also matched after the event is reconstructed using this vertex. In these events, we inspect all jets with $E_T \geq 15$ GeV and which contain at least two SVX tracks (taggable jets).

B. The low- p_T inclusive lepton sample

The efficiency of the b -tagging algorithms needs to be measured in a sample enriched in $b\bar{b}$ production. The low- p_T electron sample is collected with the L2 requirement that a CFT track with $p_T \geq 7.5$ GeV/ c is matched by an electromagnetic L2 cluster with $E_T \geq 8$ GeV. The fraction of electrons coming from semileptonic b -decays is enhanced with the selection criteria listed in Table VIII. We use electrons in the CEM fiducial region and remove photon conversion candidates. We require the lepton to be in a cone of radius 0.4 around the direction of a taggable jet. We require also the presence of at least one additional taggable jet. The b -purity of this sample is approximately 50%.

We check the results obtained using the low- p_T electron sample using a lower statistics low- p_T muon sample collected using the inclusive muon trigger. In this case, a CFT track with $p_T \geq 7.5$ GeV/ c must be matched to a reconstructed track-segment in both sets of the central muon detectors (CMU+CMU). Central muons which passed the trig-

TABLE VIII. Criteria used to select the low p_T inclusive electrons.

Variable	Cut
E_T	≥ 10 GeV
E/P	≤ 1.5
$E_{\text{had}}/E_{\text{em}}$	≤ 0.05
L_{shr}	≤ 0.2
$ \Delta x $	≤ 1.5 cm
$ \Delta z $	≤ 3.0 cm
χ_{strip}^2	≤ 10
z -vertex match	≤ 5.0 cm
I	≥ 0.1

TABLE IX. Criteria used to select isolated photons.

Variable	cut value
E_T	≥ 23 GeV
$ \eta $	≤ 1.0
$E_{\text{had}}/E_{\text{em}}$	$\leq 0.055 + 0.00045 \times E_T$
Transverse energy deposited in a cone of radius 0.7 around the γ	≤ 2 GeV
CTC tracks pointing to the γ cluster	None
χ_{strip}^2	≤ 20

ger prerequisite are selected with the same criteria used for the high- p_T muons listed in Table V (we require $I \geq 0.1$).

C. The isolated photon sample

The isolated photon sample was collected requiring a L2 isolated electromagnetic cluster with $E_T \geq 16$ GeV and with less than 5 GeV of additional energy in a 5×10 grid of calorimeter towers centered on the photon direction [18]. Photon candidates which pass the L3 trigger must be in the good fiducial region of the calorimeter and there must be less than 2 GeV in a cone of radius 0.7 around the photon direction. Table IX summarizes the offline criteria used for the selection of the photon sample. After requiring the presence of an additional jet with $E_T \geq 15$ GeV and $|\eta| \leq 2$, the final sample consists of 3000 $\gamma + \geq 1$ jet events. The expected background contamination of the sample due to π^0 and η decays is estimated to be $(45.0 \pm 4.5)\%$ [18,19].

VI. MONTE CARLO GENERATORS

In this analysis we use three Monte Carlo generators, HERWIG [7], PYTHIA [8], and VECBOS [20]. The acceptance for $t\bar{t}$ events is calculated using PYTHIA version 5.7. The $t\bar{t}$ acceptance has been also evaluated using the version 5.6 of PYTHIA and HERWIG 5.6. The HERWIG simulation, calibrated using generic-jet data as described in Sec. XI, is also used to estimate the fraction of $W + \geq 1$ jet events with heavy flavor.¹

Both HERWIG and PYTHIA generators use tree-level matrix element calculations for the parton hard scattering, convoluted with parametrizations of the parton distribution functions. The outgoing initial and final state partons are converted into a cascade of gluons and $q\bar{q}$ pairs with energy and angular distributions determined by the Altarelli-Parisi equations [21]. The strength of these generators is the modeling of the parton shower which accounts for the color correlation between the initial and final state partons. The parton shower terminates when the invariant mass of the parton falls below the perturbative QCD scale. At this level the partons are turned into colorless hadrons according to phenomenological models (the process is called hadronization or fragmenta-

tion). For b and c -quarks the fragmentation is modeled in PYTHIA with the Peterson parametrization [22]. We use the fragmentation parameter $\epsilon = 0.006$ for b -quarks and $\epsilon = 0.05$ for c -quarks. HERWIG uses its own hadronization model, the settings for which are listed in Ref. [23]. Both generators include a model of the underlying event which describes the hadronization products of the beam remnants.

The VECBOS Monte Carlo program is used to study the part of the phase-space in the $W + \geq 1$ jet production that is not treated correctly by parton shower Monte Carlos, specifically $Wb\bar{b}$ and $Wc\bar{c}$ events in which the two b or c -partons produce two well separated jets. The VECBOS Monte Carlo generator provides a parton level calculation of the $W + n$ jet cross section based on the leading order matrix elements of the hard scattering. Infrared and collinear singularities are regulated by requiring that the final-state partons have a transverse momentum exceeding a cutoff value p_T^{min} and are separated by more than R_{min} [$R = \sqrt{(\Delta\phi)^2 + (\Delta\eta)^2}$]. We use $p_T^{\text{min}} = 8$ GeV/ c and $R_{\text{min}} = 0.4$. We use the renormalization scale $Q^2 = \langle p_T \rangle^2$, where $\langle p_T \rangle$ is the average transverse momentum of the outgoing partons. We have verified that after our selection cuts the fraction of jets with heavy flavor calculated with HERWIG matches the VECBOS prediction at the R_{min} threshold. We transform the partons produced by VECBOS into hadrons and jets using the HERWIG program adapted to perform the coherent shower evolution of both initial and final-state partons [24].

In summary, we use HERWIG to predict the fraction of $W + \geq 1$ jet events in which only one jet clustered in a cone of radius 0.4 contains b or c -hadrons while we rely on VECBOS to extend the prediction to the cases in which two different jets both contain heavy-flavored hadrons.

We use the Martin-Roberts-Stirling set D'_0 (MRS D'_0) of parton distribution functions [25] to generate $W + \text{jet}$ events because it has been shown to reproduce the results of the W asymmetry measured by CDF [26].

The decay of hadrons with heavy flavor produced by the Monte Carlo generators is modeled using the CLEO Monte Carlo generator (QQ) [9]. We use the QQ table of branching ratios for each decay but our own lifetime table because decay lengths are modeled inside the detector simulation.

VII. DETECTOR SIMULATION

The QFL detector simulation is used to decay all generated particles and model their interactions with the various elements of the CDF detector. The detector response is based upon parametrizations and simple models which depend on the particle kinematics. The calorimeter simulation is based upon a parametrization of the calorimeter response to single particles parametrized as a function of the pseudorapidity and azimuthal angle (to account for cracks in the calorimetry) and of the transverse momentum using test-beam data. After the simulation of the CDF detector, the Monte Carlo events are treated as if they were real data.

A. CTC track simulation

The CTC simulation is not a hit-level simulation. It converts each particle's momentum vector at generator level into

¹We use the process 2100.

TABLE X. Track reconstruction efficiency for charged particles in the detector simulation (QFL) and for Monte Carlo tracks embedded in generic-jet data acquired in low luminosity running. The effect of the average luminosity of the data is shown separately.

	CTC track	SVX track	Luminosity effect
Embedded-track	0.94 ± 0.02	0.87 ± 0.03	0.95 ± 0.02
QFL simulation	0.993	0.983	1

a reconstructed track using covariance matrices derived from the data. Not surprisingly, the track-reconstruction efficiency in the detector simulations is higher than that measured in the data. The major factor influencing the track reconstruction efficiency is the density of hits in the tracking detector. In this respect, the problem is aggravated by the fact that the Monte Carlo generators do not contain multiple interactions.

To adjust the tracking reconstruction efficiency in the simulation, CTC hits of Monte Carlo generated tracks have been embedded in generic-jet data. The efficiency is determined by the fraction of embedded tracks which are reconstructed. The tracking efficiency is measured as a function of the hit density around the track for low luminosity runs (instantaneous luminosity $\mathcal{L}_I \leq 10^{29} \text{ cm}^{-2} \text{ s}^{-1}$), and then for runs of typical luminosities ($\mathcal{L}_I \approx 8 \times 10^{30} \text{ cm}^{-2} \text{ s}^{-1}$). Table X compares the track reconstruction efficiency in the detector simulation to the efficiency for reconstructing simulated tracks embedded in the data. The degradation of the track reconstruction efficiency is parametrized in the detector simulation as a function of the number of hits around the tracks and of the average luminosity of the data. This procedure accounts well for the dependence of the tracking efficiency on the jet transverse energy.

B. Lepton identification efficiencies

Aside from the efficiency for reconstructing a track, the primary lepton identification efficiency in the simulation depends also on how well the Monte Carlo simulation models the isolation distribution and how well the calorimeter response has been parametrized. In the simulation, the primary lepton identification efficiencies are measured as the ratio of the number of leptons passing the selection cuts listed in Tables I and IV to the number of leptons generated in the kinematical acceptance. The identification efficiencies in the simulation are $(97 \pm 2)\%$ for muons and $(87.5 \pm 2.0)\%$ for electrons. The identification efficiencies for primary leptons are degraded in the detector simulation to match the ones measured in the data (see Table III). Altogether, we degrade the rates of simulated primary leptons by the factor of 0.936 ± 0.125 (the error includes a 10% uncertainty on the muon trigger simulation).

The efficiency for identifying soft lepton tags is a far more complicated problem because some detector responses, such as dE/dx in the CTC and the CPR chambers, have not been parametrized in the detector simulation. The SLT simulation weights tracks corresponding to leptons from b and c -quark decays at generator level with a parametrization of the efficiency of each selection cut measured using the data, as described in Sec. VIII C.

C. SVX track simulation

The detector simulation becomes unwieldy when simulating tracks that are measured by both the CTC and SVX tracking detectors as is the case for input tracks to the SECVTX and jet-probability algorithms. The SVX track reconstruction is performed by assigning hits on the silicon vertex detector to previously reconstructed CTC tracks. In the data hits are assigned if they are contained in a road around the reconstructed CTC track determined by its uncertainty (4σ in the r - ϕ plane). A CTC track with at least two associated SVX hits is defined to be a SVX track and is refitted using the SVX hits and the CTC track parameters and covariance matrix. The simulation of the SVX is a hit-level simulation in which the hit resolution is taken from the data. Simulated SVX tracks are reconstructed as in the data. However, in the data we must multiply all the elements of the covariance matrix by a factor of two so that the CTC-SVX matching uncertainty agrees with the measured resolution [27] while there is no such need in the simulation.

The efficiency for finding SVX tracks in the detector simulation also needs to be degraded, by a factor determined by measuring the efficiency for reconstructing Monte Carlo generated tracks embedded at hit-level in generic-jet data (see Table X).

Having done this, the simulation is still not a perfect reflection of the data. For example, as shown in Sec. VIII B, the distribution of the impact parameter significance of SVX tracks in the data and in the detector simulation are slightly different. We conclude that it is necessary to measure the tagging efficiencies of each algorithm in the data and in the simulation and correct the detector simulation for any observed difference. This is done in Sec. IX.

VIII. DESCRIPTION OF THE TAGGING ALGORITHMS

The presence of jets originating from b quarks is one of the characteristic signatures of $t\bar{t}$ events. Following previous work [2,5], we tag b -quarks using two of their distinctive properties: the relatively long lifetime and the presence of semileptonic decays. Two tagging techniques based on tracking information using the SVX detector have been developed to identify jets containing heavy flavor. The secondary vertex tagging algorithm (SECVTX) is described in subsection A. The jet-probability algorithm, used to check SECVTX results, is described in subsection B. The soft lepton tagging algorithm (SLT) is discussed in subsection C, which also includes the evaluation of the SLT fake rate and a description of the simulation of this algorithm.

A. SECVTX algorithm

The SECVTX algorithm is described in more detail in Refs. [3,5]. SECVTX is based on the determination of the primary event vertex and the reconstruction of additional secondary vertices using displaced tracks associated with jets.

The positions of the $p\bar{p}$ interactions (primary vertices) are distributed along the beam direction according to a Gaussian with a width of approximately 28 cm. In the plane transverse

TABLE XI. Selection criteria for CTC and SVX tracks used in the SECVTX b -tagging algorithm. A good SVX hit is defined as a hit in the SVX linked to only one CTC track.

Variable	Cut
CTC track selection criteria	
No. of axial superlayers	≥ 2
No. of hits in each axial superlayer	≥ 2
No. of stereo superlayers	≥ 2
No. of hits in each stereo superlayer	≥ 2
χ^2/DOF of the track fit	≤ 6
z -vertex match	≤ 5 cm
SVX track selection criteria—Pass 1	
if $N_{\text{SVX-hits}} \geq 3$	$\begin{cases} N_{\text{SVX-hits}}^{\text{Good}} & \geq 1 \\ p_T & \geq 0.5 \text{ GeV}/c \end{cases}$
if $N_{\text{SVX-hits}} = 2$	$\begin{cases} N_{\text{SVX-hits}}^{\text{Good}} & \geq 2 \\ p_T & \geq 1.5 \text{ GeV}/c \end{cases}$
$ d $	≤ 0.1 cm
$ d /\sigma_d$	≥ 2.5
SVX track selection criteria—Pass 2	
if $N_{\text{SVX-hits}} = 4$	$\begin{cases} N_{\text{SVX-hits}}^{\text{Good}} & \geq 1 \\ p_T & \geq 1.0 \text{ GeV}/c \end{cases}$
if $N_{\text{SVX-hits}} = 3$	$\begin{cases} N_{\text{SVX-hits}}^{\text{Good}} & \geq 2 \\ p_T & \geq 1.0 \text{ GeV}/c \end{cases}$
$ d $	≤ 0.1 cm
$ d /\sigma_d$	≥ 3.0

to the beam axis, these interactions follow a distribution that is a Gaussian with a width of 25 μm in both the x and y dimensions. To reconstruct the primary event vertex, we first identify its z -position using the tracks reconstructed in the VTX detector. When projected back to the beam axis, these tracks determine the longitudinal position with a precision of about 0.2 cm.

The transverse position of the primary vertex is determined for each event by a weighted fit of all SVX tracks which have a z coordinate within 5 cm from the z position of the primary vertex associated with the trigger lepton. First, all tracks are constrained to originate from a common vertex. The position of this vertex is constrained by the transverse beam envelope described above. Tracks that have impact parameter significance $|d|/\sigma_d$, where σ_d is the estimate of the uncertainty on the impact parameter d , larger than three with respect to this vertex are removed and the fit is repeated. This procedure is iterated until all used tracks satisfy the impact parameter requirement. At least five tracks must be used in the determination of the transverse position of the primary vertex or we use the nominal beam-line position. The primary vertex coordinates transverse to the beam direction have uncertainties in the range of 10–25 μm , depending on the number of tracks and the event topology.

The search for a secondary vertex in a jet is a two stage process. In both stages, tracks in the jet are selected based on the significance of their impact parameter with respect to the primary vertex. The first stage (see Table XI) requires at least

three candidate tracks for the reconstruction of the secondary vertex. Tracks consistent with coming from the decay $K_s \rightarrow \pi^+ \pi^-$ or $\Lambda \rightarrow \pi^- p$ are not used as candidate tracks. Two candidate tracks are constrained to pass through the same space point to form a seed vertex. If at least one additional candidate track is consistent with intersecting this seed vertex, then the seed vertex is used as the secondary vertex. If the first stage is not successful in finding a secondary vertex, a second pass is attempted. More stringent track requirements (on $|d|/\sigma_d$ and p_T , for example) are imposed on the candidate tracks. All candidate tracks satisfying these stricter criteria are constrained to pass through the same space point to form a seed vertex. This vertex has an associated χ^2 . Candidate tracks that contribute too much to the χ^2 are removed and a new seed vertex is formed. This procedure is iterated until a seed vertex remains that has at least two associated tracks and an acceptable value of χ^2 . Table XI lists the selection criteria used for the determination of the secondary vertex candidates.

The decay length of the secondary vertex L_{xy} is the projection of the two-dimensional vector pointing from the primary vertex to the secondary vertex on the jet axis; if the cosine of the angle between these two vectors is positive (negative), then L_{xy} is positive (negative). Most of the secondary vertices from the decay of b and c -hadrons are expected to have positive L_{xy} . Secondary vertices from random combination of mismeasured tracks are expected to

TABLE XII. Selection criteria for tracks used by the jet-probability algorithm.

Variable	Cut
SVX track selection criteria	
$ d $	≤ 0.15 cm
p_T	≥ 1.5 GeV/ c
$N_{\text{SVX-hits}}$	≥ 2

have a symmetric distribution around $L_{xy}=0$ [28]. To reduce the background from false secondary vertices (mistags), a jet is considered tagged by SECVTX if it contains a secondary vertex with $L_{xy}/\sigma_{L_{xy}} \geq 3.0$, where $\sigma_{L_{xy}}$ is the estimated uncertainty on L_{xy} (~ 130 μm). The mistag contribution to positive SECVTX tags is evaluated starting from the rate of negative SECVTX tags and detailed in Sec. X.

B. Jet-probability algorithm

The jet-probability tagging algorithm [6] is used to cross-check the SECVTX results. The jet-probability algorithm compares track impact parameters to measured resolution functions in order to calculate for each jet a probability that there are no long lived particles in the jet cone. This probability is uniformly distributed between 0 and 1 for light quark or gluon jets, but is very small for jets containing displaced vertices from heavy flavor decays. We briefly describe the transformation from the track impact parameters to the jet-probability measure.

The track impact parameter significance S is defined as the value of the impact parameter d divided by its uncertainty σ_d . Tracks used in the calculation of jet-probability are required to satisfy the quality criteria listed in Table XII. The sign of the impact parameter significance is defined to be positive if the point of closest approach to the primary vertex lies in the same hemisphere as the jet direction, and negative otherwise. Figure 3 shows the distribution of the impact parameter significance of tracks in the JET 50 sample. This distribution is fitted with the resolution function $\mathcal{R}(S)$.

The negative side of the resolution function $\mathcal{R}(S)$ derived using JET 50 data is used to determine the probability $P(S_0)$ that the impact parameter significance S_0 of a given track is due to the detector resolution:

$$P(S_0) = \frac{\int_{-\infty}^{-|S_0|} \mathcal{R}(S) dS}{\int_{-\infty}^0 \mathcal{R}(S) dS}.$$

Figure 4 shows that the impact parameter significance distribution of tracks in the JET 50 data and in the corresponding simulation are slightly different. The resolution functions $\mathcal{R}(S)$ are therefore defined separately for the data and the simulation in order to account for the differences in the resolution between the true and the simulated detector performance.

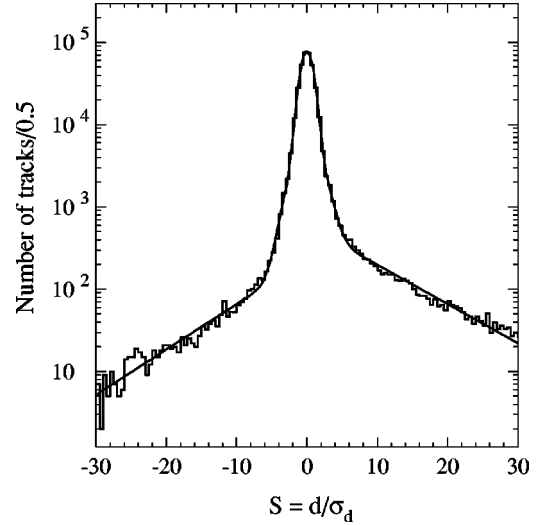


FIG. 3. Distribution of the signed impact parameter significance of tracks in the JET 50 sample. The resolution function $\mathcal{R}(S)$ is the result of a fit using two Gaussians plus an exponential function, separately for the positive and negative sides.

The probability that a jet is consistent with a zero lifetime hypothesis is defined as

$$\prod \sum_{k=0}^{N-1} \frac{(-\ln \Pi)^k}{k!}$$

where Π is the product of the individual probabilities $P(S_0)$ of the N SVX tracks in a jet which satisfy the criteria listed in Table XII. Jet-probability is defined using tracks with positive impact parameter and requiring $N \geq 2$. We also define a negative jet-probability in which we select only tracks with negative impact parameter in the calculation. This is used as a control sample and a check of our method.

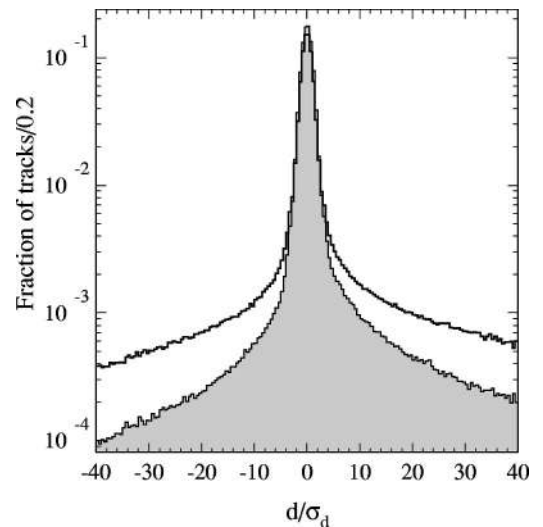


FIG. 4. Distribution of the impact parameter significance d/σ_d of tracks in the JET 50 data (histogram) and the corresponding HERWIG simulation (shaded histogram). The tracks are required to satisfy the criteria listed in Table XII.

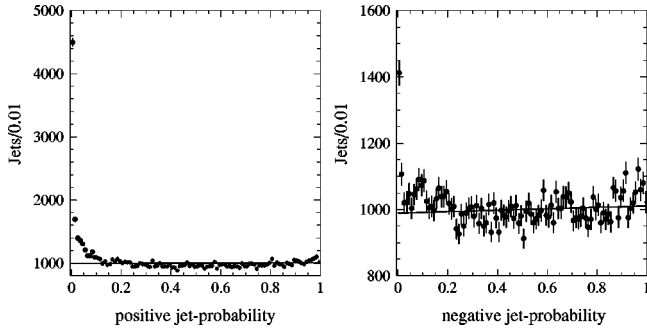


FIG. 5. Distributions of positive and negative jet-probability in a mixture of JET 50 and JET 140 data. The lines represent a fit to the negative distribution with a first order polynomial. The slope of the fit corresponds to a 1.6% change of the distribution over the entire jet-probability range.

Figure 5 shows the positive and negative jet-probability distributions in a sample of JET 50 and JET 140 data. The positive jet-probability distribution shows jets containing hadrons with heavy flavor as a large excess at jet-probabilities smaller than 0.05 over a flat distribution. A jet has a positive JPB tag if the jet-probability value is smaller than 0.05.

The negative jet-probability distribution is quite flat, as expected, since the resolution files were constructed using tracks with negative impact parameter. The small excess at negative jet-probability smaller than 0.05 (negative JPB tags) is due to the increase of the fraction of jets with heavy flavor in the JET 140 data with respect to the JET 50 data. This excess largely disappears, as shown in Fig. 6, when plotting the negative jet-probability of jets which have a large positive jet-probability (0.1–1.0). Since tracks with negative signed impact parameter in JET 50 data are used to define the resolution function, the small contribution to negative tags from jets with heavy flavor is incorrectly attributed to

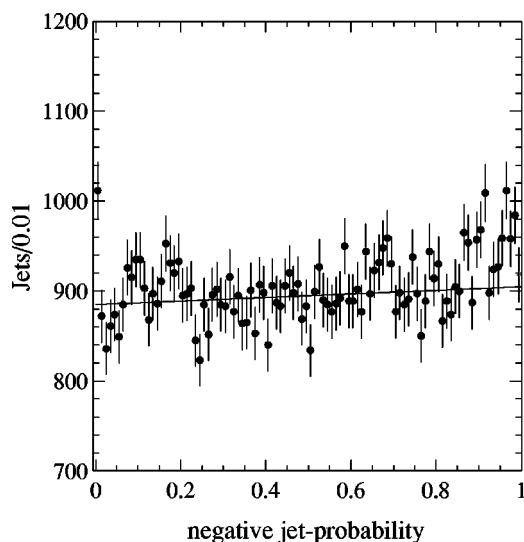


FIG. 6. Negative jet-probability distribution for jets with positive jet-probability greater than 0.1. This selection requirement removes most of the jets with heavy flavor. The line corresponds to the fit to the negative jet-probability distribution shown in Fig. 5.

the detector resolution by this procedure. It will be accounted for in the evaluation of the JPB mistags in Sec. X.

Ideally JPB tags corresponding to jet-probability values smaller than 0.05 should contain a 5% mistag rate. This expectation is tested in Fig. 6 fitting a first order polynomial function to the jet-probability distribution in the interval 0.1–1.0. The extrapolation of the fitted function predicts 4441 ± 34 negative JPB tags while 4455 are observed; this corresponds to 4.94% of the total number (101 050) of jets in the sample.

C. SLT algorithm

The SLT algorithm tags b quarks by searching for an electron or muon from their decay (low momentum leptons can also result from b -hadron decays through sequential c -decays, or τ and J/ψ cascade decays). This analysis follows the guidelines for the identification of soft electrons or soft muons documented in Refs. [5,29]. While previous measurements of the $t\bar{t}$ cross section used rates of events with SLT tags [2,3,5], in this analysis we search for soft lepton candidates only in a cone of radius 0.4 around the axis of a jet with $E_T \geq 15$ GeV and $|\eta| \leq 2$.

To search for soft electrons, every CTC track with $p_T \geq 2$ GeV/ c , which is associated to a jet, is extrapolated into the fiducial region of the calorimeter and is matched to a CES cluster. The matched CES cluster is required to be consistent in shape and position to the expectations for an electron. In addition, we require $0.7 \leq E/P \leq 1.5$ and $E_{\text{had}}/E_{\text{em}} \leq 0.1$. The energy deposited by the track in the preradiator (CPR) is required to be consistent with an electron shower. The track ionization rate (dE/dx), derived from the charge deposition of the CTC hits associated with the track, is also required to be consistent with the electron hypothesis. Electrons from photon conversions are removed. Photon conversions are identified as combinations of the electron candidate and an additional track with opposite charge passing the criteria listed in Table IV with the additional requirement that the invariant mass be smaller than 500 MeV/ c^2 . The selection criteria used to define the soft electron are described in more detail in Ref. [29]. The efficiency of each criterion used to select soft electron candidates has been measured using a sample of electrons produced by photon conversions [5] (the efficiency of the E/P and $E_{\text{had}}/E_{\text{em}}$ cuts is calculated using the simulation).

Soft muons are identified by matching CTC tracks with $p_T \geq 2$ GeV/ c to track segments in the CMU, CMP, and CMX muon chambers. Muon candidate tracks with $p_T \geq 3$ GeV/ c are extrapolated to the fiducial volume of both the CMU and CMP system and are required to be matched to track segments in both muon detectors. To maintain high efficiency for non-isolated muons, we do not impose minimum-ionization requirements on the calorimeter deposition. However, in order to reduce hadronic punch-through in the region not covered by the CMP system, we check that the energy, E_{had} , in the tower traversed by muon candidates with $p_T \geq 6$ GeV/ c is consistent with the muon hypothesis; we require $E_{\text{had}} \leq 6 + \Sigma p$, where Σp is the scalar sum of the momenta of all tracks contained in a cone of radius 0.2

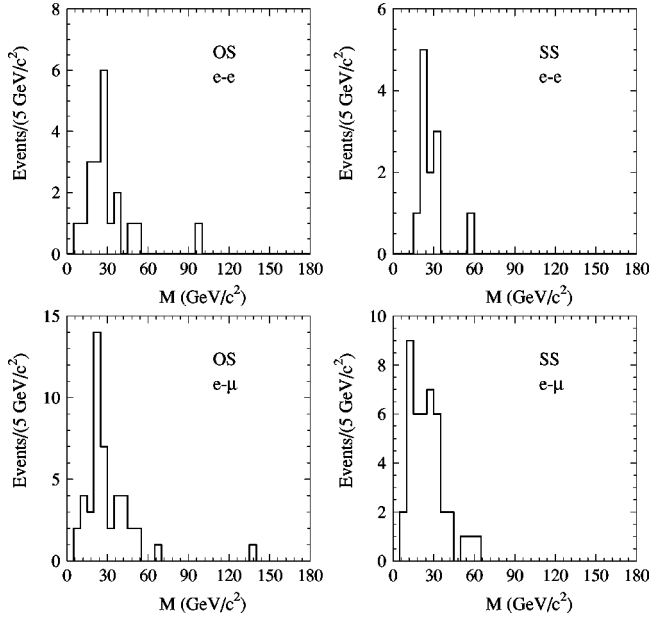


FIG. 7. Invariant mass distributions between the primary electron and the soft lepton candidates in $W+\geq 1$ events. OS and SS refer to lepton pairs with opposite and same charge, respectively.

around the muon direction. The efficiency of each selection cut has been measured using a sample of $J/\psi \rightarrow \mu^+ \mu^-$ and $Z \rightarrow \mu^+ \mu^-$ decays [5,29].

Figures 7 and 8 show distributions of the invariant mass between primary and soft leptons in all $W+\geq 1$ jet events. As shown in Fig. 8, there is a handful of events where the soft muon is consistent with being the second leg of a Z boson decay embedded in a jet. Soft muons which, when

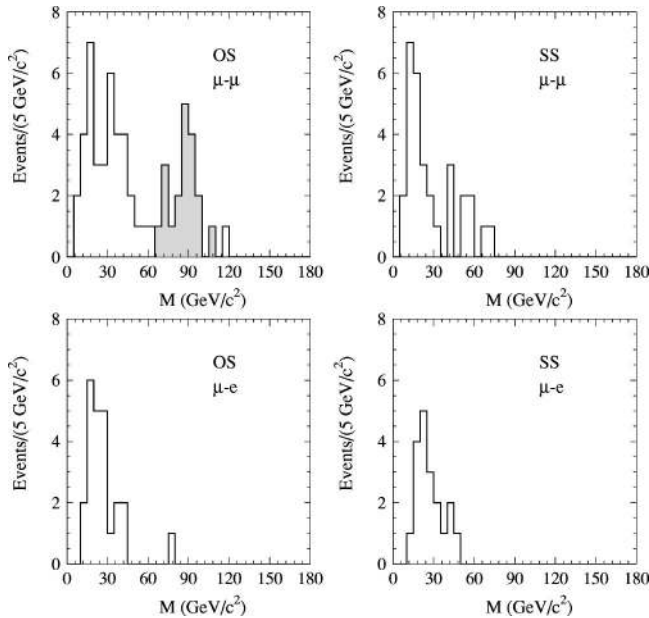


FIG. 8. Invariant mass distributions between the primary muon and the soft lepton candidates in $W+\geq 1$ events. OS and SS refer to lepton pairs with opposite and same charge, respectively. The shaded area indicates soft muons not considered tags.

combined with a primary muon of opposite charge, yield an invariant mass $70 \leq M_{\mu\mu} \leq 110 \text{ GeV}/c^2$ are not considered tags.

1. Simulation of the SLT algorithm

The soft lepton tagging algorithm has been developed studying real leptons from photon conversions and J/ψ mesons. The efficiency of each selection criterion is measured using these data. Therefore, the simulation of the soft lepton tagger does not need to rely on the QFL modeling of the detector response in order to estimate the tagging efficiency. The SLT simulation matches tracks produced by QFL to electrons and muons at generator level. The electrons or muons are required to come from b or c decay or any of their cascade decays. Electron tracks are extrapolated to the CPR and CES detectors, and required to pass fiducial cuts. Electron candidates are eliminated if they are consistent with arising from photon conversions. Muon tracks, extrapolated to the muon detectors, are required to pass the fiducial cuts and classified according to the muon detector type (CMU, CMP, and CMX). Finally tracks are weighted with the measured efficiencies of the selection criteria, which are functions of the track transverse momentum [5,29]. This procedure ensures that the simulation accurately models the soft lepton tagging efficiency.

In Sec. XI we compare rates of SLT tags in generic-jet data to the corresponding simulation to verify that the procedure has been implemented correctly. By construction, the SLT simulation does not produce mistags.

2. Fake soft lepton tags

This background includes hadrons which pass the lepton selection cuts (such as pions which fake an electron or a muon) as well as electrons from conversions or muons from pions or kaons which decay in the detector. This background is estimated using the data.

The SLT fake rate is measured starting from the ratio of the number of tracks passing the soft lepton selection criteria to the total number of tracks which satisfy the soft lepton fiducial requirements in generic-jet data [5,29]. In the JET 20, JET 50, and JET 70 samples the probability P that a track produces a SLT tag is computed separately for electrons and for different types of muon detectors. This probability is parametrized as a function of the track p_T and isolation [5,29]. Since in this analysis we search a jet for SLT candidates in a cone of radius of 0.4 around its axis, we define a SLT probability per jet $P_{\text{SLT}}^{\text{jet}}(N) = \sum_{i=1}^N P_{\text{SLT}}^{\text{jet}}(i-1) + [1 - P_{\text{SLT}}^{\text{jet}}(i-1)] \times P_i$ where N is the number of tracks contained in a cone of radius 0.4 around the jet axis.

In Table XIII the observed rates of SLT tags in various generic-jet samples are compared to the rates predicted by the probability $P_{\text{SLT}}^{\text{jet}}$ described above. Since in generic-jet data the trigger jet is biased toward a lower yield of soft muons (a jet containing a muon has a lower energy deposition in the calorimeter and therefore is less likely to be the trigger jet) the comparison is performed with and without the trigger jet. However, when more than one jet is above the trigger threshold, all jets are considered. Excluding trigger

TABLE XIII. Comparison of the observed and predicted yields of jets with SLT tags.

Samples used in the fake parametrization			
Sample	Predicted (P)	Observed (O)	(P-O)/O
JET 20	5353.9	4994	7.2%
JET 20 without leading jet	3392.4	3383	0.3%
JET 50	7082.9	6408	10.5%
JET 50 without leading jet	4947.4	4988	-0.8%
JET 70	8089.2	7277	11.2%
JET 70 without leading jet	5724.9	5678	0.8%
Independent samples			
JET 100	8603.6	7483	15.0%
JET 100 without leading jet	6109.8	5909	3.4%
JET 140	1324.1	1196	10.7%
ΣE_T 175	3392.6	3392	0.02%
ΣE_T 125 4 CL	9651.9	10095	-4.4%
ΣE_T 300	1627.1	1401	16.1%
Isolated γ	365.8	352	3.9%

jets from the comparison one observes agreement between the observed and predicted rates of tagged jets. The last seven samples shown in Table XIII were not used to determine the SLT probability per track. Predicted and observed yields of SLT tags in all samples agree within 15%. As the amount and type of heavy flavor changes appreciably in different QCD samples (see Sec. X) the apparent agreement suggests that the rate of SLT tags in generic-jet data is dominated by fakes.

The SLT fake probability is obtained by removing the contribution of SLT tags due to heavy flavor decays in the generic-jet data used to construct the SLT probability per track. For this purpose, we use the signed impact parameter significance distribution of the soft lepton tracks. The distribution observed in the data is fitted with the shape expected for leptons coming from the decay of b and c hadrons, derived using simulated events, in addition to the shape of fake SLT tags. The shape of fake SLT tags is derived using all tracks taggable² by the SLT algorithm in events which do not contain any SECVTX, JPB, or SLT tags.

Figure 9 shows the signed impact significance distribution of SLT tags in JET 50 data along with the fit result. The composition of the SLT tags determined from these fits is $(74.0 \pm 3.2)\%$ fakes, $(10.5 \pm 2.3)\%$ b 's, and $(14.5 \pm 4.3)\%$ c 's for all three generic-jet samples used to evaluate the SLT tagging probability. The fit underestimates by 5% the number of tracks with negative S_0 in Fig. 9. We take this difference as a systematic uncertainty of the fake rate contribution, which is 88% of the tracks with negative S_0 . Adding linearly this resulting 5.6% systematic uncertainty to the 4.3% error returned by the fit, we estimate a 10% error on the fraction of fake SLT tags determined by the fits. Based on this result, the SLT mistag probability per jet is obtained by rescaling the

SLT tagging probability in generic-jet data by $(74.0 \pm 7.4)\%$.

IX. EFFICIENCY OF THE SECVTX AND JPB TAGGERS

We first describe the calibration of the efficiency of the tagging algorithms in the simulation. For this purpose, we use the low- p_T inclusive electron sample described in Sec. V B and the corresponding simulation. A large fraction of the events in this sample is expected to originate from $b\bar{b}$ production in which a jet containing an electron from a semi-leptonic b -decay, called an e-jet, recoils against a jet from the other b , called the away-jet or a-jet. The tagging efficiency in the simulation, $\varepsilon_b^{\text{MC}}$, is adjusted to the value ε_b of the tag-

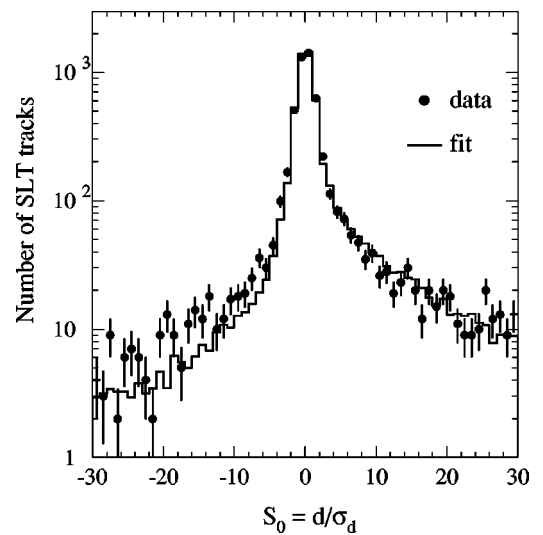


FIG. 9. Distribution of the signed impact parameter significance of SLT tracks contained in the JET 50 data (\bullet). The solid histogram represents a fit using the shapes expected for b and c semileptonic decays and for fake tags.

²Tracks with $p_T \geq 2$ GeV/ c and pointing to the fiducial volume of the electromagnetic calorimeter or the muon detector.

TABLE XIV. Fractions of electron and away-jets before and after tagging in the low- p_T inclusive electron simulation. $SN_{\text{a-jet}}^{\text{h.f.}}$ and $SN_{\text{a-jet}}^{\text{prompt}}$ are the fractions of away-jets with and without heavy flavor.

	direct production		flavor excitation		gluon splitting	
	b (%)	c (%)	b (%)	c (%)	b (%)	c (%)
$SN_{\text{e-jet}}$	20.90	3.49	39.72	10.26	19.39	6.22
$SN_{\text{a-jet}}^{\text{h.f.}}$	19.93	3.31	5.91	1.35	2.61	0.53
$SN_{\text{a-jet}}^{\text{prompt}}$	1.64	0.29	35.65	9.38	19.60	6.38
$ST_{\text{e-jet}}^{\text{SEC}}$	24.51	0.68	47.58	2.55	22.74	1.93
$ST_{\text{e-jet}}^{\text{JPB}}$	23.57	1.60	44.64	5.93	20.75	3.51
$ST_{\text{a-jet}}^{\text{SEC}}$	70.50	3.07	16.17	2.29	7.47	0.51
$ST_{\text{a-jet}}^{\text{JPB}}$	67.59	5.23	15.06	3.51	7.11	1.50
SDT^{SEC}	73.46	0.54	17.01	0.43	8.45	0.11

ging efficiency in the data using the scale factor

$$SF = \frac{\varepsilon_b}{\varepsilon_b^{\text{MC}}}.$$

Following the derivation of the scale factor, subsections A–I discuss the various sources of systematic uncertainty and also present cross-checks. In subsection J we provide an explanation for the deviation of the scale factor from unity.

The data sample consists of 55248 events. The simulated sample is generated with HERWIG [23].³ Using the generic hard parton scattering, $b\bar{b}$ and $c\bar{c}$ pairs are produced through processes of order α_s^2 as $gg \rightarrow b\bar{b}$ (direct production). Processes of order α_s^3 are implemented in the generator through flavor excitation processes such as $gb \rightarrow gb$ or gluon splitting, where the process $gg \rightarrow gg$ is followed by $g \rightarrow b\bar{b}$. We use the MRS(G) set of parton distribution functions [30]. Apart from the parton distribution functions, the simulation package is the same as that used to generate W +jet events. The generated hard scattering sample corresponds to an integrated luminosity of 83.5 pb^{-1} . In this sample we select events with an e-jet containing hadrons with heavy flavor. After applying the same selection used for the data, the simulated low- p_T electron sample contains 16547 events.

Table XIV shows the heavy flavor composition of the simulated inclusive electron sample. One notices that 80% of the e-jets are due to $b\bar{b}$ production and that only 33% of the away-jets contain heavy flavor.

In simulated events where the away jet is tagged by SECVTX ($ST_{\text{a-jet}}^{\text{SEC}}$), 94% of the electron-jets are due to $b\bar{b}$ production. It is therefore convenient to measure the b -tagging efficiency as the fraction of these events in which the electron-jet is tagged by SECVTX or JPB

TABLE XV. Number of events before and after tagging electron and away-jets. P_{QCD} is the probability of tagging away-jets if they contain the same heavy flavor fraction as generic-jets (see text).

Type	Data		Simulation	
	Observed-mistags	$P_{\text{QCD}}\%$	Type	Observed-mistags
$N_{\text{e-jet}}$	55248		$SN_{\text{e-jet}}$	16547
$T_{\text{e-jet}}^{\text{SEC}}$	8158-84.3		$ST_{\text{e-jet}}^{\text{SEC}}$	4549-0
$T_{\text{e-jet}}^{\text{JPB}}$	9123-335.3		$ST_{\text{e-jet}}^{\text{JPB}}$	5990-0
$T_{\text{a-jet}}^{\text{SEC}}$	3640-112.8	1.67	$ST_{\text{a-jet}}^{\text{SEC}}$	1832-7
DT^{SEC}	1126-23.8		SDT^{SEC}	545-1
DT^{JPB}	1225-35.3		SDT^{JPB}	743-1

$$\varepsilon_b^{\text{MC}} = \frac{SDT}{ST_{\text{a-jet}}^{\text{SEC}}} \quad (1)$$

where SDT is the number of events where both the electron and away-jet contain heavy flavor and are tagged. The $b\bar{b}$ production accounts for 99% of the simulated events with a double tag.

Table XV lists rates of tags in the data and in the simulation. In the simulation there are very few mistags and they are easily identified because the jet does not contain b or c -hadrons in a cone of radius 0.4 around its axis. In the data, the rate of mistags is evaluated using the parametrization described in Sec. X.

We use the simulation to describe F_{hf} , the fraction of data in which electron-jets contain hadrons with heavy flavor. The data contain also a relevant number of e-jets in which the electron is not associated with the production of hadrons with heavy flavor (mostly from photon conversions in jets due to light quarks or gluons). In these events, the electron-jet contributes only mistags. To describe the fraction $(1 - F_{\text{hf}})$ of the data, in which electron jets do not contain hadrons with heavy flavor, we make the additional assumption that away-jets in these events contain the same fraction of heavy flavor as generic-jets. The parametrization of the probability of tagging jets with heavy flavor in generic-jet data is derived in Sec. X. The 10% uncertainty associated with this parametrization is discussed in Sec. IX A.

We use the following procedure to derive the tagging efficiency scale factor separately for SECVTX and jet-probability, together with the heavy flavor purity F_{hf} of the data. The data and the simulation are normalized to the same number of tagged electron-jets that contain heavy flavor, $T_{\text{e-jet}}$ and $ST_{\text{e-jet}}$, through the coefficient

$$\alpha = \frac{T_{\text{e-jet}}}{ST_{\text{e-jet}}}.$$

Before tagging, the heavy flavor purity of the data is therefore given by

$$F_{\text{hf}} = \frac{\alpha \times SN_{\text{e-jet}}}{SF \times N_{\text{e-jet}}} \quad (2)$$

³We use the process 1500, generic $2 \rightarrow 2$ hard scattering with transverse momentum threshold $p_T^{\text{min}} \geq 13 \text{ GeV}/c$.

TABLE XVI. Data to Monte Carlo tagging efficiency scale factors. F_{hf} is the fraction of e-jets containing heavy flavor in the data.

Sample	SF	F_{hf}
SECVTX e-jet, SECVTX a-jet	1.23 ± 0.07	$43.5 \pm 2.9\%$
JPB e-jet, SECVTX a-jet	0.96 ± 0.05	$45.3 \pm 2.4\%$

where $N_{\text{e-jet}}$ and $SN_{\text{e-jet}}$ are the number of e-jets in the data and in the simulation and SF is the tagging efficiency scale factor. Initially, we assume $SF = 1$. In the data the number of events in which a tagged away-jet with heavy flavor is associated to an electron-jet without heavy flavor is

$$T_{\text{a-jet}}^{\text{QCD}} = (1 - F_{\text{hf}}) \times N_{\text{e-jet}} \times P_{\text{QCD}}$$

and the number of events in which a tagged away-jet containing heavy flavor is associated with an electron-jet also containing heavy flavor is

$$T_{\text{a-jet}}^{\text{SEC}} - T_{\text{a-jet}}^{\text{QCD}}$$

For the data the b -tagging efficiency, analogy of Eq. (1), is then

$$\varepsilon_b = \frac{DT}{T_{\text{a-jet}}^{\text{SEC}} - T_{\text{a-jet}}^{\text{QCD}}}$$

where, as before, DT is the number of events in which the a-jet is tagged by SECVTX and the e-jet has a SECVTX or JPB tag.

The ratio of the tagging efficiencies in the data and in the simulation yields the scale factor

$$SF = \frac{\varepsilon_b}{\varepsilon_b^{\text{MC}}}.$$

The value of the scale factor is inserted again in Eq. (2) and we iterate until the scale factor value is stable to within 1% (see Table XVI).

Using the numbers of electron and away-jets listed in Table XV, we derive $SF = 1.23 \pm 0.07$ for SECVTX and 0.96 ± 0.05 for jet-probability. The error accounts for the sample statistics (with the largest contribution coming from the simulation) and for 10% uncertainties in the evaluation of

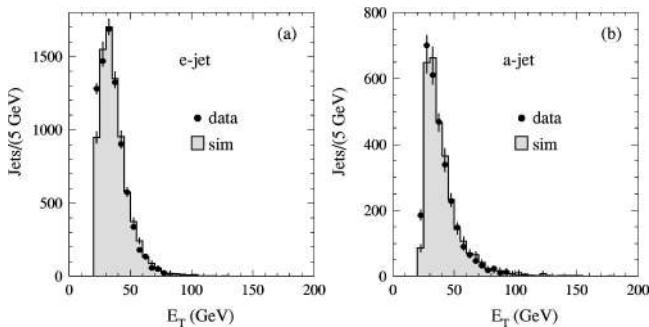


FIG. 10. Distributions of the transverse energy of electron-jets (a) and away-jets (b) tagged by SECVTX.

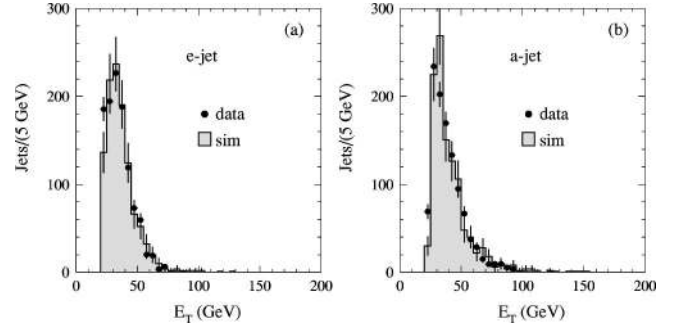


FIG. 11. Distributions of the transverse energy of electron-jets (a) and away-jets (b) in events with double SECVTX tags.

the mistag rates and in the prediction of the rate of tags in generic-jets with heavy flavor.

The b -purity of the e-jets before tagging, $F_{\text{hf}} = (43.5 \pm 2.9)\%$, is in agreement with the measurement in Ref. [5], $(37 \pm 8)\%$, using the fraction of tagged electron-jets that also contain a muon of opposite charge.

The average SECVTX tagging efficiency is $(36.7 \pm 1.9)\%$ in the data and $(29.8 \pm 1.1)\%$ in the simulation. The corresponding numbers for jet-probability are $(39.2 \pm 2.1)\%$ and $(40.7 \pm 1.1)\%$, respectively.

Since the tagging efficiencies depend on the jet energy, it is important to show that jet energy distributions are similar in the data and the simulation (see Figs. 10 and 11). The distributions of the lifetime and invariant mass of the SECVTX tags are shown in Fig. 12 and support our determination of the b -purity of the sample. The lifetime of a SECVTX tag is defined as

$$\text{pseudo-}\tau = \frac{L_{xy} \times M^{\text{SVX}}}{c \times p_T^{\text{SVX}}}$$

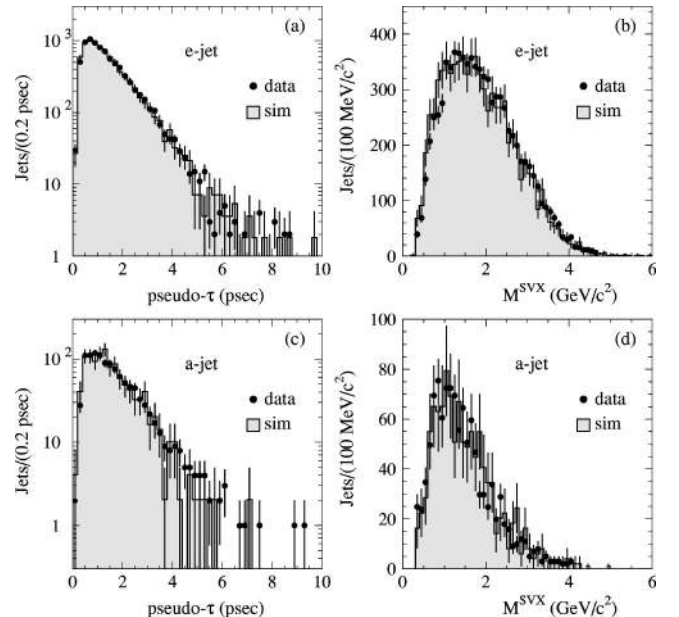


FIG. 12. Distributions of pseudo- τ (a) and of the invariant mass (b) of SECVTX tags in electron-jets; (c) and (d) are the analogous distributions for away-jets in events with double tags.

TABLE XVII. Rates of events in which the electron jet is due to a photon conversion before and after tagging. The heavy flavor purity of this sample is $F_{\text{hf}} = (8.7 \pm 0.9)\%$. Events where the e-jet contains heavy flavor are described with the HERWIG simulation. In the remaining events, the rate of tagged away-jets (QCD) is predicted using the probability for tagging jets with heavy flavor in generic-jet data. Mistags have been removed from the data and simulation.

Type	Data	Simulation	QCD	Prediction
$N_{\text{e-jet}}$	4027	350 ± 37	3677 ± 37	4027
$T_{\text{e-jet}}^{\text{SEC}}$	108.3 ± 10.6	114 ± 12	0	114 ± 12
$T_{\text{e-jet}}^{\text{JPB}}$	133.1 ± 12.5	126 ± 13	0	126 ± 13
$T_{\text{a-jet}}^{\text{SEC}}$	102.2 ± 10.5	41.6 ± 5.0	60.2 ± 6.0	101.8 ± 7.8
$T_{\text{a-jet}}^{\text{JPB}}$	135.0 ± 13.7	45.0 ± 4.5	86.7 ± 8.7	131.7 ± 9.8

where M^{SVX} and p_T^{SVX} are the invariant mass and the transverse momentum of all tracks forming the SECVTX tag.

A. Check of the background parametrization using a photon conversion sample

In events where the e-jet does not contain heavy flavor, we predict the rate of tagged away-jets containing heavy flavor using the probability of tagging jets with heavy flavor as measured in generic-jet data. We test this method in a sample of data where the electrons in the e-jet are due to photon conversions. The criteria used to identify photon conversions are listed in Table II. In this case we require that an electron is matched by a second track consistent with a photon conversion and that it is not matched by a track segment in the VTX detector. Otherwise, we select this sample as the inclusive electron sample where in contrast conversions were removed.

Following the procedure used in the previous section, we determine the fraction of events with heavy flavor to be $F_{\text{hf}} = (8.7 \pm 0.9)\%$ from the number of e-jets with a SECVTX or JPB tag. Tagging rates in events due to heavy flavor production are described using the HERWIG simulation as in the previous section. In the remaining 91.3% of the events, we describe the rates of tagged away-jets using the parametrization derived from generic jets.

Table XVII shows that this procedure correctly predicts the rates of tags observed in the data. We take the 10% statistical error of this comparison as the systematic uncertainty of the method.

B. Sensitivity of the scale factor to the modeling of c -jets

In the simulation the tagging efficiency is defined as the ratio of events with double tags to all events where the away-jet is tagged by SECVTX. As shown in Table XIV, the HERWIG simulation predicts that 94% of the a-jets with a SECVTX tag are due to $b\bar{b}$ production. The remaining 6% of the a-jets are due to $c\bar{c}$ production and are accounted for by the simulation but in principle this could be improperly modeled. In events where a-jets have a JPB tag, the fraction of $c\bar{c}$ production increases to 11% (see Table XIV). If SECVTX

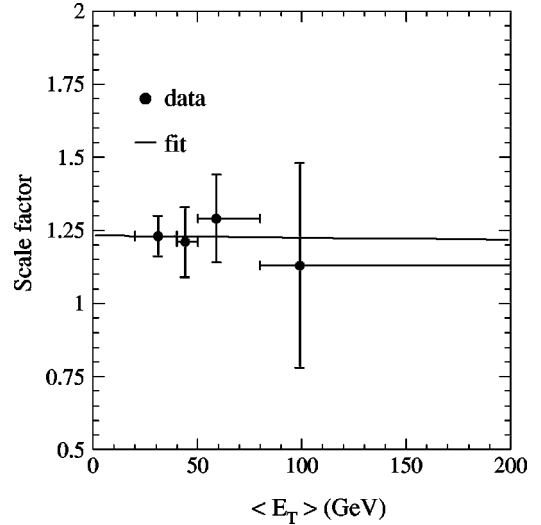


FIG. 13. SECVTX tagging efficiency scale factor as a function of the average transverse energy $\langle E_T \rangle$ of the electron-jet. The line represents a fit with a first degree polynomial.

and JPB scale factors are determined using a-jets tagged by JPB instead of a-jets tagged by SECVTX, both scale factors change by less than 1%. Therefore, we conclude that the modeling of c -jets is satisfactory for the determination of the b -tagging efficiency scale factor.

C. Dependence of the scale factor on the gluon splitting cross section

As shown in Table XIV, a fraction of the events in the inclusive electron sample is due to gluon splitting to heavy flavor quarks. The calibration of the HERWIG simulation using generic-jet data in Sec. XI shows that the direct production and the heavy flavor excitation as implemented in HERWIG provide a fair description of the data, but the gluon splitting cross section requires a $(40 \pm 20)\%$ correction. We repeat the calculation of the scale factor using this larger gluon splitting cross section. We find that the SECVTX scale factor increases from 1.23 to 1.25. The final scale factor we use will be this latter value.

D. E_T dependence of the scale factor

Jets produced directly in association with a W boson have transverse energies comparable to the jets in the low- p_T inclusive electron sample. However, b -jets produced by top quark decays have substantially higher transverse energies. In this section, we investigate a possible E_T dependence of the scale factor using two methods.

First, we derive the value of the SECVTX scale factor in four different bins of the electron-jet transverse energy. In each bin, we calculate the average e-jet transverse energy $\langle E_T \rangle$ and the scale factor using the iterative procedure previously described. The result of the study is shown in Fig. 13. A fit of the scale factor as a function of the transverse energy with a first order polynomial yields a χ^2 of 0.3 for 2 DOF and

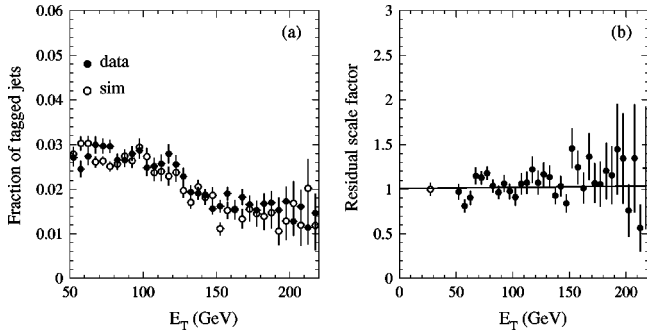


FIG. 14. Fractions of tagged jets (a) as a function of the jet transverse energy. The residual scale factor (b) is defined as the ratio of these fractions in the data and the simulation. The open circle in (b) represents the inclusive electron sample result.

$$SF(E_T) = (1.23 \pm 0.17) - (0.1 \pm 4.0) \times 10^{-3} \times \langle E_T \rangle \text{ (GeV)}$$

with a correlation $\rho = -0.95$ between the two fit parameters. The result of this fit is therefore consistent with a constant scale factor.

In the second method, we compare the fraction of jets with heavy flavor tagged by SECVTX in JET 50 and in JET 100 data and in the corresponding HERWIG simulation tuned as in Sec. XI. The b -tagging efficiency in the detector simulation is increased by the factor 1.25 independently of the jet transverse energy. The ratio RSF of the fractions of tagged jets in the data and in the simulation is sensitive to any residual E_T dependence of the scale factor. The result of this method is shown in Fig. 14. We fit the ratio RSF of the tagging efficiencies in the data to the simulation as a function of the jet transverse energy with a first order polynomial. The fit yields a χ^2 of 51 for 49 DOF and

$$RSF(E_T) = (1.01 \pm 0.05) + (1.3 \pm 4.6) \times 10^{-4} \times E_T \text{ (GeV)}$$

with a correlation $\rho = -0.92$ between the two fit parameters. The fit result is consistent with a constant scale factor.

E. Uncertainty of the scale factor

The SECVTX b -tagging efficiency scale factor measurement using the inclusive electron sample has a 5.6% uncertainty. The uncertainty of the calibration of the gluon splitting cross section predicted by HERWIG results in an additional 0.8% uncertainty of the scale factor. By folding the E_T spectrum of b -jets from top quark decays with the E_T parametrization of the scale factor from the fit shown in Fig. 13 (a variation of the fit parameters by $\pm 1\sigma$ yields a $\pm 4.2\%$ change in the efficiency for tagging b -jets and $\pm 3.9\%$ change in the efficiency to tag events), we estimate a 4% uncertainty from any residual E_T dependence. These errors are mostly systematic and in general highly correlated. Altogether, we assign a 10% error to the determination of the scale factor after combining linearly the above contributions. Our final estimate of the b -tagging efficiency scale factor for the SECVTX algorithm is $SF = 1.25 \pm 0.13$ and for the jet-probability algorithm is $SF = 0.96 \pm 0.10$. The latter is consistent with unity.

F. Check of the scale factor using a low- p_T inclusive muon sample

The low- p_T inclusive muon sample is analogous to the electron sample in that a muon with $p_T \geq 10$ GeV/ c is required in place of an electron with $E_T \geq 10$ GeV (see Sec. VB). It provides an independent sample for checking the tagging efficiency scale factor. The low- p_T muon sample consists of 10393 events. In these events muon-jets without heavy flavor are due to fake muons arising from non-interacting hadrons or in-flight decays of K and π mesons. We compare to a simulated sample also generated using the option 1500 of HERWIG which consists of 4280 events. The same procedure described above yields a SECVTX tagging efficiency scale factor of 1.24 ± 0.10 , in agreement with the value 1.23 ± 0.07 derived in the inclusive electron sample (before correcting the gluon splitting cross section). At the same time the heavy flavor purity of the low- p_T muon sample is measured to be $F_{\text{hf}} = (59.7 \pm 3.6)\%$.

G. Check of the scale factor in jets containing inclusive b decays

In this section we investigate whether the scale factor is different in jets containing semileptonic b -decays and inclusive b -decays. We use the low- p_T inclusive electron sample and normalize the data and the simulation to the same number of electron-jets with a SECVTX tag after mistag removal. In the simulation, the rate of gluon splitting to $b\bar{b}$ and $c\bar{c}$ pairs is corrected as in Sec. XI. We compare rates of away-jets which are taggable and which are tagged by SECVTX. We find that the simulation predicts correctly the amount of taggable away-jets but it underestimates by a factor 1.23 ± 0.08 the rate of SECVTX tags with respect to the data.

H. Check of the scale factor using rates of double tags in generic-jet data

The studies of the E_T dependence of the SECVTX scale factor performed in Sec. IX D depend upon the assumption that HERWIG models correctly the fractional yield of jets with heavy flavor as a function of their transverse energy. We use the JET 50 and JET 100 data and simulation for a test independent of this assumption. We select events with only two jets: one taggable jet with transverse energy larger than the trigger threshold and one taggable jet with $E_T \geq 15$ GeV in the opposite hemisphere. We compare the number of events with double JPB tags and double SECVTX tags in the data and in the HERWIG simulation after mistag removal. In the simulation, 92% of these double tags are due to $b\bar{b}$ production. The ratio of double SECVTX to double JPB tags in the data and in the simulation is

$$R_{\text{data}} = 0.92 \pm 0.18 \quad \text{and} \quad R_{\text{sim}} = 0.61 \pm 0.05.$$

This ratio does not depend on the absolute cross section for producing jets with heavy flavor. From the equivalence

$$\frac{R_{\text{data}}}{R_{\text{sim}}} = \left(\frac{SF^{\text{SEC}}}{SF^{\text{JPB}}} \right)^2,$$

we measure $SF^{\text{SEC}}/SF^{\text{JPB}} = 1.24 \pm 0.13$ using generic jets with high transverse energy, in agreement with the value $SF^{\text{SEC}}/SF^{\text{JPB}} = 1.28 \pm 0.10$ measured in the low- p_T inclusive electron sample.

I. SECVTX efficiency for tagging c jets

Since we need to apply a large correction to the simulated SECVTX efficiency for tagging b -jets, it is worth investigating differences between data and simulation for tagging c -jets. For this purpose, we compare rates of tags in the JET 50 and JET 100 data to the corresponding HERWIG simulation, described in Sec. XI normalized to the same number of events.

We define R as the ratio of the number of SECVTX to JPB tags after mistag removal. In the data $R = 0.77 \pm 0.07$. Under the assumption that the heavy flavor composition of the data is modeled correctly by HERWIG, the SECVTX scale factor for c -jets, SF_c^{SEC} , can then be derived solving the equivalence

$$R = \frac{T_b^{\text{SEC}} \times SF_b^{\text{SEC}} + T_c^{\text{SEC}} \times SF_c^{\text{SEC}}}{T^{\text{JPB}} \times SF^{\text{JPB}}}$$

where $T_b^{\text{SEC}} = 5354$ and $T_c^{\text{SEC}} = 2477$ are the number of simulated b and c -jets tagged by SECVTX, and $T^{\text{JPB}} = 11958$ is the number of JPB tags. Using $SF_b^{\text{SEC}} = 1.23 \pm 0.07$ and $SF^{\text{JPB}} = 0.96 \pm 0.05$, we derive that the SECVTX scale factor for tagging c -jets is $SF_c^{\text{SEC}} = 0.92 \pm 0.28$. The error is determined by the uncertainty of the heavy flavor composition (see Sec. XI) and by the errors of the scale factors SF_b^{SEC} and SF^{JPB} .

J. Understanding of the scale factor

In an effort to explain the 25% difference of the SECVTX tagging efficiency in the data and the simulation we uncovered three oversights in the simulation package used in this and in some previous CDF analyses [2,3]. A significant fraction of the difference is due to the use of an outdated version of the CLEO decay tables and to outdated B -lifetimes in the CDF particle database. The above two inaccuracies account for $\sim 40\%$ of the difference of the SECVTX scale factor from unity. Small inconsistencies in the implementation of the SVX geometry in the simulation contribute an additional 16% to this difference. If we corrected for these effects, the new determination of the SECVTX scale factor would be 1.09 ± 0.11 ; the uncertainty includes the error on the b -lifetime ($\sim 3\%$) and the uncertainty of the track degradation procedure described in Sec. VII ($\sim 8\%$). The efficiency of jet-probability is not affected by these changes in the QFL simulation.

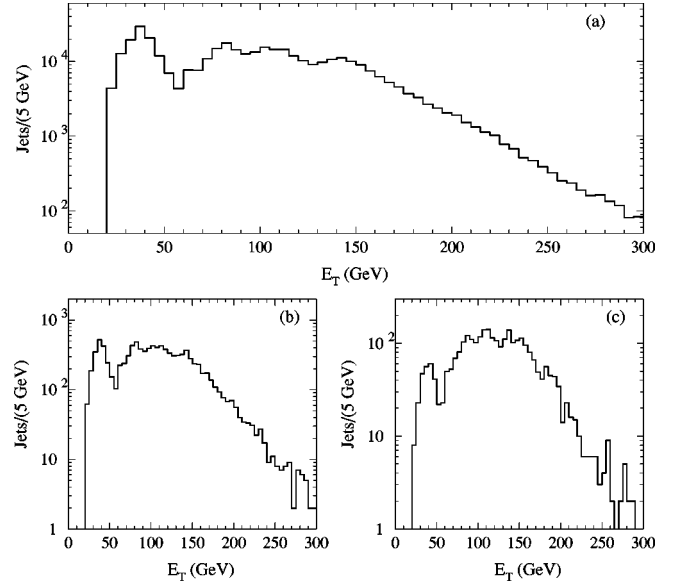


FIG. 15. Transverse energy distributions of (a) taggable jets, and jets with positive (b) and (c) negative SECVTX tags.

X. SECVTX AND JPB MISTAGS

In this section we estimate the SECVTX and JPB mistag rate in a variety of control samples before applying it to W +jet and Z +jet events in Secs. XII and XIII. Tags in jets without heavy flavor, which we call mistags, are caused by detector resolution effects. SECVTX mistags are poorly reproduced by our detector simulation and traditionally CDF removed this background from the data using a parametrization of the probability of finding negative SECVTX tags in JET 50 data [2,3,5]. We derive a new parametrization of the mistag rate using the JET 20, JET 50, JET 70, JET 100, and ΣE_T 300 data described in Sec. V A. Even if JPB mistags are well reproduced by the detector simulation, we derive a mistag parametrization also for JPB tags because this algorithm has a higher rate of mistags than SECVTX and provides a better check of the method.

The method to evaluate the mistag probability starts with the measurement of the number of positive and negative tags in generic-jet data and their parametrization as a function of the jet E_T and the jet track multiplicity, $N_{\text{TRK}}^{\text{SVX}}$. The tagging probability is derived as a ratio of the number of tags to the number of taggable jets in bins of transverse energy and track multiplicity. We use only jets that are far away from calorimeter cracks and correct the jet energy for the detector response and out-of-cone losses (see Sec. III D).

Negative tags are also produced in jets containing heavy flavor. In particular, the probability of producing negative tags is different for jets initiated by a heavy-quark or by gluon splitting to a pair of heavy quarks. Since this contribution to negative tags must be accounted for and subtracted in order to obtain the mistag rate, it is important to parametrize the rate of negative tags in a sample in which the composition of quark and gluon jets is well understood and is not subject to the additional uncertainty of the simulation. For this reason, in each generic-jet sample, we use only jets with transverse energy above the trigger threshold (leading

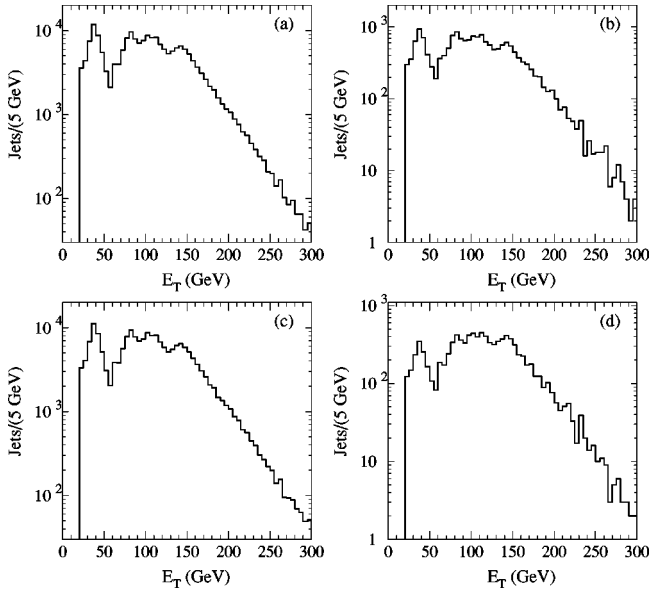


FIG. 16. Transverse energy distributions of jets with (a) at least two JPB tracks with positive impact parameter significance, (b) with positive JPB tags, (c) with two or more JPB tracks with negative impact parameter significance, and (d) with negative JPB tags.

jets): jets with corrected $E_T \geq 30, 70, 90, 120,$ and 160 GeV in the JET 20, JET 50, JET 70, JET 100, and ΣE_T 300 data, respectively. In the generic-jet simulation, 95% of the leading jets with a tag contain just one heavy-flavored hadron (a large fraction of these leading jets is produced by heavy quarks from flavor excitation or direct production). The E_T region below 30 GeV is mapped selecting events containing two leading jets, but using only the additional jets in the event; in the simulation, 96% of the tagged nonleading jets contain two hadrons with heavy flavor produced by a gluon splitting process.

Transverse energy distributions of the jets used to measure the tagging probability are shown in Figs. 15 and 16. Projections of the tagging probability matrices are shown in Figs. 17 and 18.

Figure 19 shows that the tagging probability parametrization derived using jets with well measured energies works well for all jets.

Since the heavy flavor contribution to negative tags is expected to be small, the number of tags due to heavy flavor in a given E_T bin of the tagging probability matrix is estimated as $P-N$, the difference between the numbers of positive (P) and negative (N) tags in this bin. In simulated jets with heavy flavor, we measure the ratio $R=N/(P-N)$ as a function of the jet transverse energy. We measure this ratio separately for jets which contain only one hadron with heavy flavor (R_1) and for jets which contain two hadrons with heavy flavor (R_2). The following empirical parametrization provides a good description of R for jets containing b as well as c -hadrons:

$$R_1(E_T) = \begin{cases} 0.0088 + 0.000158 \times E_T \text{ GeV} & \text{for SECVTX} \\ 0.039 + 0.00117 \times E_T \text{ GeV} & \text{for JPB} \end{cases}$$

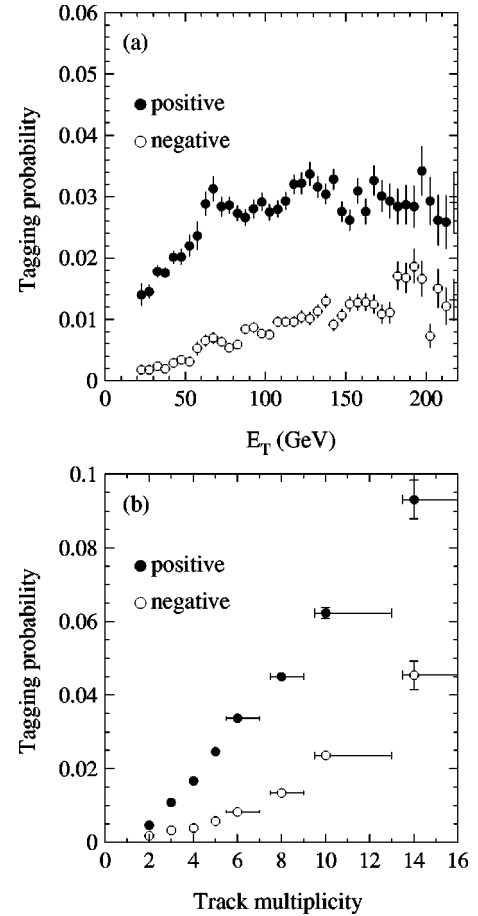


FIG. 17. The positive and negative SECVTX tagging probability as a function of (a) the jet E_T and (b) the number of SVX tracks in a jet.

$$R_2(E_T) = \begin{cases} 0.075 + 0.000158 \times E_T \text{ GeV} & \text{for SECVTX} \\ 0.14 + 0.00117 \times E_T \text{ GeV} & \text{for JPB.} \end{cases}$$

With this parametrization we construct the mistag probability matrix by correcting each bin of the negative tagging probability matrix by the factors:

$$N - (P - N) \times R_1(E_T) \quad \text{for jets with } E_T \geq 30 \text{ GeV}$$

$$N - (P - N) \times R_2(E_T) \quad \text{for jets with } E_T \leq 30 \text{ GeV.}$$

The fraction of negative tags contributed by heavy flavors is shown in Table XVIII.

In the generic-jet samples used to derive the mistag matrices, approximately 70% of the events contain additional interactions. The rate of multiple interactions is different in other samples, e.g., W + multi-jet events where we require an isolated primary lepton. The negative tagging rate in the generic-jet data depends on the number of additional interactions.

Figure 20 shows the relative negative tagging probability, normalized to the average, as a function of the sum of the transverse momenta of all tracks associated with additional vertices displaced by more than 5 cm from the primary ver-

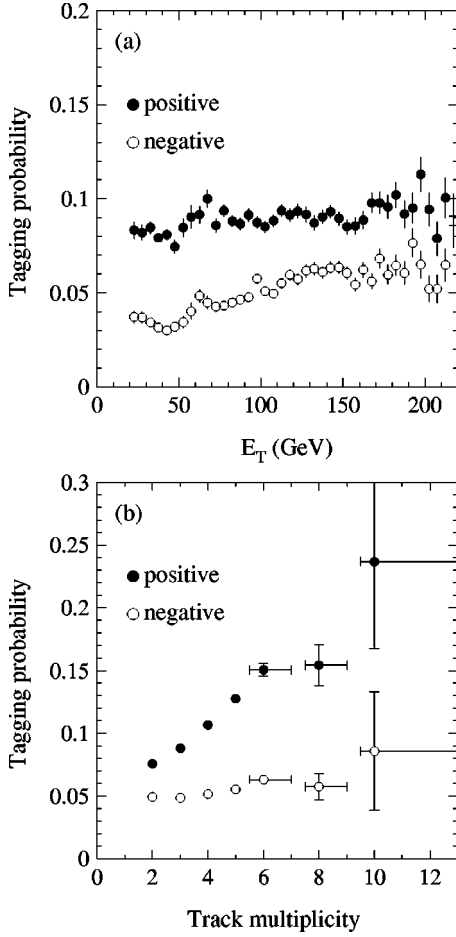


FIG. 18. The positive and negative JPB tagging probability as a function of (a) the jet E_T and (b) the number of SVX tracks in a jet.

tex Σp_T^V . Accordingly, the mistag rate is parametrized with the additional empirical function for both SECVTX and JPB:

$$F(\Sigma p_T^V) = \begin{cases} 0.8 + 0.0128 \times \Sigma p_T^V & \text{for } \Sigma p_T^V < 60 \text{ GeV}/c \\ 1.57 & \text{for } \Sigma p_T^V \geq 60 \text{ GeV}/c. \end{cases}$$

A. Check of the SECVTX mistag parametrization

In this section, we test the capability of our model to predict the rate of negative tags in all available generic-jet samples.

Figure 21 serves to illustrate the procedure followed to predict the rates of negative tags. They are evaluated as the sum of the mistags plus the heavy flavor contribution using

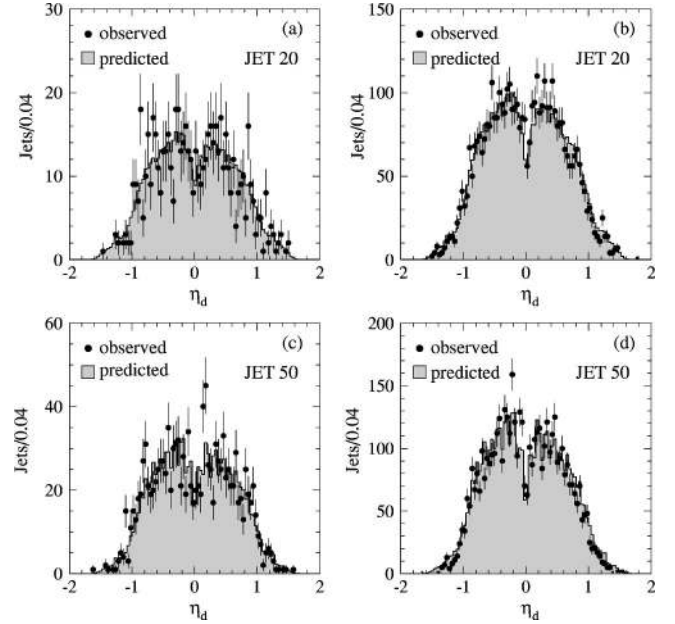


FIG. 19. Pseudorapidity distributions of all jets tagged by SECVTX (\bullet) are compared to the prediction derived using only jets away from calorimeter cracks (shaded histogram) in JET 20 and JET 50 data. (a) and (c) are negative tags; (b) and (d) are positive tags.

the R_1 and R_2 parametrizations derived in the previous section. This procedure requires the knowledge of the fraction of quark and gluon jets as a function of jet- E_T in each data sample (literally, we need to know the fraction of jets containing one or two hadrons with heavy flavor). In the JET 20, JET 50, JET 70, JET 100, ΣE_T 175, and ΣE_T 300 samples we make the assumption, corroborated by the corresponding simulations, that all jets below trigger threshold are gluon jets and all jets above trigger threshold are quark jets.

Figure 21(a) shows the number of observed positive tags and predicted mistags as a function of the jet E_T . Figure 21(b) compares rates of negative tags to the predicted mistags. The mistag rate does not include any heavy flavor contribution and is lower than the observed rate of negative tags. Figure 21(c) compares the rate of mistags and the heavy flavor contribution to the negative tags obtained by multiplying the difference between positive tags and predicted mistags in Fig. 21(a) by R_1 (R_2) if the jet E_T is above (below) the trigger threshold. Figure 21(d) compares the observed and predicted yield of negative tags. The predicted yield of negative tags is derived by adding the two distributions shown in Fig. 21(c).

TABLE XVIII. Fraction of negative tags (%) due to heavy flavor as a function of the E_T of the jet.

Jet E_T (GeV)	SECVTX	JPB	Jet E_T (GeV)	SECVTX	JPB
$0 \leq E_T \leq 20$		10	$80 \leq E_T \leq 100$	6	12
$20 \leq E_T \leq 35$	12	19	$100 \leq E_T \leq 120$	6	12
$35 \leq E_T \leq 50$	10	15	$120 \leq E_T \leq 150$	6	10
$50 \leq E_T \leq 65$	7	13	$150 \leq E_T \leq 180$	5	12
$65 \leq E_T \leq 80$	8	15	$180 \leq E_T$	5	12

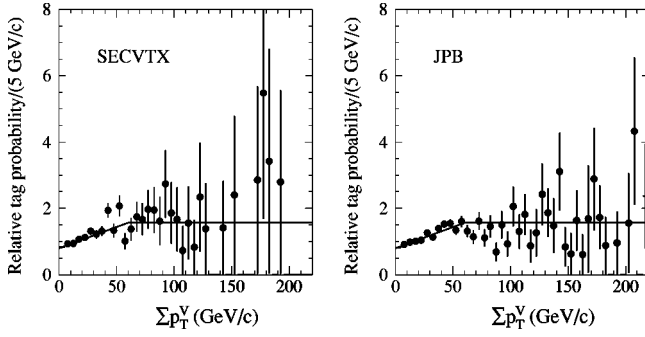


FIG. 20. Yield of the negative tagging probability as a function of Σp_T^V for (a) SECVTX and (b) JPB. The solid line represents an empirical parametrization described in the text.

Following the same procedure, comparisons between the corrected jet E_T distributions of observed and predicted negative SECVTX tags are shown in Figs. 22–24. In the case of the ΣE_T 125 4 CL sample, the ratio of quark to gluon jets (1/6, independent of E_T) is evaluated using the corresponding HERWIG simulation. In the inclusive photon sample, we use only the R_1 parametrization as the simulation shows that the main contribution to tagged jets comes from the γ Compton production.

The inclusive low- p_T electron sample, used to measure the tagging efficiency scale factor, is also a good sample to test the validity of the R_1 and R_2 parametrizations because it is enriched in heavy flavor content. We compare rates of

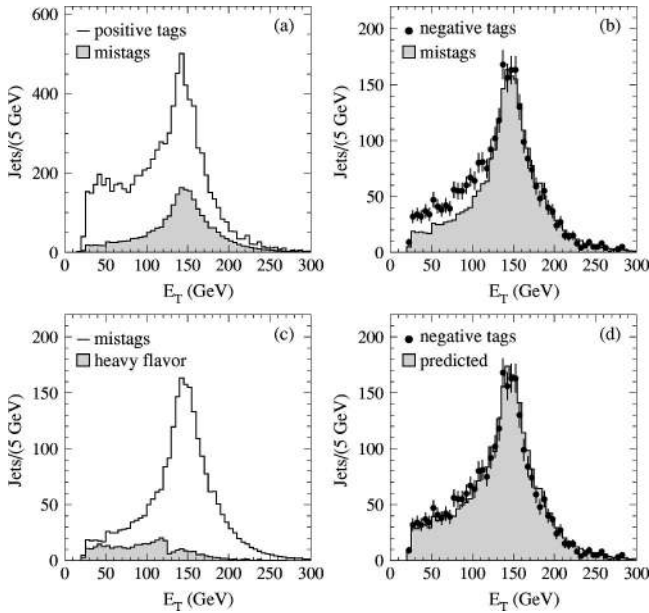


FIG. 21. E_T distributions of jets with SECVTX tags in the JET 100 sample. On (a), observed positive tags (histogram) are compared to the predicted mistags (shaded histograms). On (b), observed negative tags (\bullet) are compared to the predicted mistags (shaded histogram). On (c), predicted mistags (histogram) are compared to the predicted heavy flavor contribution to the negative tags (shaded histograms). On (d), observed negative tags (\bullet) are compared to the sum of the predicted mistags and heavy flavor contribution to the negative tags (shaded histogram).

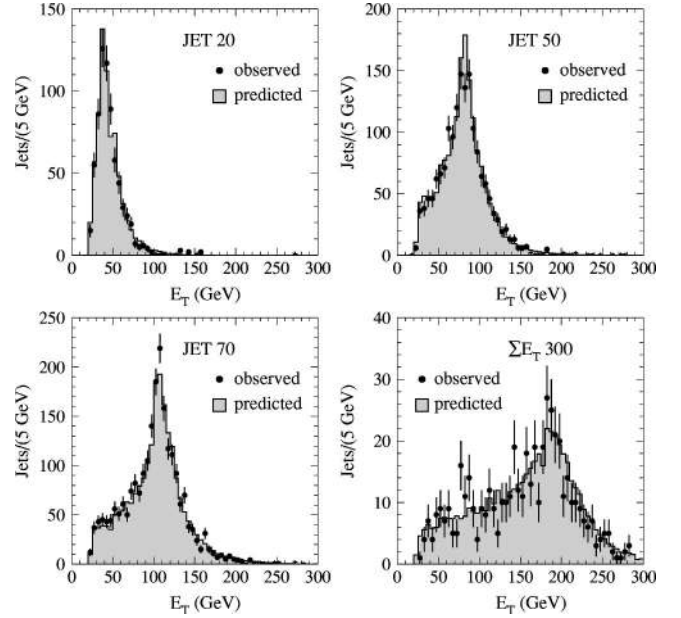


FIG. 22. Transverse energy distributions of jets with negative SECVTX tags. The four data samples were used for the construction of the mistag probability matrix.

observed and predicted negative tags both in the data and in the corresponding HERWIG simulation. The fraction of gluon jets in the simulation is taken from Table XIV and is increased by 40% according to the calibration of the HERWIG simulation performed in Sec. XI. Comparisons between observed and predicted rates of negative tags are shown in Fig. 25 for the data and Fig. 26 for the simulation.

Table XIX summarizes the rates of observed and predicted negative SECVTX tags in all generic-jet samples. Based on the observed agreement a 10% systematic error is assigned to the estimate of the SECVTX mistag probability.

B. Check of the JPB mistag parametrization

We follow the same procedure of the previous section to test the parametrization of the mistag rate of jet-probability. Figures 27–29 compare E_T distributions of observed and predicted jets with negative JPB tags for all generic-jet samples. Rates of JPB tags are summarized in Table XX. As

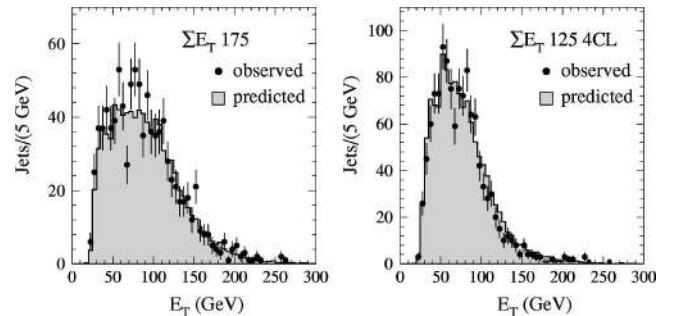


FIG. 23. Transverse energy distributions of jets with negative SECVTX tags in the ΣE_T 175 (a) and ΣE_T 125 4CL (b) samples, which were not used for the construction of the mistag probability matrix.

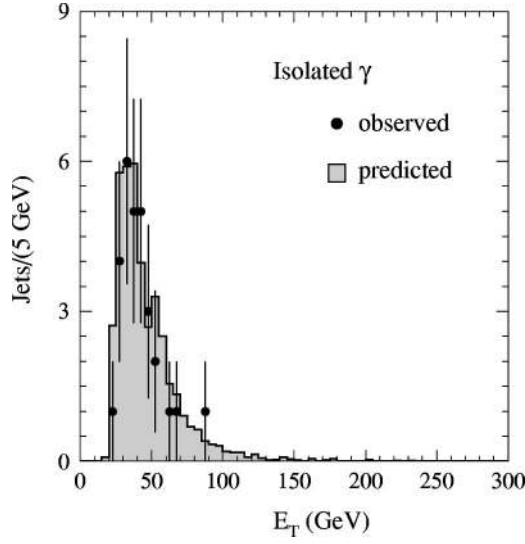


FIG. 24. Transverse energy distributions of jets with negative SECVTX tags in the isolated photon sample.

before, by comparing the observed and predicted number of negative tags, we assign a 10% systematic error to the parametrization of the JPB mistags.

XI. CALIBRATION OF THE FRACTION OF W +JET EVENTS WITH HEAVY FLAVOR

$Wb\bar{b}$ and $Wc\bar{c}$ events are produced through the so-called gluon splitting process, where an initial or final state gluon branches into a heavy quark pair. In this analysis the fraction of W +jet events containing heavy flavor is estimated using

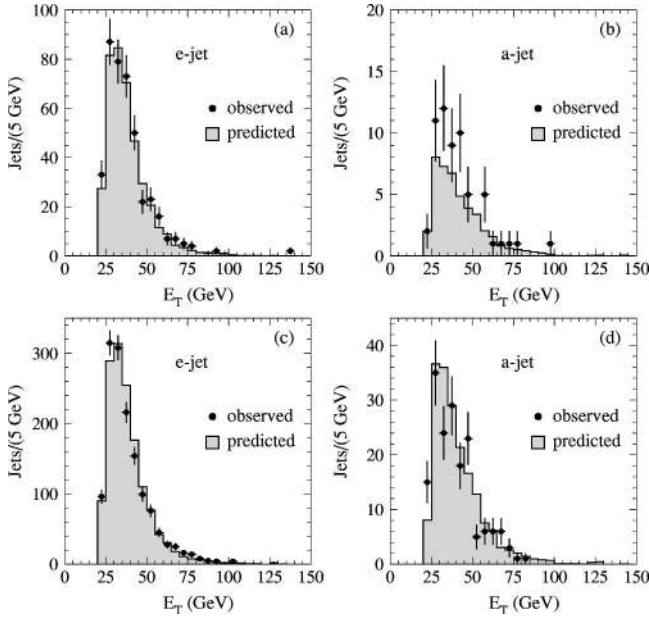


FIG. 25. Transverse energy distributions in the inclusive electron data. In (a) e-jets with a negative SECVTX tag; (b) a-jets with a negative SECVTX tag in events where the e-jet is tagged by SECVTX; (c) e-jets with a negative JPB tag; (d) a-jets with a negative JPB tag in events where the e-jet is tagged by SECVTX.

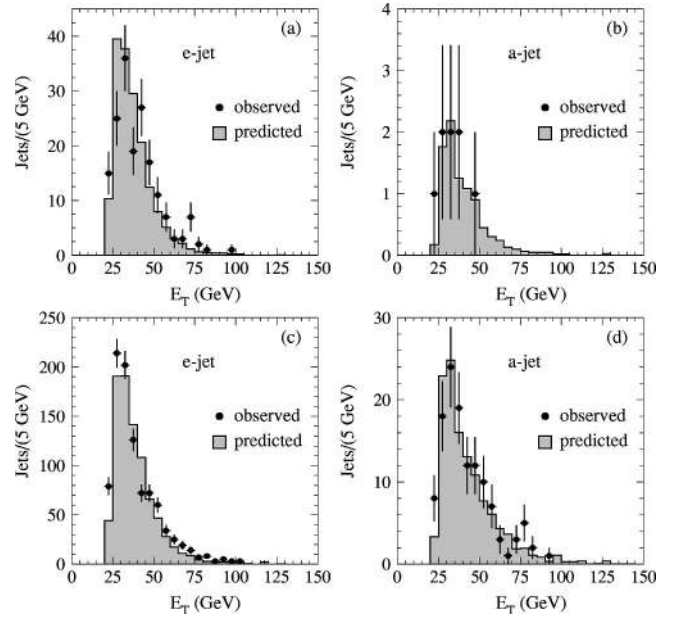


FIG. 26. Transverse energy distributions in the inclusive electron simulation. In (a) e-jets with negative SECVTX tags; (b) a-jets with negative SECVTX tag; (c) e-jets with negative JPB tags; (d) a-jets with negative JPB tag.

the HERWIG generator. The uncertainty in the rate of gluons splitting into heavy quarks based on the parton shower approach is estimated to be approximately 40% in Ref. [31] and approximately 25% in Ref. [32]. Because of this large uncertainty we calibrate the gluon splitting cross section calculated by HERWIG using generic-jet data. Heavy flavor in generic-jet data stems from three primary sources: (1) direct production (e.g., $gg \rightarrow b\bar{b}$); (2) flavor excitation (e.g., $gb \rightarrow gb$); and (3) gluon splitting. The calibration of the simulation package is performed by tuning the various cross sections calculated by HERWIG to reproduce the tagging rate observed in the JET 50 and JET 100 data. In these samples, the gluon splitting contribution is comparable to the other production mechanisms. In the JET 20 simulation, the gluon

TABLE XIX. Numbers of observed positive and negative SECVTX tags in all generic-jet samples. The method for predicting the number of negative tags, P_N , is explained in the text.

Samples used in the mistag parametrization				
Sample	Pos. tags	Neg. tags	Mistags	P_N
JET 20	4731	699	652	722
JET 50	6874	1648	1426	1695
JET 70	7758	2248	1858	2192
JET 100	8335	2723	2385	2756
ΣE_T 300	1507	501	438	521
Independent samples				
ΣE_T 175	3790	947	675	908
ΣE_T 125 4 CL	5637	1203	897	1249
Isolated γ	284	29	35	40

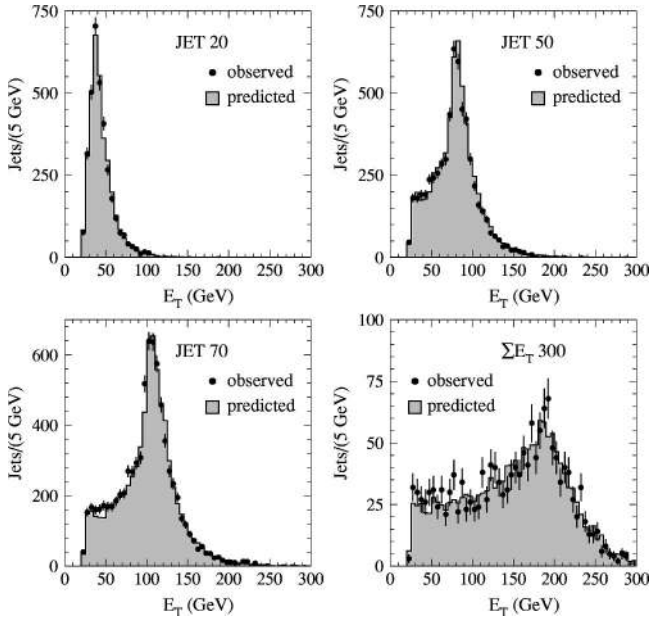


FIG. 27. Transverse energy distributions of jets with a negative JPB tag. The four samples were used for the construction of the mistag probability matrix.

splitting contribution is negligible compared to the other processes; we compare observed and predicted rates of tags in this sample using the tuned simulation as a check that we disentangled correctly the different heavy flavor production mechanisms.

In each generic-jet sample we count the number of SECVTX tags in taggable jets. Mistags are evaluated using the mistag probability evaluated in Sec. X.

The simulated samples (corresponding to the JET 20, JET 50, and JET 100 data) are generated using option 1500 of HERWIG and requiring hard scattering partons with $|\eta| \leq 4.5$ and $p_T^{\min} \geq 10, 40, \text{ and } 80 \text{ GeV}/c$, respectively [23]. We use the MRS(G) set of structure functions [30]. Generated events are simulated with the standard package discussed in Sec. VII. As in the data, we select events containing at least one jet above the trigger threshold.

In the simulation a jet is classified as a b or a c -jet if it contains a b or a c -hadron in a cone of radius 0.4 around its

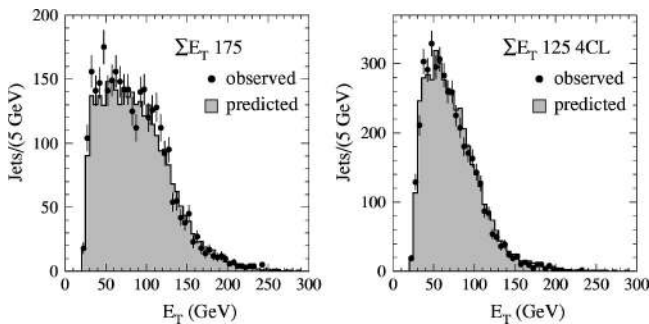


FIG. 28. Transverse energy distributions of jets with negative JPB tags in the $\Sigma E_T 175$ (a) and $\Sigma E_T 125 4 \text{ CL}$ (b) samples, which were not used for the construction of the mistag probability matrix.

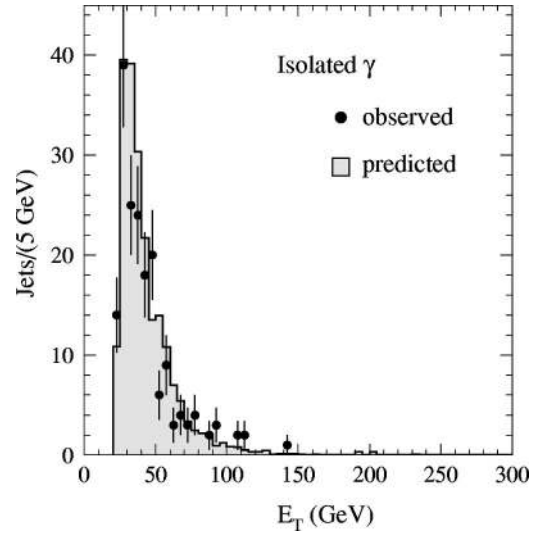


FIG. 29. Transverse energy distributions of jets with negative JPB tags in the isolated photon sample.

axis. Hadrons with heavy flavor resulting from the fragmentation of one of the hard scattering partons are indicative of direct production or flavor excitation (if one of the incoming partons of the hard scattering has heavy flavor we attribute the process to flavor excitation; in this case a second hadron of the same flavor is produced by the backward-evolution of the structure functions). All pairs of hadrons with heavy flavor of the same type which do not come from the hadronization of the hard scattering partons are attributed to gluon splitting. Table XXI lists the rate of jets containing heavy flavor per event in the simulated JET 50 and JET 100 samples.

In the data, we use intuitive kinematical differences in order to distinguish gluon splitting from the rest of the heavy flavor production. Jets from heavy flavor direct production are expected to be produced back-to-back and are more likely to produce double tags. In events produced by heavy flavor excitation, jets produced by the backward-evolution of the structure functions tend to be at large pseudorapidities

TABLE XX. Numbers of observed positive and negative JPB tags in all generic-jet samples. The method for predicting the number of negative tags, P_N , is explained in the text.

Samples used in the parametrization				
Sample	Pos. tags	Neg. tags	Mistags	P_N
JET 20	8418	3414	2919	3421
JET 50	12124	5970	4948	6156
JET 70	13254	7567	6020	7437
JET 100	14528	8827	7010	8721
$\Sigma E_T 300$	2712	1581	1162	1566
Independent samples				
$\Sigma E_T 175$	6217	3235	2227	3069
$\Sigma E_T 125 4 \text{ CL}$	9283	4407	3166	4481
Isolated γ	537	179	176	209

TABLE XXI. Average numbers of jets containing heavy flavor per event in the JET 50 and JET 100 samples generated with HERWIG, split by flavor type and production mechanism.

Sample	direct production+flavor excitation		gluon splitting		Total
	b -jets	c -jets	$g \rightarrow b\bar{b}$	$g \rightarrow c\bar{c}$	
JET 50	2.14×10^{-2}	3.04×10^{-2}	1.67×10^{-2}	3.79×10^{-2}	10.64×10^{-2}
JET 100	2.15×10^{-2}	2.89×10^{-2}	2.58×10^{-2}	5.73×10^{-2}	13.35×10^{-2}

and out of the SVX acceptance. On the other hand, gluon splitting produces pairs of jets with heavy flavor at small separation $\Delta R = \sqrt{(\Delta\phi)^2 + (\Delta\eta)^2}$. Most of the time the two hadrons with heavy flavor produced by gluon splitting reside in the same jet. Figure 30 shows distributions of the distance between two b -jets for the different production mechanisms in a simulated sample. In addition, the relative gluon splitting contribution increases with the jet multiplicity.

This motivates us to compare data and simulation in the following classes of SECVTX tags:

- (1) number of tagged jets per event with at least one taggable jet;
- (2) number of tagged jets per event with at least one taggable jet and with three or more jets with $E_T \geq 15$ GeV and $|\eta| \leq 2$;
- (3) twice the number of events with two tagged jets per event with two or more taggable jets.

We also compare the data to the simulation for:

- (4) the fraction of (1) in which the tagged jet has a companion jet with $E_T \geq 10$ GeV in a cone of radius 1.2 around its axis;

- (5) the fraction of events with double tags where the two tagged jets are at a distance $\Delta R \leq 1.2$. Table XXII lists the yields of these tags in the data and in the simulation.

In the simulation, one notes that after tagging with SECVTX the contribution of c -jets is reduced by more than a factor of four and becomes negligible in events with double tags. However, the ratio of double to single SECVTX tags does not discriminate between $b\bar{b}$ and $c\bar{c}$ production for this ratio is similarly small for $b\bar{b}$ production through flavor excitation and gluon splitting.

We discriminate the flavor type with the additional comparison of rates of JPB tags (JPB has about the same tagging efficiency of SECVTX for b -jets and is more than twice as efficient for tagging c -jets). Since we use JPB tags only to disentangle between b and c -production, we compare data and simulations in only two classes of JPB tags:

- (6) number of tagged jets per event with at least one taggable jet;
- (7) twice the number of events with two tagged jets per event with two or more taggable jets. Table XXIII lists the yields of JPB tags in the data and in the simulation.

We fit the data with the simulation in order to evaluate the correction for the simulated rates of $g \rightarrow b\bar{b}$ and $g \rightarrow c\bar{c}$. When fitting the simulation to the data, the yield of simulated SECVTX and JPB tags is corrected for the tagging efficiency scale factors measured in Sec. IX. The 10% uncertainty in the scale factor determination is included in the error of the

simulated rates of tags. In the fit, we also compare five distributions in each generic-jet sample and in the corresponding simulation:

- (1) the yield of the fraction of SECVTX tags per taggable jet as a function of the jet- E_T .
- (2) The distributions of the distance ΔR between a jet tagged by SECVTX and a companion jet as defined above.
- (3) The distributions of the distance ΔR between a jet tagged by JPB and a companion jet as defined above.
- (4) The distributions of the distance ΔR between two jets tagged by SECVTX.
- (5) The distributions of the distance ΔR between two jets tagged by JPB.

In the comparison, the area of each distribution is normalized to unity. For each distribution we compute a reduced χ^2

$$\chi_D^2 = \frac{1}{N} \sum_{i=1}^N \frac{[d(i) - sd(i)]^2}{ed(i)^2 + esd(i)^2}$$

where N is the number of bins in each distribution, $d(i)$ and

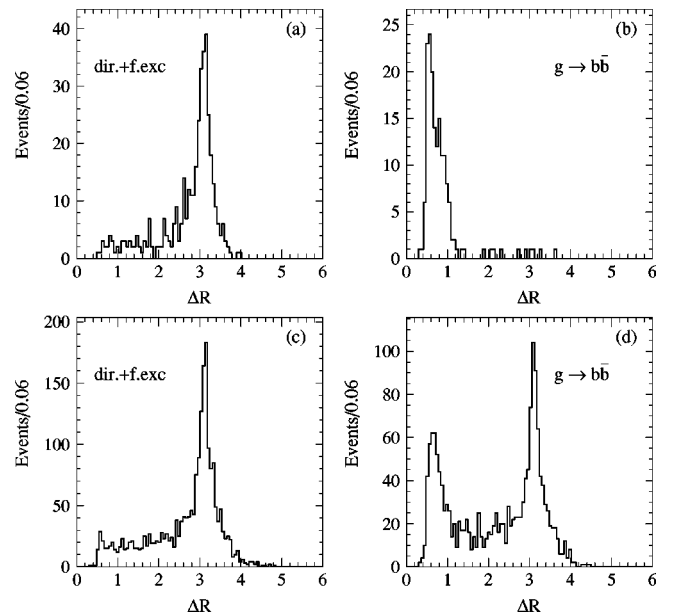


FIG. 30. Distributions of the distance ΔR between two b -jets tagged by SECVTX in JET 50 simulated events contributed by (a) direct production and flavor excitation or (b) gluon splitting. (c) and (d) are the distributions of the distance between a b -jet tagged by SECVTX and the closest jet in the event with $E_T \geq 10$ GeV.

TABLE XXII. Yields ($\times 10^{-3}$) of SECVTX tags in generic-jet data and in simulated samples generated with HERWIG. Rows 1, 2, and 3 represent the average number of tags per event; rows 4 and 5 represent the fraction of 1 and 3, respectively. Rates of simulated tags are not yet corrected for the tagging efficiency scale factor measured in Sec. IX.

		JET 50					
		direct production		flavor excitation		gluon splitting	
Class	Data	b -jets	c -jets	b -jets	c -jets	$g \rightarrow b\bar{b}$	$g \rightarrow c\bar{c}$
1	34.20 ± 1.05	2.90 ± 0.11	0.72 ± 0.02	6.53 ± 0.17	2.63 ± 0.11	7.37 ± 0.18	4.17 ± 0.14
2	43.00 ± 1.37	2.31 ± 0.16	0.53 ± 0.08	6.36 ± 0.26	2.26 ± 0.16	9.71 ± 0.33	5.32 ± 0.24
3	7.50 ± 0.65	2.00 ± 0.18	0.16 ± 0.04	0.94 ± 0.13	0.07 ± 0.03	0.65 ± 0.10	0.09 ± 0.02
4	5.60 ± 0.38	0.23 ± 0.03	0.04 ± 0.01	0.71 ± 0.06	0.25 ± 0.03	2.17 ± 0.10	0.86 ± 0.06
5	0.58 ± 0.08	0.00 ± 0.08	0.00	0.08 ± 0.03	0.00	0.26 ± 0.05	0.00

		JET 100					
		direct production		flavor excitation		gluon splitting	
Class	Data	b -jets	c -jets	b -jets	c -jets	$g \rightarrow b\bar{b}$	$g \rightarrow c\bar{c}$
1	42.05 ± 1.84	4.31 ± 0.22	1.23 ± 0.12	5.57 ± 0.25	2.24 ± 0.16	11.85 ± 0.37	6.88 ± 0.28
2	51.50 ± 2.04	3.51 ± 0.27	0.86 ± 0.13	5.71 ± 0.35	1.97 ± 0.20	15.06 ± 0.56	8.40 ± 0.42
3	15.50 ± 0.92	2.68 ± 0.29	0.26 ± 0.09	1.08 ± 0.18	0.05 ± 0.03	1.42 ± 0.21	0.10 ± 0.05
4	6.36 ± 0.41	0.64 ± 0.09	0.09 ± 0.03	0.97 ± 0.10	0.31 ± 0.06	5.03 ± 0.24	2.10 ± 0.15
5	1.10 ± 0.11	0.00 ± 0.03	0.00	0.06 ± 0.03	0.00	0.54 ± 0.09	0.00

$sd(i)$ are the contents of the bin i of the distribution in the data and in the simulation, respectively, with $ed(i)$ and $esd(i)$ their errors. The simulated jet- E_T distributions have a systematic uncertainty due to the trigger simulation which is cumbersome to account for in the fit. Simulated distributions of distances between tagged jets have systematic uncertainties due to how well the parton shower generator models gluon splitting at distances $\Delta R \geq 1.2$. We use the reduced χ_D to diminish the importance of these comparisons with respect to the classes of absolute tagging rates. The data are fitted to the simulation using a minimum χ^2 method. We minimize the function

$$\chi^2 = \sum_{\text{JET50}}^{\text{JET100}} \left(\sum_{j=1}^7 \frac{[D(j) - S(j)]^2}{ED(j)^2 + ES(j)^2} + \sum_{k=1}^5 \chi_D^k \right)$$

TABLE XXIII. Fractions ($\times 10^{-3}$) of JPB tags per event in generic-jet data and in simulated samples generated with HERWIG. Fractions of tags are not yet corrected for the tagging efficiency scale factor measured in Sec. IX.

		JET 50					
		direct production		flavor excitation		gluon splitting	
Class	Data	b -jets	c -jets	b -jets	c -jets	$g \rightarrow b\bar{b}$	$g \rightarrow c\bar{c}$
6	45.20 ± 3.19	3.84 ± 0.13	1.87 ± 0.09	7.97 ± 0.19	6.28 ± 0.17	9.11 ± 0.21	8.67 ± 0.20
7	4.75 ± 0.28	1.62 ± 0.12	0.26 ± 0.05	0.81 ± 0.09	0.23 ± 0.05	0.89 ± 0.09	0.52 ± 0.06

		JET 100					
		direct production		flavor excitation		gluon splitting	
Class	Data	b -jets	c -jets	b -jets	c -jets	$g \rightarrow b\bar{b}$	$g \rightarrow c\bar{c}$
6	53.07 ± 5.09	5.72 ± 0.26	2.66 ± 0.18	6.86 ± 0.29	5.69 ± 0.26	14.22 ± 0.42	13.13 ± 0.40
7	5.50 ± 0.34	2.11 ± 0.19	0.39 ± 0.08	0.78 ± 0.11	0.25 ± 0.06	1.69 ± 0.17	1.06 ± 0.13

where the index k runs over the 5 kinematic distributions described in the previous paragraph, $D(j)$ are the yields of tags observed in the data for the seven classes listed in Tables XXII and XXIII, and

$$S(j) = \sum_{n=1}^6 P(n) \times C_H(j, n) * SF^\alpha$$

is the corresponding yield of simulated tags. The contributions $C_H(j, n)$ of different flavor types and production mechanisms, as listed in Tables XXII and XXIII, are weighted with the fit parameters $P(n)$. SF is the tagging efficiency scale factor and $\alpha=0$ for c -jet, 1 for events with one tagged b -jet, and 2 for events with two tagged b -jets.

In the fit, the b -to- c ratio for direct production is constrained to the default value with a 14% Gaussian error. Op-

TABLE XXIV. Results of the fit of the HERWIG simulation to the JET 50 and JET 100 data (see text).

Process	Cross section weight
b direct production+flavor excitation	1.09 ± 0.15
$g \rightarrow b\bar{b}$	1.40 ± 0.19
b Total	1.22 ± 0.12
c direct production+flavor excitation	1.12 ± 0.28
$g \rightarrow c\bar{c}$	1.35 ± 0.36
c Total	1.25 ± 0.20
$b+c$ direct production+flavor excitation	1.11 ± 0.16
$g \rightarrow b\bar{b}, c\bar{c}$	1.36 ± 0.22
$b+c$ Total	1.24 ± 0.12

tion 1500 of HERWIG evaluates the direct production cross section of massless quarks. The 14% uncertainty accounts for having neglected the quark masses (estimated using option 1700 of HERWIG) and for the uncertainty in the fragmentation process (estimated using the PYTHIA generator).

The b -to- c ratio for flavor excitation is also constrained to the default value with a 28% Gaussian error. This uncertainty accounts for the largest variation of this ratio observed using a wide range of structure functions in the PDF library [33].

The ratio of the $g \rightarrow b\bar{b}$ to $g \rightarrow c\bar{c}$ is also constrained to the default value with a 28% Gaussian error. The uncertainty accounts for a ± 0.5 GeV change of the b and c -quark masses around the default value.

The fit has 21 degrees of freedom and yields a χ^2 of 22. The fit results are shown in Table XXIV. The weights of the gluon splitting cross sections will be used to rescale the fraction of W +jet events with heavy flavor predicted by HERWIG. These rescaling factors are of the same size as those measured by the SLC and LEP experiments for the rate of $g \rightarrow b\bar{b}$ and $g \rightarrow c\bar{c}$ in Z decays [34], and are consistent with the estimated theoretical uncertainties [31,32].

Figure 31 compares the E_T distributions of tagged jets in the data and in the fitted simulation. Similarly, Figs. 32 and 33 compare distributions of distances between tagged jets.

Table XXV compares rates of tags in generic-jet data and in the HERWIG simulation calibrated according to Table XXIV. The JET 20 sample was not used to calibrate the simulation package. Similarly, the SLT algorithm was not used in the HERWIG calibration. The comparison of the number of SLT tags in the data and in the simulation serves to check independently the calibration of the HERWIG production cross section and the SLT tagging efficiency in the simulation.

XII. COMPOSITION OF THE $W+\geq 1$ JET SAMPLE

The background to the $t\bar{t}$ production is determined using the data or the simulation calibrated as described in Secs. IX and XI. The $t\bar{t}$ production cross section is determined by attributing the excess of tagged $W+\geq 3$ jet events to $t\bar{t}$ production. $W+1$ and $W+2$ jet events provide a check of the background calculation. The evaluation of the backgrounds

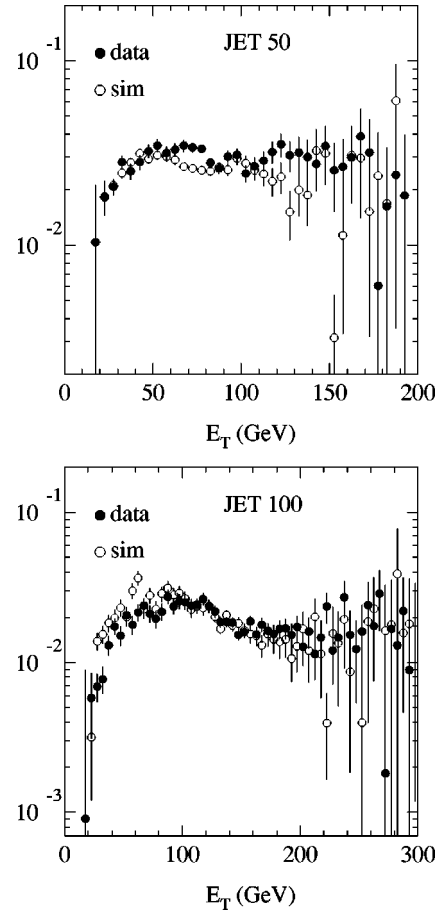


FIG. 31. Fractions of taggable jets with a SECVTX tag as a function of jet E_T in the data and in the fitted simulation. The distributions of the data and the fitted simulation are normalized to unit area.

to $t\bar{t}$ events is detailed in the subsections A–H. The results of these background determinations are listed in Sec. XV where the cross section is calculated. The following two Secs. XIII and XIV provide checks of these background estimates.

A. Non- W background

As in previous analyses [35], the background from non- W sources, including $b\bar{b}$ production, is determined directly from the data by studying the isolation of primary lepton candidates in the low ($\cancel{E}_T \leq 10$ GeV) and in the high ($\cancel{E}_T \geq 20$ GeV) \cancel{E}_T region. The number of non- W events in each jet-bin is evaluated as

$$N_{\text{non-}W} = N_C \times \frac{N_A}{N_B}$$

where N_A , N_B , and N_C are the number of events in regions A, B, and C of Fig. 34. The corresponding number of tagged events is

$$N_{\text{non-}W}^{\text{tag}} = N_{\text{non-}W} \times P^{\text{tag}}$$

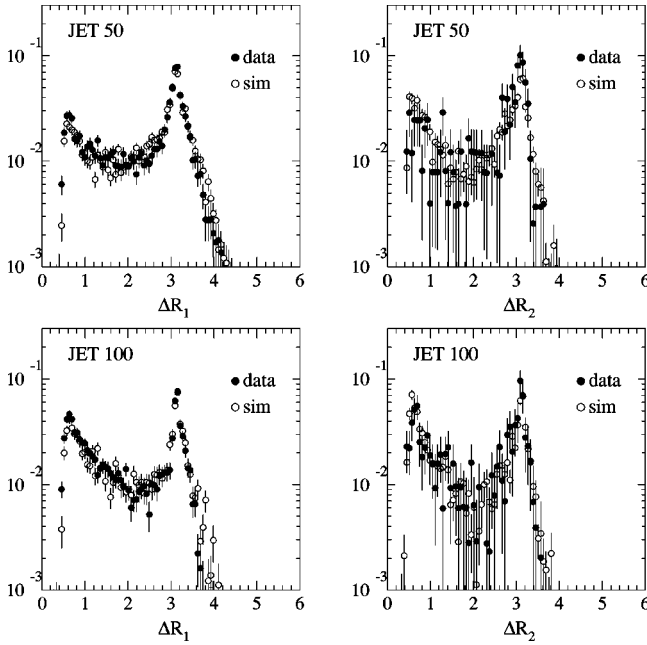


FIG. 32. Distributions of the distance ΔR_1 between a jet tagged by SECVTX tag and the closest jet in the event and of the distance ΔR_2 between two jets tagged by SECVTX. The distributions of the data and the fitted simulation are normalized to unit area.

where P^{tag} is the tagging probability measured in region A. The yield of P^{tag} as a function of the lepton isolation is shown in Fig. 35.

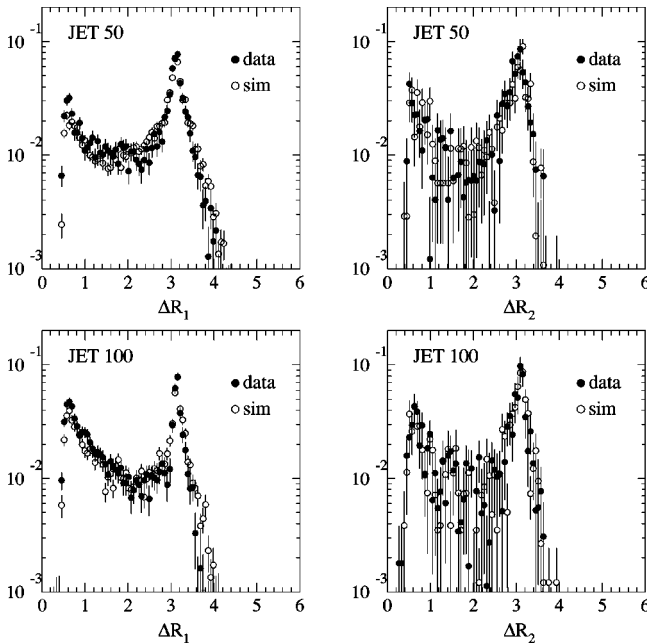


FIG. 33. Distributions of the distance ΔR_1 between a jet with a JPB tag and the closest jet in the event and of the distance ΔR_2 between two jets with a JPB tag. The distributions of the data and the fitted simulation are normalized to unit area.

TABLE XXV. Number of tagged jets with heavy flavor in generic-jet data and in the calibrated HERWIG simulation. Data and simulation are normalized to the same number of events. The second and third columns list the number of tags and removed mistags in the data.

JET 20 (194 009 events)				
Tag type	Tags	Mistags	Data	Simulation
SECVTX	4674	616	4058 ± 92	4052 ± 143
JPB	8343	2801	5542 ± 295	5573 ± 173
SLT	4994	3962	1032 ± 402	826 ± 122
JET 50 (151 270 events)				
Tag type	Tags	Mistags	Data	Simulation
SECVTX	6536	1360	5176 ± 158	5314 ± 142
JPB	11533	4700	6833 ± 482	6740 ± 171
SLT	6408	5241	1167 ± 530	1116 ± 111
JET 100 (129 434 events)				
Tag type	Tags	Mistags	Data	Simulation
SECVTX	7682	2227	5455 ± 239	5889 ± 176
JPB	13365	6494	6871 ± 659	7263 ± 202
SLT	7483	6367	1116 ± 642	1160 ± 168

B. $Z \rightarrow \tau^+ \tau^-$ events

The $Z \rightarrow \tau^+ \tau^-$ contributions is estimated using the PYTHIA generator (option MSEL=13). The simulation is normalized to the same number of $Z \rightarrow \mu^+ \mu^-, e^+ e^-$ events observed in the data for each jet-bin.

C. Single top quark production

The single top quark contribution via the W -gluon fusion channel is estimated with HERWIG using the process 2000. The single top production for the annihilation process $q\bar{q} \rightarrow W^* \rightarrow t\bar{b}$ is estimated using the PYTHIA generator (option MSEL=12). We use the cross sections $\sigma_{W-g} = 1.5 \pm 0.4$ pb

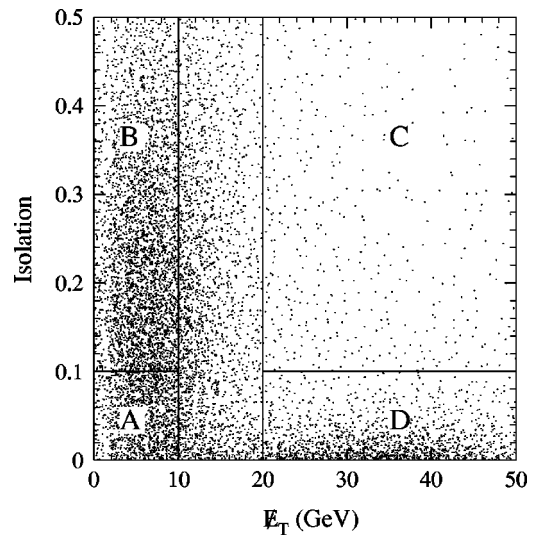


FIG. 34. Distributions of the primary lepton isolation vs E_T in $W + \geq 1$ jet candidate events. The three regions A, B, C are used to evaluate the non- W contribution in the region D, which defines the W signal.

TABLE XXVI. Fraction of $W+\geq 1$ jet events with heavy flavor jets as a function of the jet multiplicity.

Sample	$Wb\bar{b}$		$Wc\bar{c}$	
	F_1^b (%)	F_2^b (%)	F_1^c (%)	F_2^c (%)
$W+1$ jet	0.80 ± 0.11		2.01 ± 0.54	
$W+2$ jet	1.28 ± 0.18	1.20 ± 0.38	3.73 ± 1.00	1.40 ± 0.52
$W+3$ jet	1.88 ± 0.31	1.90 ± 0.62	5.31 ± 1.48	2.30 ± 0.91
$W+\geq 4$ jet	3.54 ± 1.06	2.40 ± 0.77	6.08 ± 2.45	3.00 ± 1.13

for $W-g$ fusion derived using the NLO calculation in Ref. [36] and $\sigma_{W^* \rightarrow t\bar{b}} = 0.74 \pm 0.05$ pb for the annihilation process [36].

D. Diboson production

The contribution of the ZZ , WZ , and WW production is estimated using the PYTHIA generator (options MSEL=15 and ISUB=22, 23, and 25, respectively). We use the cross sections $\sigma(WW) = 9.5 \pm 0.7$ pb, $\sigma(WZ) = 2.6 \pm 0.34$ pb, and $\sigma(ZZ) = 1.0 \pm 0.2$ pb [37].

E. Mistags

The SECVTX and SLT mistags are calculated weighting each jet in the W sample with the mistag probability matrices derived in Sec. X and Sec. VIII C 2, respectively. The re-evaluation of the SECVTX mistag matrix has resulted in a reduced estimate of this background in the signal region by $(50 \pm 5)\%$ compared with the previous estimates of Refs. [2,3].

For the jet-probability algorithm, each simulated background also includes the contribution of mistags. The number of JPB mistags is evaluated only for the fraction of W + jet events which is not simulated, i.e., W + jet direct production without heavy flavor.

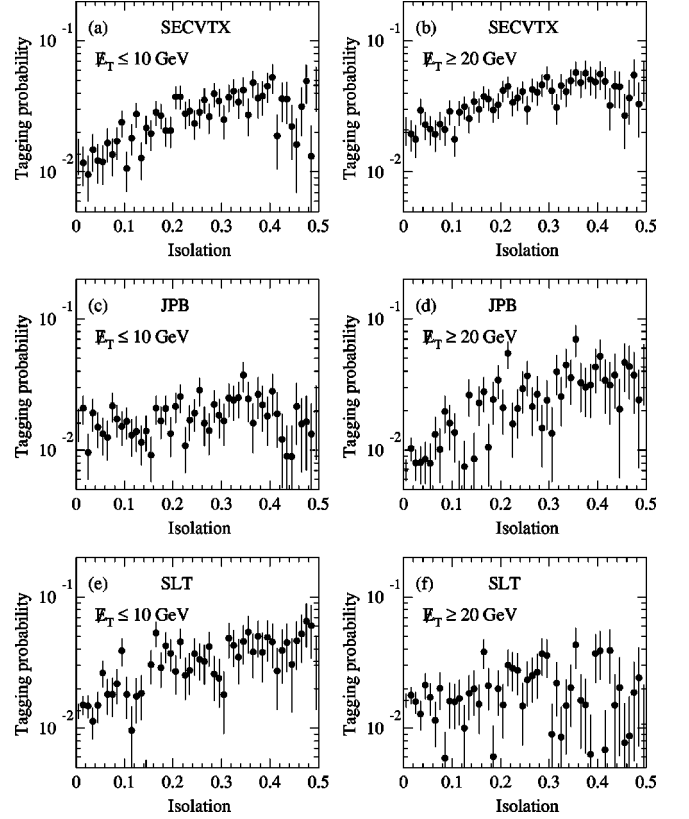


FIG. 35. The tagging probability as a function of the isolation of the primary lepton.

F. The $W+b\bar{b}$ and $W+c\bar{c}$ contribution

We use the HERWIG generator (process 2100 with hard scattering $p_T^{\min} \geq 10$ GeV/ c) to estimate the fraction of $W+\geq n$ jet events, F_1^α , in which only one jet contains hadrons with heavy flavor resulting from gluon splitting (α refers to the flavor type). The fraction of $W+\geq 2$ jet events, F_2^α , in which two different jets contain hadrons with heavy flavor is calculated using the VECBOS generator (see Sec. VI). The

TABLE XXVII. Tagging efficiencies (ε) in $Wb\bar{b}$ and $Wc\bar{c}$ simulated events.

Sample	$Wb\bar{b}$		SECVTX			
	$\varepsilon_{1\text{tag}}^{1b}$ (%)	$\varepsilon_{1\text{tag}}^{2b}$ (%)	$\varepsilon_{2\text{tag}}^{2b}$ (%)	$\varepsilon_{1\text{tag}}^{1c}$ (%)	$\varepsilon_{1\text{tag}}^{2c}$ (%)	$\varepsilon_{2\text{tag}}^{2c}$ (%)
$W+1$ jet	24.6 ± 0.8			4.56 ± 0.29		
$W+2$ jet	21.6 ± 1.7	45.8 ± 1.8	10.6 ± 1.2	3.59 ± 0.49	11.7 ± 1.1	0.4 ± 0.2
$W+\geq 3$ jet	20.6 ± 4.4	46.8 ± 4.0	10.7 ± 2.8	3.59 ± 1.26	14.3 ± 2.3	0.0 ± 0.0
Sample	$Wb\bar{b}$		JPB			
	$\varepsilon_{1\text{tag}}^{1b}$ (%)	$\varepsilon_{1\text{tag}}^{2b}$ (%)	$\varepsilon_{2\text{tag}}^{2b}$ (%)	$\varepsilon_{1\text{tag}}^{1c}$ (%)	$\varepsilon_{1\text{tag}}^{2c}$ (%)	$\varepsilon_{2\text{tag}}^{2c}$ (%)
$W+1$ jet	23.8 ± 0.7			9.8 ± 0.4		
$W+2$ jet	20.3 ± 1.4	40.7 ± 1.5	10.0 ± 0.9	7.8 ± 0.7	25.0 ± 1.4	2.8 ± 0.5
$W+\geq 3$ jet	21.7 ± 3.8	43.2 ± 3.4	9.3 ± 1.9	13.0 ± 2.2	25.6 ± 2.9	1.7 ± 0.8
Sample	$Wb\bar{b}$		SLT			
	$\varepsilon_{1\text{tag}}^{1b}$ (%)	$\varepsilon_{1\text{tag}}^{2b}$ (%)	$\varepsilon_{2\text{tag}}^{2b}$ (%)	$\varepsilon_{1\text{tag}}^{1c}$ (%)	$\varepsilon_{1\text{tag}}^{2c}$ (%)	$\varepsilon_{2\text{tag}}^{2c}$ (%)
$W+1$ jet	7.7 ± 0.9			3.7 ± 0.5		
$W+2$ jet	6.9 ± 1.2	13.2 ± 1.7	0.6 ± 0.3	3.7 ± 0.6	6.2 ± 1.0	0.1 ± 0.1
$W+\geq 3$ jet	7.1 ± 2.6	9.6 ± 2.3	0.5 ± 0.5	5.2 ± 1.6	8.0 ± 2.0	0.0 ± 0.0

TABLE XXVIII. Fractions of Wc events.

Sample	F_{Wc} (%)
$W+1$ jet	4.8 ± 1.4
$W+2$ jet	7.2 ± 2.2
$W+3$ jet	7.5 ± 2.3
$W+\geq 4$ jet	7.5 ± 2.3

fractions of W +jet events with heavy flavor content are listed in Table XXVI. We use the HERWIG and VECBOS simulations also to determine the efficiency for finding events with one or two tagged jets, as listed in Table XXVII.

It follows that the number of tagged $Wb\bar{b}$ and $Wc\bar{c}$ events are

$$N_{1\text{tag}}^\alpha = N_W \times (F_1^\alpha \times \varepsilon_{1\text{tag}}^{1\alpha} + F_2^\alpha \times \varepsilon_{1\text{tag}}^{2\alpha})$$

$$N_{2\text{tag}}^\alpha = N_W \times F_2^\alpha \times \varepsilon_{2\text{tag}}^{2\alpha}$$

where N_W is the number of W events in the data after removing the predicted number of non- W , di-boson, single top, unidentified Z and $t\bar{t}$ events.

G. The Wc contribution

The fraction F_{Wc} of $gs \rightarrow Wc$ and $gd \rightarrow Wc$ events is evaluated using the HERWIG simulation and is shown in Table XXVIII. The estimated uncertainty on F_{Wc} which is dominated by the uncertainty in the strange sea content of the proton, has been evaluated by examining a wide range of different structure functions in Ref. [5]. The tagging efficiencies for this process are listed in Table XXIX.

H. Direct production of Z +jet with heavy flavor

We use the PYTHIA generator (option MSEL=13) to estimate the number of unidentified Z +jet events passing our selection. The simulation is normalized to the number of $Z \rightarrow ll$ observed in the data for each jet-bin. We would like to use a simulation calibrated using the data to evaluate the fraction of Z +jet events containing heavy flavor. The HERWIG generator was tuned using generic-jet data (see Sec. XI), but the HERWIG version used in this analysis does not contain the $Z+1$ jet matrix element. Therefore, we first estimate the ratio of the fraction of Z +jet events which contain heavy flavor to the fraction of W +jet events which contain heavy flavor by using the PYTHIA simulation which has both $Z+1$ and $W+1$ jet matrix elements. We find that the fraction of Zc events is 30% of the fraction of Wc events, the fractions of

TABLE XXIX. Tagging efficiencies in Wc events.

Sample	$\varepsilon_{Wc}^{\text{SEC}}$ (%)	$\varepsilon_{Wc}^{\text{JPB}}$ (%)	$\varepsilon_{Wc}^{\text{SLT}}$ (%)
$W+1$ jet	4.1 ± 0.4	8.7 ± 0.4	3.3 ± 0.4
$W+2$ jet	4.2 ± 0.6	10.8 ± 1.0	5.2 ± 0.7
$W+\geq 3$ jet	4.5 ± 0.6	16.7 ± 2.9	6.9 ± 2.0

TABLE XXX. Composition of the $Z+\geq 1$ jet sample before tagging. We use $\sigma_{t\bar{t}} = 5$ pb from Ref. [1].

Source	$Z+1$ jet	$Z+2$ jet	$Z+3$ jet	$Z+\geq 4$ jet
Data	1148	159	16	4
WW	0.8 ± 0.2	0.2 ± 0.1	0.0 ± 0.0	0.0 ± 0.0
WZ	2.2 ± 0.5	1.7 ± 0.4	0.3 ± 0.1	0.1 ± 0.0
ZZ	1.2 ± 0.3	1.6 ± 0.4	0.3 ± 0.1	0.0 ± 0.0
Zc	16.5 ± 4.9	3.3 ± 1.0	0.3 ± 0.1	0.1 ± 0.0
$Zb\bar{b}$	18.3 ± 2.5	7.6 ± 1.3	1.1 ± 0.2	0.4 ± 0.1
$Zc\bar{c}$	23.0 ± 6.1	7.9 ± 1.7	1.1 ± 0.3	0.3 ± 0.1
Z +jet without h.f.	1085.3 ± 8.3	135.3 ± 2.5	12.2 ± 0.4	2.9 ± 0.1
Single top quark	0.1 ± 0.0	0.0 ± 0.0	0.0 ± 0.0	0.0 ± 0.0
$t\bar{t}$	0.6 ± 0.1	1.4 ± 0.3	0.5 ± 0.1	0.2 ± 0.0

$Zc\bar{c}$ and $Wc\bar{c}$ events are the same, and the fraction of $Zb\bar{b}$ events is a factor of two larger than the fraction of $Wb\bar{b}$ events. The fraction of Z +jet events with heavy flavor is then estimated multiplying by the above factors the fraction of W +jet events with heavy flavor listed in Table XXVI.

XIII. CHECK OF THE BACKGROUND CALCULATION USING THE $Z+\geq 1$ JET SAMPLE

The production mechanisms of W and Z bosons in association with jets are very similar and the $t\bar{t}$ contribution to the Z +jet events is negligible. This sample provides a good benchmark for our background calculation. The selection of the $Z+\geq 1$ jet event sample is described in Sec. IV A. Table XXX shows the predicted composition of the $Z+\geq 1$ jet sample before tagging. In this table, the number of Z +jet events without heavy flavor is derived from the data by subtracting the WW , WZ , ZZ , $t\bar{t}$, and single top quark contribution. The measured and predicted rates of events with SECVTX, JPB, and SLT tags are shown in Tables XXXI–XXXIII. The product of the probabilities that the ob-

TABLE XXXI. Summary of observed and predicted number of Z events with one (ST) and two (DT) SECVTX tags.

Source	$Z+1$ jet	$Z+2$ jet	$Z+3$ jet	$Z+\geq 4$ jet
Mistags	1.27 ± 0.13	0.34 ± 0.03	0.08 ± 0.01	0.01 ± 0.01
WW , WZ , ZZ	0.09 ± 0.03	0.18 ± 0.05	0.03 ± 0.01	0.00 ± 0.00
Zc	0.67 ± 0.21	0.15 ± 0.05	0.02 ± 0.00	0.00 ± 0.00
$Zc\bar{c}$, $Zb\bar{b}$ (ST)	5.56 ± 0.70	2.59 ± 0.46	0.40 ± 0.08	0.14 ± 0.03
$Zc\bar{c}$, $Zb\bar{b}$ (DT)		0.39 ± 0.13	0.06 ± 0.03	0.02 ± 0.01
Single top quark	0.01 ± 0.01	0.00 ± 0.00	0.00 ± 0.00	0.00 ± 0.00
$t\bar{t}$ (ST)	0.22 ± 0.05	0.44 ± 0.09	0.20 ± 0.05	0.03 ± 0.01
$t\bar{t}$ (DT)		0.23 ± 0.06	0.07 ± 0.02	0.03 ± 0.01
Prediction (ST)	7.83 ± 0.74	3.70 ± 0.47	0.73 ± 0.10	0.20 ± 0.03
Prediction (DT)		0.62 ± 0.14	0.13 ± 0.03	0.04 ± 0.01
Data (ST)	10	3	0	1
Data with (DT)		2	0	0

TABLE XXXII. Summary of observed and predicted number of Z events with one (ST) and two (DT) JPB tags.

Source	$Z+1$ jet	$Z+2$ jet	$Z+3$ jet	$Z+\geq 4$ jet
Mistags	5.65 ± 0.57	1.51 ± 0.15	0.34 ± 0.04	0.05 ± 0.01
WW, WZ, ZZ	0.13 ± 0.03	0.24 ± 0.06	0.02 ± 0.01	0.02 ± 0.01
Zc	1.39 ± 0.44	0.35 ± 0.11	0.05 ± 0.02	0.01 ± 0.00
$Zc\bar{c}, Zb\bar{b}$ (ST)	6.63 ± 0.87	2.85 ± 0.45	0.50 ± 0.09	0.17 ± 0.03
$Zc\bar{c}, Zb\bar{b}$ (DT)		0.42 ± 0.13	0.06 ± 0.02	0.02 ± 0.01
Single top quark	0.01 ± 0.00	0.00 ± 0.00	0.00 ± 0.00	0.00 ± 0.00
$t\bar{t}$ (ST)	0.17 ± 0.02	0.43 ± 0.06	0.19 ± 0.03	0.04 ± 0.01
$t\bar{t}$ (DT)		0.17 ± 0.02	0.06 ± 0.01	0.03 ± 0.00
Prediction (ST)	13.98 ± 1.13	5.37 ± 0.49	1.11 ± 0.10	0.30 ± 0.04
Prediction (DT)		0.59 ± 0.13	0.12 ± 0.02	0.05 ± 0.01
Data (ST)	11	5	1	2
Data (DT)		0	0	0

served number of tags in each of the four jet bins is a Poisson fluctuation of the prediction is $P_0=1.2\times 10^{-3}$ for Table XXXI, $P_0=2.1\times 10^{-4}$ for Table XXXII, and $P_0=1.0\times 10^{-3}$ for Table XXXIII. With a Monte Carlo simulation, in which we fluctuate the predicted rates by their uncertainty according to a Gaussian distribution, we estimate that the likelihood of observing a probability no larger than P_0 is 33.8% for events with SECVTX tags, 17.9% for events with JPB tags and 41.1% for events with SLT tags. In Z +jet events the background prediction agrees with the data.

XIV. RATES OF NEGATIVE TAGS IN THE $W+\geq 1$ JET SAMPLE

As shown in Sec. X, the mistag rates plus the estimated heavy flavor contribution to the negative tags account for the observed rates of negative tags in all generic-jet data. A similar test in the $W+\geq 1$ jet sample offers an additional check of the mistag rate predictions and a complementary test of

the method used to estimate the background contribution to the $t\bar{t}$ signal.

The rate of negative tags for each process is calculated from the corresponding simulation or using the data as we do for positive tags. We use the sample composition before tagging listed in Tables XXXVI and XXXVIII for SECVTX and JPB, respectively. Table XXXIV compares numbers of observed and predicted negative SECVTX tags as a function of the jet multiplicity. The analogous comparison for negative JPB tags is shown in Table XXXV. Data and predictions agree within the estimated uncertainties.

XV. MEASUREMENT OF THE $t\bar{t}$ PRODUCTION CROSS SECTION

The $t\bar{t}$ production cross section is

$$\sigma_{t\bar{t}} = \frac{N_{\text{tag}}^{\text{obs}} - N_{\text{tag}}^{\text{bkg}}}{\mathcal{A}_{t\bar{t}} \epsilon_{\text{tag}} \int \mathcal{L} dt}$$

TABLE XXXIII. Summary of observed and predicted number of Z events with one (ST) and two (DT) SLT tags.

Source	$Z+1$ jet	$Z+2$ jet	$Z+3$ jet	$Z+\geq 4$ jet
Mistags	12.65 ± 1.27	3.66 ± 0.37	0.57 ± 0.06	0.15 ± 0.02
WW, WZ, ZZ	0.04 ± 0.02	0.09 ± 0.03	0.01 ± 0.01	0.01 ± 0.01
Zc	0.55 ± 0.17	0.17 ± 0.05	0.02 ± 0.01	0.01 ± 0.00
$Zc\bar{c}, Zb\bar{b}$ (ST)	2.26 ± 0.36	1.10 ± 0.19	0.16 ± 0.03	0.06 ± 0.01
$Zc\bar{c}, Zb\bar{b}$ (DT)		0.02 ± 0.01	0.00 ± 0.00	0.00 ± 0.00
Single top quark	0.00 ± 0.00	0.00 ± 0.00	0.00 ± 0.00	0.00 ± 0.00
$t\bar{t}$ (ST)	0.04 ± 0.00	0.19 ± 0.02	0.08 ± 0.01	0.01 ± 0.00
$t\bar{t}$ (DT)		0.00 ± 0.00	0.00 ± 0.00	0.00 ± 0.00
Prediction (ST)	15.54 ± 1.33	5.21 ± 0.42	0.85 ± 0.07	0.24 ± 0.02
Prediction (DT)		0.03 ± 0.01	0.01 ± 0.00	0.00 ± 0.00
Data (ST)	16	3	0	1
Data (DT)		0	0	0

TABLE XXXIV. Summary of the predicted and observed number of W +jet events with negative SECVTX tags. The contribution of each process before tagging is taken from Table XXXVII.

Source	$W+1$ jet	$W+2$ jet	$W+3$ jet	$W+\geq 4$ jet
Mistags	10.82 ± 1.08	3.80 ± 0.38	0.99 ± 0.10	0.35 ± 0.04
Non- W	0.30 ± 0.15	0.30 ± 0.21	0.00 ± 0.35	0.00 ± 0.14
WW, WZ, ZZ	0.00 ± 0.00	0.04 ± 0.04	0.00 ± 0.00	0.00 ± 0.00
Single top quark	0.07 ± 0.02	0.05 ± 0.02	0.01 ± 0.00	0.00 ± 0.00
Wc	0.69 ± 0.32	0.34 ± 0.15	0.12 ± 0.09	0.02 ± 0.02
$Wc\bar{c}$ (ST)	0.34 ± 0.15	0.18 ± 0.07	0.07 ± 0.05	0.01 ± 0.01
$Wc\bar{c}$ (DT)		0.00 ± 0.00	0.00 ± 0.00	0.00 ± 0.00
$Wb\bar{b}$ (ST)	1.42 ± 0.26	0.32 ± 0.09	0.08 ± 0.05	0.02 ± 0.02
$Wb\bar{b}$ (DT)		0.00 ± 0.00	0.00 ± 0.00	0.00 ± 0.00
$Z \rightarrow \tau\tau$	0.00 ± 0.00	0.00 ± 0.00	0.00 ± 0.00	0.00 ± 0.00
Zc	0.01 ± 0.00	0.00 ± 0.00	0.00 ± 0.00	0.00 ± 0.00
$Zc\bar{c}$ (ST)	0.01 ± 0.00	0.00 ± 0.00	0.00 ± 0.00	0.00 ± 0.00
$Zc\bar{c}$ (DT)		0.00 ± 0.00	0.00 ± 0.00	0.00 ± 0.00
$Zb\bar{b}$ (ST)	0.08 ± 0.01	0.02 ± 0.01	0.01 ± 0.01	0.00 ± 0.00
$Zb\bar{b}$ (DT)		0.00 ± 0.00	0.00 ± 0.00	0.00 ± 0.00
$t\bar{t}$ (ST)	0.01 ± 0.00	0.12 ± 0.03	0.31 ± 0.08	0.27 ± 0.07
$t\bar{t}$ (DT)		0.00 ± 0.00	0.00 ± 0.00	0.00 ± 0.00
Prediction (ST)	13.74 ± 1.18	5.18 ± 0.48	1.60 ± 0.39	0.69 ± 0.17
Prediction (DT)		0.00 ± 0.00	0.00 ± 0.00	0.00 ± 0.00
Data (ST)	19	7	2	0
Data (DT)		0	0	0

TABLE XXXV. Summary of the predicted and observed number of W +jet events with negative JPB tags. The contribution of each process before tagging is taken from Table XXXIX.

Source	$W+1$ jet	$W+2$ jet	$W+3$ jet	$W+\geq 4$ jet
Mistags	41.81 ± 4.24	12.99 ± 1.35	2.25 ± 0.28	0.25 ± 0.19
Non- W	2.74 ± 0.45	1.42 ± 0.43	0.39 ± 0.19	0.16 ± 0.08
WW, WZ, ZZ	0.50 ± 0.15	0.74 ± 0.19	0.36 ± 0.13	0.02 ± 0.01
Single top quark	0.23 ± 0.05	0.34 ± 0.08	0.09 ± 0.03	0.02 ± 0.01
Wc	9.31 ± 2.91	1.82 ± 0.67	0.46 ± 0.21	0.04 ± 0.03
$Wc\bar{c}$ (ST)	4.55 ± 1.27	0.71 ± 0.25	0.26 ± 0.12	0.03 ± 0.02
$Wc\bar{c}$ (DT)		0.00 ± 0.00	0.00 ± 0.00	0.00 ± 0.00
$Wb\bar{b}$ (ST)	3.14 ± 0.50	1.77 ± 0.36	0.39 ± 0.11	0.06 ± 0.04
$Wb\bar{b}$ (DT)		0.01 ± 0.01	0.01 ± 0.01	0.00 ± 0.00
$Z \rightarrow \tau\tau$	0.44 ± 0.20	0.52 ± 0.21	0.09 ± 0.09	0.00 ± 0.00
Zc	0.08 ± 0.02	0.02 ± 0.01	0.01 ± 0.00	0.00 ± 0.00
$Zc\bar{c}$ (ST)	0.12 ± 0.04	0.02 ± 0.01	0.01 ± 0.01	0.00 ± 0.00
$Zc\bar{c}$ (DT)		0.00 ± 0.00	0.00 ± 0.00	0.00 ± 0.00
$Zb\bar{b}$ (ST)	0.17 ± 0.03	0.10 ± 0.02	0.04 ± 0.02	0.01 ± 0.01
$Zb\bar{b}$ (DT)		0.00 ± 0.00	0.00 ± 0.00	0.00 ± 0.00
$t\bar{t}$ (ST)	0.12 ± 0.03	1.21 ± 0.26	2.98 ± 0.65	3.35 ± 0.73
$t\bar{t}$ (DT)		0.06 ± 0.01	0.09 ± 0.02	0.26 ± 0.06
Prediction (ST)	63.21 ± 5.34	21.65 ± 1.67	7.35 ± 0.80	3.93 ± 0.76
Prediction (DT)		0.08 ± 0.02	0.10 ± 0.02	0.26 ± 0.06
Data (ST)	66	23	8	5
Data (DT)		1	0	1

TABLE XXXVI. Composition of the $W + \geq 1$ jet sample before tagging using $\sigma_{t\bar{t}} = 5.08 \pm 1.54$ pb.

Source	$W + 1$ jet	$W + 2$ jet	$W + 3$ jet	$W + \geq 4$ jet
Data	9454	1370	198	54
Non- W	560.1 ± 14.9	71.2 ± 2.7	12.4 ± 2.0	5.1 ± 1.7
WW	31.2 ± 5.4	31.1 ± 5.4	5.2 ± 1.0	0.8 ± 0.2
WZ	4.4 ± 0.9	4.8 ± 1.0	0.9 ± 0.2	0.1 ± 0.0
ZZ	0.3 ± 0.1	0.4 ± 0.1	0.1 ± 0.0	0.0 ± 0.0
Unidentified- Z	234.8 ± 14.5	38.5 ± 5.9	7.9 ± 2.4	0.7 ± 0.7
Single top quark	14.1 ± 2.1	7.9 ± 1.7	1.7 ± 0.4	0.3 ± 0.1
Wc	413.1 ± 123.9	86.8 ± 26.1	11.2 ± 3.4	1.9 ± 0.7
$Wb\bar{b}$	69.0 ± 9.5	29.7 ± 5.1	5.7 ± 1.1	1.5 ± 0.5
$Wc\bar{c}$	173.1 ± 46.2	61.9 ± 13.6	11.4 ± 2.6	2.3 ± 0.9
$W + \text{jet without h.f.}$	7952.0 ± 133.6	1027.7 ± 31.1	121.1 ± 7.7	19.9 ± 6.1
$t\bar{t}$	1.8 ± 0.5	10.1 ± 2.8	20.3 ± 5.7	21.3 ± 5.9

where $N_{\text{tag}}^{\text{obs}}$ is the number of tagged $W + \geq 3$ jet events, $N_{\text{tag}}^{\text{bkg}}$ is the background prediction, $\mathcal{A}_{t\bar{t}}$ is the detector acceptance for $t\bar{t}$ events, ϵ_{tag} is the efficiency for tagging top quark events, and $\int \mathcal{L} dt = 105.1 \pm 4.0 \text{ pb}^{-1}$ is the total integrated luminosity.

The acceptance for $t\bar{t}$ events is evaluated with a simulation which uses the PYTHIA generator and is $(7.8 \pm 1.3)\%$ for a top mass of $175 \text{ GeV}/c^2$. The 17% systematic error accounts for all uncertainties in the simulation which come

from the following: lepton identification and trigger simulation ($\pm 14\%$), jet energy scale ($\pm 5\%$), modeling of initial state gluon radiation ($\pm 2\%$), final state gluon radiation ($\pm 5\%$), Monte Carlo modeling of the $t\bar{t}$ production ($\pm 5\%$), detector resolution effects ($\pm 2\%$), and instantaneous luminosity dependence ($\pm 2\%$).

The tagging efficiencies are evaluated using the same simulation and are 0.505 ± 0.051 , 0.455 ± 0.046 , and 0.157 ± 0.016 for SECVTX, JPB, and SLT, respectively.

TABLE XXXVII. Summary of the predicted and observed number of W events with one (ST) and two (DT) SECVTX tags.

Source	$W + 1$ jet	$W + 2$ jet	$W + 3$ jet	$W + \geq 4$ jet
Mistags	10.82 ± 1.08	3.80 ± 0.38	0.99 ± 0.10	0.35 ± 0.04
Non- W	8.18 ± 0.78	1.49 ± 0.47	0.76 ± 0.38	0.31 ± 0.16
WW, WZ, ZZ	0.52 ± 0.14	1.38 ± 0.28	0.40 ± 0.13	0.00 ± 0.00
Single top quark	1.36 ± 0.35	2.38 ± 0.54	0.63 ± 0.14	0.14 ± 0.03
Wc	16.89 ± 5.38	3.94 ± 1.30	0.51 ± 0.17	0.09 ± 0.04
$Wc\bar{c}$ (ST)	7.89 ± 2.17	3.54 ± 0.88	0.77 ± 0.25	0.16 ± 0.07
$Wc\bar{c}$ (DT)		0.06 ± 0.04	0.00 ± 0.00	0.00 ± 0.00
$Wb\bar{b}$ (ST)	17.00 ± 2.41	8.35 ± 1.74	1.62 ± 0.40	0.41 ± 0.14
$Wb\bar{b}$ (DT)		1.51 ± 0.52	0.31 ± 0.13	0.07 ± 0.03
$Z \rightarrow \tau\tau$	0.96 ± 0.30	0.70 ± 0.25	0.17 ± 0.12	0.00 ± 0.00
Zc	0.14 ± 0.04	0.03 ± 0.01	0.01 ± 0.00	0.00 ± 0.00
$Zc\bar{c}$ (ST)	0.22 ± 0.06	0.10 ± 0.03	0.04 ± 0.02	0.00 ± 0.00
$Zc\bar{c}$ (DT)		0.00 ± 0.00	0.00 ± 0.00	0.00 ± 0.00
$Zb\bar{b}$ (ST)	0.93 ± 0.14	0.46 ± 0.12	0.17 ± 0.06	0.02 ± 0.02
$Zb\bar{b}$ (DT)		0.08 ± 0.03	0.03 ± 0.02	0.00 ± 0.00
Total background (ST)	64.90 ± 6.45	26.26 ± 2.51	6.11 ± 0.68	1.50 ± 0.23
Total background (DT)		1.65 ± 0.52	0.34 ± 0.13	0.07 ± 0.03
$t\bar{t}$ (ST)	0.54 ± 0.14	3.34 ± 0.87	6.76 ± 1.76	7.42 ± 1.93
$t\bar{t}$ (DT)		0.76 ± 0.20	2.88 ± 0.75	3.96 ± 1.03
$t\bar{t}$ + background (ST)	65.44 ± 6.45	29.61 ± 2.66	12.87 ± 1.89	8.92 ± 1.95
$t\bar{t}$ + background (DT)		2.41 ± 0.56	3.23 ± 0.76	4.03 ± 1.03
Data (ST)	66	35	10	11
Data (DT)		5	6	2

TABLE XXXVIII. Composition of the $W+\geq 1$ jet sample before tagging using $\sigma_{t\bar{t}}=8.02\pm 2.16$ pb.

Source	W+1jet	W+2jet	W+3jet	W+ ≥ 4 jet
Data	9454	1370	198	54
Non-W	560.1 \pm 14.9	71.2 \pm 2.7	12.4 \pm 2.0	5.1 \pm 1.7
WW	31.2 \pm 5.4	31.1 \pm 5.4	5.2 \pm 1.0	0.8 \pm 0.2
WZ	4.4 \pm 0.9	4.8 \pm 1.0	0.9 \pm 0.2	0.1 \pm 0.0
ZZ	0.3 \pm 0.1	0.4 \pm 0.1	0.1 \pm 0.0	0.0 \pm 0.0
Unidentified-Z	234.8 \pm 14.5	38.5 \pm 5.9	7.9 \pm 2.4	0.7 \pm 0.7
Single top quark	14.1 \pm 2.1	7.9 \pm 1.7	1.7 \pm 0.4	0.3 \pm 0.1
Wc	413.1 \pm 123.9	86.4 \pm 25.9	10.3 \pm 3.2	1.0 \pm 0.7
Wb \bar{b}	69.0 \pm 9.5	29.5 \pm 5.1	5.3 \pm 1.0	0.8 \pm 0.5
Wc \bar{c}	173.1 \pm 46.2	61.6 \pm 13.5	10.5 \pm 2.5	1.2 \pm 0.8
W+jets without h.f.	7951.0 \pm 133.5	1022.7 \pm 31.1	111.6 \pm 9.2	10.3 \pm 8.3
$t\bar{t}$	2.9 \pm 0.7	15.9 \pm 3.8	32.1 \pm 7.7	33.6 \pm 8.1

In the background calculation the rate of W +jet events with heavy flavor is estimated from the number of events due to W +jet direct production using the fraction of heavy flavor determined in Sec. XIF. Therefore the contribution of $t\bar{t}$ events must be removed from the data. This is done by iterating. The $t\bar{t}$ cross section is first estimated from the excess of tagged $W+\geq 3$ jet events over the background calculated assuming $\sigma_{t\bar{t}}=0$. The resulting $\sigma_{t\bar{t}}$ is used to evaluate the number of $t\bar{t}$ events before tagging; this contribution is sub-

tracted from the data to obtain the contribution of the W +jet direct production. The amount of W +jet with heavy flavor is recalculated and $\sigma_{t\bar{t}}$ is updated. The procedure is repeated until $\sigma_{t\bar{t}}$ is stable to within 1%.

In the sample of 252 $W+\geq 3$ jet events, there are 29 events with at least one jet tagged by the SECVTX algorithm. Using the procedure described above, the background estimate is 8.0 ± 1.0 events. Assuming that all the excess is due to $t\bar{t}$ production, the resulting $t\bar{t}$ cross section is 5.08

TABLE XXXIX. Summary of the predicted and observed number of W events with one (ST) and two (DT) jet-probability tags.

Source	W+1jet	W+2jet	W+3jet	W+ ≥ 4 jet
Mistags	41.80 \pm 4.24	12.78 \pm 1.33	2.19 \pm 0.27	0.25 \pm 0.19
Non-W	12.55 \pm 0.95	2.53 \pm 0.61	0.57 \pm 0.33	0.24 \pm 0.14
WW,WZ,ZZ	1.15 \pm 0.26	2.39 \pm 0.43	0.74 \pm 0.19	0.05 \pm 0.04
Single top quark	1.32 \pm 0.32	2.19 \pm 0.51	0.59 \pm 0.14	0.11 \pm 0.03
Wc	34.80 \pm 10.58	9.02 \pm 2.84	1.67 \pm 0.59	0.16 \pm 0.11
Wc \bar{c} (ST)	17.02 \pm 4.60	7.24 \pm 1.73	1.70 \pm 0.45	0.20 \pm 0.14
Wc \bar{c} (DT)		0.47 \pm 0.20	0.05 \pm 0.03	0.01 \pm 0.01
Wb \bar{b} (ST)	16.43 \pm 2.32	7.47 \pm 1.52	1.47 \pm 0.35	0.21 \pm 0.14
Wb \bar{b} (DT)		1.42 \pm 0.48	0.25 \pm 0.10	0.03 \pm 0.02
$Z\rightarrow\tau\tau$	2.35 \pm 0.47	1.13 \pm 0.32	0.17 \pm 0.12	0.09 \pm 0.09
Zc	0.28 \pm 0.09	0.08 \pm 0.03	0.03 \pm 0.01	0.00 \pm 0.00
Zc \bar{c} (ST)	0.46 \pm 0.13	0.20 \pm 0.06	0.09 \pm 0.04	0.01 \pm 0.01
Zc \bar{c} (DT)		0.01 \pm 0.01	0.00 \pm 0.00	0.00 \pm 0.00
Zb \bar{b} (ST)	0.90 \pm 0.14	0.42 \pm 0.10	0.16 \pm 0.06	0.02 \pm 0.02
Zb \bar{b} (DT)		0.07 \pm 0.03	0.03 \pm 0.01	0.00 \pm 0.00
Total background (ST)	129.08 \pm 12.56	45.53 \pm 4.00	9.43 \pm 0.97	1.34 \pm 0.34
Total background (DT)		1.97 \pm 0.52	0.33 \pm 0.10	0.04 \pm 0.02
$t\bar{t}$ (ST)	0.80 \pm 0.17	4.77 \pm 1.04	9.93 \pm 2.17	10.61 \pm 2.32
$t\bar{t}$ (DT)		1.10 \pm 0.24	3.90 \pm 0.85	5.46 \pm 1.19
$t\bar{t}$ +background (ST)	129.87 \pm 12.56	50.30 \pm 4.14	19.37 \pm 2.38	11.95 \pm 2.35
$t\bar{t}$ +background (DT)		3.07 \pm 0.57	4.23 \pm 0.86	5.50 \pm 1.20
Data (ST)	124	62	21	12
Data (DT)		6	5	3

TABLE XL. The composition of the $W+\geq 1$ jet sample before tagging using $\sigma_{t\bar{t}}=9.18\pm 4.26$ pb.

Source	W+1jet	W+2jet	W+3jet	W+ ≥ 4 jet
Data	9454	1370	198	54
Non-W	560.1 ± 14.9	71.2 ± 2.7	12.4 ± 2.0	5.1 ± 1.7
WW	31.2 ± 5.4	31.1 ± 5.4	5.2 ± 1.0	0.8 ± 0.2
WZ	4.4 ± 0.9	4.8 ± 1.0	0.9 ± 0.2	0.1 ± 0.0
ZZ	0.3 ± 0.1	0.4 ± 0.1	0.1 ± 0.0	0.0 ± 0.0
Unidentified-Z	234.8 ± 14.5	38.5 ± 5.9	7.9 ± 2.4	0.7 ± 0.7
Single top quark	14.1 ± 2.1	7.9 ± 1.7	1.7 ± 0.4	0.3 ± 0.1
Wc	413.1 ± 123.9	86.3 ± 25.9	10.0 ± 3.2	0.6 ± 1.3
$Wb\bar{b}$	69.0 ± 9.5	29.5 ± 5.1	5.1 ± 1.1	0.5 ± 1.0
$Wc\bar{c}$	173.1 ± 46.2	61.5 ± 13.5	10.1 ± 2.6	0.8 ± 1.6
W+jet without h.f.	7950.6 ± 133.5	1020.8 ± 31.8	107.8 ± 17.3	6.6 ± 17.5
$t\bar{t}$	3.3 ± 1.5	18.2 ± 8.2	36.7 ± 16.5	38.5 ± 17.3

± 1.54 pb (the statistical error is ± 1.30 pb and the systematic ± 0.82 pb). The estimated breakdown of the $W+\geq 1$ jet sample before and after tagging is shown in Tables XXXVI and XXXVII.

As a cross-check, we calculate $\sigma_{t\bar{t}}$ using rates of JPB tags. There are 41 events with at least one jet tagged by the jet-probability algorithm with a background of 11.1 ± 1.3 events. The observed excess of events yields $\sigma_{t\bar{t}}=8.02\pm 2.16$ pb. The estimated breakdown of the $W+\geq 1$ jet sample before and after tagging is shown in Tables XXXVIII and XXXIX.

There are 25 events with at least one jet tagged by the SLT algorithm with a background of 13.2 ± 1.2 events. The observed excess of events yields $\sigma_{t\bar{t}}=9.18\pm 4.26$ pb (the statistical error is ± 3.89 pb and the systematic ± 1.72 pb). The estimated breakdown of the $W+\geq 1$ jet sample before and after tagging is shown in Tables XL and XLI.

There is a small dependence of the acceptance and the tagging efficiencies on the top quark mass. The cross sections evaluated using SECVTX and JPB tags change by $\pm 1.8\%$ and the cross section calculated using SLT tags

TABLE XLI. Summary of the predicted and observed number of W events with one (ST) and two (DT) SLT tags.

Source	W+1jet	W+2jet	W+3jet	W+ ≥ 4 jet
Mistags	101.92 ± 10.19	30.90 ± 3.09	7.34 ± 0.73	3.01 ± 0.30
Non-W	8.96 ± 0.84	2.09 ± 0.56	0.38 ± 0.27	0.16 ± 0.11
WW,WZ,ZZ	0.50 ± 0.16	0.88 ± 0.22	0.10 ± 0.05	0.00 ± 0.00
Single top quark	0.38 ± 0.10	0.67 ± 0.15	0.18 ± 0.05	0.05 ± 0.01
Wc	13.12 ± 4.27	4.26 ± 1.45	0.65 ± 0.29	0.04 ± 0.09
$Wc\bar{c}$ (ST)	6.41 ± 1.89	2.68 ± 0.66	0.61 ± 0.21	0.05 ± 0.10
$Wc\bar{c}$ (DT)		0.02 ± 0.02	0.00 ± 0.00	0.00 ± 0.00
$Wb\bar{b}$ (ST)	5.31 ± 0.96	2.84 ± 0.67	0.41 ± 0.13	0.04 ± 0.08
$Wb\bar{b}$ (DT)		0.09 ± 0.05	0.01 ± 0.01	0.00 ± 0.00
$Z\rightarrow\tau\tau$	0.43 ± 0.20	0.09 ± 0.09	0.09 ± 0.09	0.00 ± 0.00
Zc	0.11 ± 0.04	0.04 ± 0.01	0.01 ± 0.01	0.00 ± 0.00
$Zc\bar{c}$ (ST)	0.17 ± 0.05	0.08 ± 0.02	0.03 ± 0.01	0.00 ± 0.00
$Zc\bar{c}$ (DT)		0.00 ± 0.00	0.00 ± 0.00	0.00 ± 0.00
$Zb\bar{b}$ (ST)	0.29 ± 0.06	0.16 ± 0.04	0.05 ± 0.02	0.01 ± 0.01
$Zb\bar{b}$ (DT)		0.00 ± 0.00	0.00 ± 0.00	0.00 ± 0.00
Total background (ST)	137.60 ± 11.29	44.66 ± 3.60	9.86 ± 0.88	3.35 ± 0.36
Total background (DT)		0.10 ± 0.05	0.01 ± 0.01	0.00 ± 0.00
$t\bar{t}$ (ST)	0.25 ± 0.11	2.44 ± 1.07	5.14 ± 2.25	6.08 ± 2.66
$t\bar{t}$ (DT)		0.07 ± 0.03	0.24 ± 0.10	0.32 ± 0.14
$t\bar{t}$ +background (ST)	137.85 ± 11.29	47.10 ± 3.75	15.00 ± 2.41	9.43 ± 2.68
$t\bar{t}$ +background (DT)		0.17 ± 0.06	0.25 ± 0.10	0.32 ± 0.14
Data (ST)	146	56	17	8
Data (DT)		0	0	0

TABLE XLII. Summary of old and new CDF $t\bar{t}$ production cross section results.

Channel	Previous result	New result
Lepton+jets (SVX)	$6.2_{-1.7}^{+2.1}$ pb	5.1 ± 1.5 pb
Lepton+jets (SLT)	$9.2_{-3.6}^{+4.3}$ pb	9.2 ± 4.3 pb
Dilepton	$8.2_{-3.4}^{+4.4}$ pb	$8.4_{-3.5}^{+4.5}$ pb
All-hadronic	$10.1_{-3.6}^{+4.5}$ pb	$7.6_{-2.7}^{+3.5}$ pb

changes by $\pm 2.3\%$ for a ± 5 GeV/ c^2 variation of the top quark mass.

XVI. COMBINED $t\bar{t}$ PRODUCTION CROSS SECTION

The best measurement of the $t\bar{t}$ cross section comes from combining the results of this analysis with the dilepton and all-hadronic analyses [16,38]. The revised b -tagging efficiency reported in this paper effects the cross section measured in the all-hadronic channel. The details of this analysis have not changed from those reported in Ref. [38]. The cross section measurement from the dilepton channel [16] does not require b -tagging information and so is unchanged by the revisions reported here. It is affected slightly by the revised determination of the total integrated luminosity as are all measurements. A comparison between the previously published results and the revised cross sections used for the new combined result is shown in Table XLII.

We combine the measurements from the SVX and SLT tagged lepton+jets, all-hadronic, and dilepton channels, using a maximum likelihood technique similar to that described in Refs. [3,5]. This procedure properly accounts for correlated systematic uncertainties, such as the uncertainties in the b -tagging efficiency, the luminosity, the kinematic acceptance, and some of the calculated backgrounds. In all channels the acceptances are calculated with M_{top}

$= 175$ GeV/ c^2 . The resulting combined $t\bar{t}$ production cross section is

$$\sigma_{t\bar{t}} = 6.5_{-1.4}^{+1.7} \text{ pb}$$

where the quoted uncertainties include both statistical and systematic effects, which are approximately equal in magnitude.

XVII. CONCLUSIONS

Having improved the method for determining the b -tagging efficiency and the method for calculating the backgrounds to $t\bar{t}$ production, we revise our previous measurements of $\sigma_{t\bar{t}}$ in the lepton+jets channel [2]. We find $\sigma_{t\bar{t}} = 5.08 \pm 1.54$ pb and $\sigma_{t\bar{t}} = 9.18 \pm 4.26$ pb using events with SECVTX and SLT tags, respectively. We have used the jet-probability algorithm as a cross-check and find that it gives a result consistent with these measurements. The measurement of the $t\bar{t}$ cross section, obtained by combining the results of this analysis with the dilepton and all-hadronic analyses, is $\sigma_{t\bar{t}} = 6.5_{-1.4}^{+1.7}$ pb, in agreement with the SM predictions [1] and the measurement performed by the DØ Collaboration [39].

ACKNOWLEDGMENTS

We thank the Fermilab staff and the technical staff of the participating institutions for their contributions. This work was supported by the U.S. Department of Energy and National Science Foundation, the Istituto Nazionale di Fisica Nucleare, the Ministry of Education and Culture of Japan, the Natural Science and Engineering Research Council of Canada, the National Science Council of the republic of China, the Swiss National Science Foundation, the A. P. Sloan Foundation; the Bundesministerium fuer Bildung und Forschung, and the Korea Science and Engineering Founda-

-
- [1] F. Bonciani *et al.*, Nucl. Phys. **B529**, 450 (1998); S. Catani *et al.*, Phys. Lett. B **378**, 329 (1996); E. Berger and H. Contopanagos, Phys. Rev. D **54**, 3085 (1996); E. Laenen *et al.*, Phys. Lett. B **321**, 254 (1994).
- [2] CDF Collaboration, F. Abe *et al.*, Phys. Rev. Lett. **80**, 2773 (1998).
- [3] F. Abe *et al.*, Phys. Rev. Lett. **74**, 2626 (1995).
- [4] F. Abe *et al.*, Phys. Rev. Lett. **80**, 2767 (1998).
- [5] F. Abe *et al.*, Phys. Rev. D **50**, 2966 (1994).
- [6] D. Buskulic *et al.*, Phys. Lett. B **313**, 535 (1993).
- [7] G. Marchesini and B. R. Webber, Nucl. Phys. **B310**, 461 (1988); G. Marchesini *et al.*, Comput. Phys. Commun. **67**, 465 (1992).
- [8] T. Sjöstrand, Report No. CERN-TH-6488/92, 1992. (URL: http://wwwcn.cern.ch/asdoc/pythia_html3/pythia57.html). PYTHIA v5.7 is used.
- [9] P. Avery, K. Read, and G. Trahern, Cornell Internal Note CSN-212, 1985. We use Version 9_1 of the CLEO simulation. The lifetime is set at 1.45 ps for all b -hadrons and the 1993 PDG values are used for the charmed hadron lifetimes.
- [10] F. Abe *et al.*, Nucl. Instrum. Methods Phys. Res. A **271**, 387 (1988).
- [11] D. Amidei *et al.*, Nucl. Instrum. Methods Phys. Res. A **350**, 73 (1994).
- [12] F. Abe *et al.*, Phys. Rev. D **50**, 5550 (1994); D. Cronin-Hennessy *et al.*, Nucl. Instrum. Methods Phys. Res. A **443**, 37 (2000).
- [13] D. Amidei *et al.*, Nucl. Instrum. Methods Phys. Res. A **269**, 51 (1988); P. Azzi *et al.*, *ibid.* **360**, 137 (1994).
- [14] F. Abe *et al.*, Phys. Rev. D **45**, 1448 (1992).
- [15] F. Abe *et al.*, Phys. Rev. D **47**, 4857 (1993).
- [16] F. Abe *et al.*, Phys. Rev. Lett. **80**, 2779 (1998).
- [17] The track isolation requirement is that the sum of the transverse momentum of all tracks in a cone of radius around the candidate track direction be less than 4 GeV/ c .
- [18] F. Abe *et al.*, Phys. Rev. Lett. **73**, 2662 (1994).
- [19] S. Kuhlmann, Report No. FERMILAB-CONF-94/148-E, 1994.

- [20] F. A. Berends, W. T. Giele, H. Kuijf, and B. Tausk, Nucl. Phys. **B357**, 32 (1991).
- [21] G. Altarelli and G. Parisi, Nucl. Phys. **B126**, 298 (1977).
- [22] C. Peterson *et al.*, Phys. Rev. D **27**, 105 (1983).
- [23] We use HERWIG v5.6 with $m_b = 4.75 \text{ GeV}/c^2$ and $m_c = 1.50 \text{ GeV}/c^2$ for the b - and c -quark masses, respectively. The value of the parameter VGCUT in the parton shower is set to VGCUT=0.06 and the value of the parameter CLPOW in the cluster hadronization is set to CLPOW=1.3. The generic-jet and low- p_T Monte Carlo samples use the MRS(G) structure functions, while all the other Monte Carlo samples use the MRSD₀ structure functions.
- [24] J. Benlloch, in *Proceedings of the 1992 DPF Meeting*, Batavia, Illinois, 1992, edited by C. H. Albright *et al.* (World Scientific, Singapore, 1993), p. 1091.
- [25] A. D. Martin, R. G. Roberts, and W. J. Stirling, Phys. Lett. B **306**, 145 (1993); **309**, 492(E) (1993).
- [26] F. Abe *et al.*, Phys. Rev. Lett. **74**, 850 (1995).
- [27] F. Abe *et al.*, Phys. Rev. D **53**, 3496 (1996).
- [28] F. Abe *et al.*, Phys. Rev. D **57**, 5382 (1998).
- [29] D. Kestenbaum, Ph.D. dissertation, Harvard University, 1996.
- [30] A. D. Martin, R. G. Roberts, and W. J. Stirling, Phys. Lett. B **354**, 155 (1995).
- [31] M. Mangano, Nucl. Phys. **B405**, 536 (1993).
- [32] M. Seymour, Nucl. Phys. **B436**, 163 (1995).
- [33] H. Plochow-Besch, "PDFLIB: Nucleon, Pion and Photon Parton Density Functions and alpha_s Calculations," User's Manual—Version 6.06, W5051 PDFLIB, 1995.03.15, CERN-PPE.
- [34] A. Ballestrero *et al.*, hep-ph/0006259; M. Mangano, hep-ph/9911256.
- [35] F. Abe *et al.*, Phys. Rev. D **52**, 2624 (1995).
- [36] T. Stelzer, Z. Sullivan, and S. Willenbrock, Phys. Rev. D **56**, 5919 (1997); M. Smith and S. Willenbrock, *ibid.* **54**, 6696 (1996).
- [37] J. Ohnemus and J. F. Owens, Phys. Rev. D **43**, 3626 (1991); J. Ohnemus, *ibid.* **43**, 3626 (1991); **44**, 1403 (1991).
- [38] F. Abe *et al.*, Phys. Rev. Lett. **79**, 1992 (1997).
- [39] B. Abbott *et al.*, Phys. Rev. D **60**, 012001 (1999).